UNIVERSITY OF THE PHILIPPINES

UPPER OCEAN RESPONSE TO TROPICAL CYCLONES OFF EASTERN PHILIPPINES

by

IAN QUINO D.G. FERNANDEZ

A Master's Thesis Submitted to the
Marine Science Institute
College of Science
University of the Philippines
Diliman, Quezon City

In Partial Fulfillment of the Requirements
For the Degree of
Master of Science in Marine Science

April 2014

Upper Ocean Response to Tropical Cyclones off Eastern Philippines
by Ian Quino D.G. Fernandez
MS Thesis, Marine Science Institute
University of the Philippines, Diliman
April 2014

Classification*: P
* I – Invention or creation; P – Publication; C – Confidential Information

Available to the general Public	No
Available only after consultation with author/adviser for thesis/dissertation	No
Available only to those bound by nondisclosure or confidentiality agreement	Yes

_____
Ian Quino D.G. Fernandez
Student

_____
Cesar L. Villanoy, Ph.D.
Thesis Adviser

This is to certify that this master's thesis entitled, "**UPPER OCEAN RESPONSE TO TROPICAL CYCLONES OFF EASTERN PHILIPPINES**" and submitted by IAN QUINO FERNANDEZ to fulfill part of the requirements for the degree of **Master of Science** in **Marine Science** was successfully defended and approved on **March 3, 2014**.

CESAR L. VILLANOY, Ph.D.
Thesis Adviser

PIERRE FLAMENT, Ph.D.
Thesis Reader

The **Marine Science Institute** endorses acceptance of this master's thesis as partial fulfillment of the requirements for the degree of **Master of Science** in **Marine Science**.

MARIE ANTONETTE J. MEÑEZ, Ph.D.
Director, Marine Science Institute

The master's thesis is hereby officially accepted as partial fulfillment of the requirements for the degree of **Master of Science** in **Marine Science**.

JOSE MARIA P. BALMACEDA, Ph.D.
Dean, College of Science

THE MARINE SCIENCE INSTITUTE
College of Science
University of the Philippines
Diliman, Quezon City

ANNOUNCEMENT OF THE MASTER'S EXAMINATION

of

MR. IAN QUINO FERNANDEZ

in defense of his master's thesis

"UPPER OCEAN RESPONSE TO TROPICAL CYCLONES OFF EASTERN PHILIPPINES"

for the degree of Master of Science in Marine Science

1:00 P.M., Monday, 3 March 2014
Audio-Visual Room, MSI Building
U.P. Diliman, Quezon City

THESIS ADVISER
Dr. Cesar L. Villanoy
Professor
Marine Science Institute
College of Science
U.P. Diliman, Quezon City

THESIS READER
Dr. Pierre Flament
Professor
Department of Oceanography
School of Ocean and Earth Sciences & Technology
University of Hawai'i at Manoa
Honolulu, Hawai'I 96822

THESIS EXAMINER
Dr. Laura T. David
Professor
Marine Science Institute
College of Science
U.P. Diliman, Quezon City

THESIS EXAMINER
Dr. Gerry Bagtasa
Assistant Professor
Institute of Environmental Science & Meteorology
College of Science
U.P. Diliman, Quezon City

ENDORSED BY:

Dr. Marie Antonette J. Meñez
Director
Marine Science Institute

AUTHORIZED BY:

Dr. Jose Maria P. Balmaceda
Dean
College of Science

ACKNOWLEDGEMENT

“No words can express but

Glory to GOD”

ABSTRACT

The tropical Western North Pacific, east of the Philippines, is a region where most of the strongest typhoons of the world originate and is associated with the bifurcation of the North Equatorial Current forming the Kuroshio Current to the north and Mindanao Current to the south. The variability of the NEC bifurcation latitude (seasonally and inter-annually) may alter the origins of the Kuroshio and modify the intensity of semi-permanent oceanic features that may alter temperature field affecting the strength of the typhoons and upper ocean response. The general objective of this study is to determine upper ocean response to tropical cyclones off Eastern Philippines based on background thermal structure and different oceanic features. This was conducted by computing the upper ocean response based on maximum change in sea surface temperature (SST) and recovery period derived from numerical experiments and actual satellite data from 2003 to 2012.

Upper ocean response generally summarized as the SST response due to tropical cyclones with higher sea surface temperature anomaly (SSTA) induced cooling (local minimum) and is associated with longer SST recovery period and is either enhanced by with increasing tropical cyclone (TC) strength and slower translation speed. On the other hand, SST response also varies based on different background conditions. Two general regions were identified, BN (> 15°N) and BS (<15°N) differentiated by their mean background thermal structure parameterized as mean SST, mixed layer depth (MLD), mixed layer temperature (MLT), Average temperature in the top 100m (T100) and depth of the 26°C isotherm (D26). The BN region, characterized with a shallow MLD and D26, and colder SST, T100 and MLT showed higher seasonal variability; while BS region with deeper MLD and D26 (>100m), and warmer SST, T100 and MLT were more consistent throughout the year. The BS region is associated with the NEC bifurcation window where the deeper D26 contributes to warmer waters in the region. Results shows that the BN region is more susceptible to oceanic cooling with at most 2°C (0.5°C) observed and computed difference in local minimum for slow (fast) moving and strong (weak) TC than the BS region. Moreover, SST response based on different oceanic features and its response to the shifting of the NEC bifurcation latitude was also investigated. Results show highest local minimum, alongside longest SST recovery, are associated with negative features (SSHA <-6 cm) as a result of turbulent mixing given a shallow D26 (~40m), while lowest local minimum, alongside fastest recovery are associated with positive features (SSHA > 6 cm) as effect of warm water entrainment, given a deeper D26 (~100m) serving as insulation. The northward migration of the NEC results to an

increase in the number of negative features while a southward shift results to an increase in positive features. A region of high correlation (R^2>=0.5) was also identified on 6°N to 18°N latitude and 125° to 170°E (RCORR region). SST response on this shows no significant differences. However, the percentage of slow moving typhoons and strong typhoons were observed during a northward shift while an increase in moderate moving and the number of tropical storms and depression during a southward shift.

SST response is dependent on oceanic features related to a background upper ocean thermal structure that varies with latitude, seasonally and interannually. Variations in magnitude and direction may play an important role in the relative strength of tropical cyclones and associated sea surface response. This shows that the NEC, off Eastern Philippines plays an important role in manipulating control of the atmosphere at a given favorable atmospheric conditions.

TABLE OF CONTENTS

ACKNOWLEDGEMENT V

ABSTRACT VI

TABLE OF CONTENTS VIII

LIST OF TABLES X

LIST OF FIGURES XI

CHAPTER 1 1

Introduction 1
Tropical Cyclogenesis 3
Ocean Response to Tropical Cyclone 4
SSH Response 7
SST Response 8
Upper Structure in Relation to the passage of Typhoons 9
Northwest Pacific Basin 12

Objectives of the Study 14

Datasets 15

CHAPTER 2. SEA SURFACE TEMPERATURE RESPONSE TO TROPICAL CYCLONES OFF EASTERN PHILIPPINES: DEPENDENCE ON BACKGROUND THERMAL STRUCTURE 17

Introduction 17
Background Climatological Condition 18

Methodology 22
SST Response 22
Numerical Modeling 23

Results 25
SST Response 25
Numerical Experiments 27
SST Response in the BN and BS Region 29

Discussion 33

Summary and Conclusion 37

CHAPTER 3. SEA SURFACE TEMPERATURE RESPONSE TO TROPICAL CYCLONES OFF EASTERN PHILIPPINES: DEPENDENCE ON OCEANIC FEATURES 38

Introduction 38

Methodology 39
SST Response 39
Oceanic Features 39
Numerical Modeling 40
NEC Bifurcation Latitude 40

Results 42
Numerical Experiments 42
SST Response: dependence on oceanic features 44
Migration of the NEC Bifurcation Latitude 46
SST Response with the NEC Bifurcation 50

Discussion 52

Summary and Conclusion 55

CHAPTER 4. SYNTHESIS 56

REFERENCES 58

APPENDIX 65
Supplementary Figures – Chapter 2 65
Supplementary Figures – Chapter 3 68

LIST OF TABLES

Table 1. Saffir Simpson Scale for Hurricane Classification and associated Wind Speed, Pressure and Storm Surge Height 1

Table 2. Mean and standard deviation of Upper Ocean Thermal Parameters (T100 in °C, MLT in °C, MLD in meters, and D26 in meters) using annual, typhoon season (June to November) and outside the typhoon season (December to May) along the region bounded by 0-30°N, 120-150°E, and at BN (15-30°N) and BS (0-15°N) based on ARGO float data from 2003-2012. 19

Table 3. Input Momentum Flux or Wind Stress (τ_{wind}) representing different TC scales based on the Saffir-Simpson Hurricane Scale (SSHS) 24

Table 4. Mean Local Minima (°C) induced by Tropical Cyclones 25

Table 5. Pre and post typhoon parameters (T100, MLT, D26 and MLD) for both BN and BS Region. 28

Table 6. Comparison of Maximum SSTA changes based on Numerical Experiments and Observation Data in degree Celsius for Both BN and BS region 33

Table 7. Comparison of Maximum SSTA changes based on Numerical Experiments and Observation Data in degree Celsius for different oceanic features (Negative, Neutral and Positive) 53

LIST OF FIGURES

Figure 1. Saffir-Simpson Hurricane Scale with associated Wind Speed (mph), Pressure (mbars), Storm surge (ft) and Damage level (SOURCE: National Weather Service) 2

Figure 2. Philippine Area of Responsibility bounded by dotted red lines. 2

Figure 3. Frequency of Tropical Cyclones from 2003-2012 affecting the Philippine Area of Responsibility summarized according to year (a), and month (b). Lower plots show monthly frequency categorized by year (c) and Normalized monthly events over the total events from 2003-2012 (d). 3

Figure 4. Regional map showing the tracks of tropical cyclones during the period 2003–2012, with green circles indicating where they formed. The background color is the satellite-derived mean sea surface temperature from 2003 to 2012. 4

Figure 5. Cross-section schematic of the physical processes that alter the mixed layer depth (MLD) (h: light gray line) forced by Tropical Cyclone winds (u_*) such as shear-induced mixing ($\partial v/\partial z$=shear) and MLD changes (Dh: dark gray line), upwelling (w) due to transport (arrows) by currents away from the storm center relative to the surface depression (Z_0), and surface heat fluxes (Q_o) from the ocean to the atmosphere, all of which may contribute to ocean cooling during TC passage (Shay, 2001). 5

Figure 6. Effect of Winds in the Northern Hemisphere. (a) Cyclonic Wind on surface waters and (b) corresponding shape of the sea surface and thermocline; (c) Anticyclonic wind on surface waters and (d) corresponding shape of the sea surface and thermocline (from Collins, 2000) 6

Figure 7. Wind Fields during the passage of Typhoon Lupet on October 22-23, 2009 passing through along the east coast of Luzon (http://earthobservatory.nasa.gov/NaturalHazards./vew.php?id=40882) 6

Figure 8. Ekman Transport along the Coast (along western boundary). (Left) wind blowing to the north, transport is away from the coast causing coastal upwelling (Right) wind blowing to the south, Transport towards the coast will cause coastal downwelling 7

Figure 9. Biological responses (a) before and (b) after passage of Tropical Cyclones (Hung and Gong, 2011) 8

Figure 10. Schematic of the time series of SSTA in terms of full recovery time, and e-folding period as a response to TC passage adapted from Dare and McBride, 2011 (right) and actual data (left) 9

Figure 11. (a) Relationship of the Upper thermal structure associated with Sea surface height anomaly (SSHA) including the Mixed Layer Thickness and the Depth of 26°C and 20°C isotherm (D26 and D20, respectively) (http://www.aoml.noaa.gov/phod/cyclone/data/method.html) 10

Figure 12. The three-dimensional schematic of the temperature distribution in the upper ocean shown above illustrates the impact of a hurricane passing over the ocean when the oceanic mixed layer is thin (left) and thick (right). In both cases, the hurricane propagates down and left over the warm sea surface (red), creating a cold wake behind the storm as colder water (blue) is brought towards the sea surface by the hurricane's wind stress. The thin oceanic mixed layer (left) favors formation of the cold wake making the hurricane weaker than a thick oceanic mixed layer (right). (Scrowcroft et al, 2011) 11

Figure 13. Structure of the barrier layer in association with the mixed layer depth (Mignot et al, 2009) 11

Figure 14. Main Development Region (MDR) for typhoon formation and intensification area average of the depth of 26°C isotherm (D26) and Tropical Cyclone Heat Potential (TCHP) during the peak of typhoon season (July-October) from 1993 to 2011 (left); Region enclosed in red rectangle (right) is the MDR (122°-170°E; 10°-26°N) (Pun et al, 2013). 13

Figure 15. General Diagram illustrating bifurcation of the NEC into the Kuroshio Current to the North and Mindanao Current to the South (Rudnick et al, 2011) 14

Figure 16. Tropical Cyclone Tracks affecting Philippine Area of Responsibility from 2003 to 2012. 15

Figure 17. Number of Tropical Cyclone affecting (a) Western North Pacific Region (b) Philippine Area of Responsibility. TS includes Tropical Storm and Tropical Depression, TY includes typhoons from Cat 1-3 while STY includes typhoons from Cat 4-5 based on the Saffir-Simpson Hurricane Scale 15

Figure 18. Spatial Distribution of Available ARGO Profiles from 2003 to 2012 16

Figure 19. Climatological data based on (a) Sea Surface Temperature (SST) Mean Climatological for the entire region (black solid lines); at BN (LAT > 15°N) (gray broken line line); and at BS (LAT < 15°N) (gray solid line) 18

Figure 20. (a) Normalized distribution to the total number of occurrences of Tropical Cyclones affecting the Philippine Area of Responsibility – Typhoon peak season is enclosed in black broken line rectangular box; Climatological (b) Sea Surface Temperature (SST) (c) Mixed Layer Depth (MLD) (d) Mixed Layer Temperature (MLT) averaged during the peak of the typhoon season (June to October) 19

Figure 21. Mean temperature Profile derived from ARGO Float Data from 2003 to 2012 associated with (e) BS Region and (f) BN Region. Identified regions are BN (Latitude > 15°N), enclosed in a black broken line rectangular box and BS (Latitude < 15°N), enclosed in solid black line rectangular box. 20

Figure 22. Meridional Plot of (top) Depth of 26°C Isotherm (D26); and (bottom) Depth Averaged Temperature up to 100m (T100) from 0° to 30°N Latitude derived from ARGO Float data. Dotted box is the Bifurcation window, 10-15°N (Qiu and Chen, 2010); dashed line showing boundary below and above -100m D26 isotherm (top) 21

Figure 23. Number of occurrence the day of local SSTA minima relative to TC passage, compiled from 3426 Data Points from TCs affecting the Philippine Area of Responsibility from 2003 to 2012; Highlighted in red box is the events considered in the study 22

Figure 24. Relationship between Translation speeds versus wind duration derived from TC track data translation speed and radius of maximum wind. Line graph show mean values; Error bar are standard deviations. 24

Figure 25. Mean SSTA Time Series for dataset with local minima occurring from Day -1 to Day 3 using (b) actual time series (c) adjusted local minima of the time series to Day 1. 25

Figure 26. Mean and standard deviation for Local Minimum SSTA versus Recovery Time at 0.5°C increment for (a) Global dataset (Dare and McBride, 2011) (b) East of the Philippines; Mean and standard deviation for Local Minimum versus e-Folding Period at 0.5°C increment for (c) Global Dataset (Dare and McBride, 2011) (d) East of the Philippines. 26

Figure 27.Relationship between varying TC translation speed on local minima SSTA and recovery period. Translation Speed expressed as slow (0-5 ms^{-1}); Moderate (5-10 ms^{-1}) and Fast (>10 ms^{-1}). 27

Figure 28. Relationship between varying TC Strength on local minima SSTA and recovery period. TC Strength labeled as TS/TD for tropical storms and depression; TYP for Cat 1 to 3 and STYP for Cat 4 to 5. 27

Figure 29. SSTA response (local minimum) derived from numerical experiments by varying TC strength and wind duration forcing time for (left) BN; and (right) BS region. 28

Figure 30. Temperature profile during a pre- and post-TC condition (top) and temperature profile changes (bottom) of a simulated Category 3 typhoon after 3 hours of wind forcing at (left) BN; and (right) BS region. 29

Figure 31. Difference on SST Response on BS region subtracted from the SST response on the BN region derived from numerical experiments 29

Figure 32. SSTA response (local minimum) (top) and Recovery Period (bottom) from observations at varying translation speed and TC strength for BS (left) and BN (right) region. Translation Speed are considered slow for 0-4 ms^{-1}; Moderate for 4-8 ms^{-1} and Fast for >8 ms^{-1}; TC Strength is TS/TD for Tropical Storms and Depression, TYP for CAT 1 to 3 and STYP for CAT 4 to 5 30

Figure 33. Relationship between translation speed on local minima and recovery period for BS (top) and BN (bottom) region. Translation Speed are considered slow for 0-4 ms^{-1}; Moderate for 4-8 ms^{-1} and Fast for >8 ms^{-1} 31

Figure 34. Actual number of occurrence of events (a, b) and percentage occurrence (c, d) based on TC strength (a, c) and based on translation speed (b, d) in both BS (blue) and BS (red) region. 31

Figure 35. Number of Occurrence for local minimum SSTA classes with respect to TC Strength (Left) and translation Speed (Right) for regions, BS (Top) and BN (Bottom);

Strength is TS/TD for Tropical Storms and Depression, TYP for CAT 1 to 3 and STYP for CAT 4 to 5; Translation Speed is SLOW for 0-5 m/s, MOD for 5-10 m/s and FAST for > 15 m/s. 32

Figure 36. Number of Occurrence for recovery period classes with respect to TC Strength (Left) and translation Speed (Right) for regions, BS (Top) and BN (Bottom); Strength is TS/TD for Tropical Storms and Depression, TYP for CAT 1 to 3 and STYP for CAT 4 to 5; Translation Speed is SLOW for 0-5 m/s, MOD for 5-10 m/s and FAST for > 15 m/s. 32

Figure 37. Meridional variation of Local Minimum (°C) (left) and Recovery Period (days) (right) at an increments of 0° from 0 to 30°N at 5° increment. Error bars are standard deviation. 35

Figure 38. Meridional Climatological Background Conditions from 2003 to 2012 during the peak of the Typhoon Season (June to November) based on Temperature (T100, MLT and SST) (left) and Depth (D26 and MLD) (right) at an increments of 5° from 0 to 30°N. 35

Figure 39. Monthly variation of Local Minimum (°C) on BS (left) and BN (right) Error bars are standard deviation. 36

Figure 40. Monthly variation of D26 (m) (top-left); MLD (m) (top-right); T100 (°C) (bottom-left) and MLT (°C) (bottom-right) for both the BS (gray) and BN (black) region. 36

Figure 41. Mean Temperature Profile using ARGO Profiles from 2003 to 2012 at different Oceanic Feature (a) Negative Features (SSHA < -6cm) (b) Neutral Feature (SSHA>-6 cm and SSHA <6 cm) and (c) Positive Features (SSHA > 6cm); Also highlighted red dashed line showing the depth of 26°C isotherm (D26). Black arrow indicating estimated value of SST. 40

Figure 42. SSTA response (local minimum) from numerical experiments by varying TC strength and wind duration forcing time at different oceanic features (left) negative; (middle) neutral and (right) positive. 42

Figure 43. Temperature profile of pre and post-TC condition (top) and temperature profile changes (bottom) of a simulated Category 3 typhoon after 3 hours of wind forcing different background profiles on (left) negative features; (middle) neutral features and (right) positive features. Light red solid line and light blue solid line indicating pre and post-storm D26, respectively. 43

Figure 44. Difference on SSTA Response on negative (SSHA <-6cm) (left) and positive (SSHA >6cm) (right) features relative to SSTA response occurring in neutral (SSHA >-6cm and SSHA <6cm) features derived from numerical experiments 43

Figure 45. SSTA response (local minimum) (top) and Recovery Period (bottom) from observations at varying translation speed and TC strength for different oceanic features – Negative Features (Left); Neutral Features (Center) and Positive Features (Right). Translation Speed are considered slow for 0-4 ms^{-1}; Moderate for 4-8 ms^{-1} and Fast for >8 ms^{-1}; TC Strength is TS/TD for Tropical Storms and Depression, TYP for CAT 1 to 3 and STYP for CAT 4 to 5 44

Figure 46. Relationship between translation speed on local minimum (°C) (left) and recovery period (days) (right) for different oceanic feature [positive (Δ), neutral (○) and blue (□) features] at varying TC Strength (top) and translation speed (bottom) derived from observation data. Error bars are standard deviation.[TC Strength: TS/TD – Tropical Storms/Depression; TYP – CAT 1 to 3; STYP – CAT 4 to 5.Translation Speed: SLOW – 0-4ms^{-1}; MODERATE – 4-8ms^{-1}; FAST - >8ms^{-1}] 45

Figure 47. Mean and standard deviation of the local minimum (°C) (top) and ΔSSHA (cm) (bottom) for different oceanic features [NEG+, SSHA <-18cm; NEG, SSHA >-18cm & SSHA <-6cm; NEU, SSHA >-6cm & SSHA <6cm; POS, SSHA >6cm & SSHA <18cm; POS+, SSHA >18cm] derived from observation data. Error bars are standard deviation. [TC Strength: TS/TD – Tropical Storms/Depression; TYP – CAT 1 to 3; STYP – CAT 4 to 5.Translation Speed: SLOW – 0-4ms^{-1}; MODERATE – 4-8ms^{-1}; FAST - >8ms^{-1}] 46

Figure 48. NEC Bifurcation Latitude (Yp) derived from satellite-derived SSHA from 1993 to 2013 47

Figure 49. (left) Monthly Mean D26 along the NEC Bifurcation window (10-15°N) with the bifurcation latitude (R=0.91347) and (right) Monthly Mean T100 along the NEC Bifurcation window with the bifurcation latitude (R=-78187) 47

Figure 50. Northerly Bifurcation (2003): (a) Annual Sea Surface Height with Yp = 13.7503°N (b) Annual Sea Surface Height Anomaly associated with cold core eddies near the coast; Southerly Bifurcation (2008): (c) Annual Sea Surface Height with Yp = 10.43333 (d) Annual Sea Surface Height Anomaly associated with warm core eddies near the coast. Values are in cm. 48

Figure 51. Spatial distribution of the correlation coefficient (r) [top left] and squared correlation coefficient (r^2) [bottom left] of the bifurcation latitude (Yp) versus SSHA derived from 1993 to 2012 satellite altimetry data; On the enclosed box labeled as the RCORR region (Latitude: 6 °N to 18°N and Longitude: 125°E to 170°E) where monthly mean D26 [top right] and T100 [bottom right] derived from ARGO float data from 2003 to 2012 showing correlation of R_{D26}=0.82 and R_{T100}=-0.61 with the bifurcation latitude (Yp). 49

Figure 52. Correlation between bifurcation latitude (Yp) and the percentage of occurrence of negative (top left), neutral (top right), positive (bottom left) and positive+neutral (bottom right) oceanic features along 6-18°N, 125-170°E. 49

Figure 53. Mean SSTA Response versus recovery period based on actual data during events with Bifurcation latitude (Yp) > 11°N (North, Δ) and < 11°N (South, □) in 6°-18°N (left) and 0°-30°N (right); Error bars are standard deviations. 50

Figure 54. Percentage number of occurrences of different TC Translation Speed (top) and Strength (bottom) classes for RCORR (left); MDR (center) and entire dataset (right) during a northerly bifurcation (YP > 11°N, red) and southerly bifurcation (YP <=11°N, blue). TC Strength: TS/TD – Tropical Storms/Depression; TYP – CAT 1 to 3; STYP – CAT 4 to 5.Translation Speed: SLOW – 0-4ms^{-1}; MODERATE – 4-8ms^{-1}; FAST - >8ms^{-1}. 51

Figure 55. Seasonal trend of the NEC Bifurcation Latitude adapted from Qiu and Chen, 2010 54

Figure 56. Temperature profile forced at wind stress at associated with different TC strength after 3 hours at BN as result of numerical experiments (Pre-Typhoon Profile – solid red line; Post Typhoon Profile –broken blue line). From top left to top right (TD, TS, C1, C2); bottom left to bottom right (C3, C4, C5) 65

Figure 57. Temperature profile differences forced at wind stress at associated with different TC strength after 3 hours at BN as result of numerical experiments (Pre-Typhoon Profile – solid red line; Post Typhoon Profile –broken blue line). From top left to top right (TD, TS, C1, C2); bottom left to bottom right (C3, C4, C5) 65

Figure 58. SST profile forced at wind stress associated with different TC strength after 3 hours at BS as result of numerical experiments (Pre-Typhoon Profile – solid red line; Post Typhoon Profile –broken blue line). From top left to top right (TD, TS, C1, C2); bottom left to bottom right (C3, C4, C5) 66

Figure 59. Temperature profile differences forced at wind stress at associated with different TC strength after 3 hours at BS as result of numerical experiments (Pre-Typhoon Profile – solid red line; Post Typhoon Profile –broken blue line). From top left to top right (TD, TS, C1, C2); bottom left to bottom right (C3, C4, C5) 66

Figure 60. Relationship between translation speed on local minima and recovery period for BS (top) and BN (bottom) region at varying TC Strength; Color bar denotes TC Strength is classified as TS/TD (blue) for Tropical Storms and Depression, TYP (green) for CAT 1 to 3 and STYP (red) for CAT 4 to 5; Translation Speed are considered slow for 0-5 m/s; Moderate for 5-10 m/s and Fast for >10 m/s; 67

Figure 61. Meridional variations of mean and standard variation of (c) Local Minimum and (d) Recovery Time based on Translation Speed [Slow (blue) – Translation Speed < 4 m/s; Moderate (green) – Translation Speed > 4 & <8 m/s; Fast (red) – Translation Speed > 8 m/s]; Meridional variation of (c) Local Minimum and (d) Recovery Time for different typhoon intensities based on Saffir-Simpson Hurricane Scale (SSHS) [TS/TD (blue) – Tropical Storms and Depression; TYP (green) – Category 1 to Category 3; STYP (red) – Category 4 and 5] 67

Figure 62. SST profile forced at associated with different TC strength after 3 hours for a negative feature as result of numerical experiments (Pre-Typhoon Profile – solid red line; Post Typhoon Profile –broken blue line). From top left to top right (TD, TS, C1, C2); bottom left to bottom right (C3, C4, C5) 68

Figure 63. Temperature profile differences forced at wind stress at associated with different TC strength after 3 hours for a negative feature as result of numerical experiments (Pre-Typhoon Profile – solid red line; Post Typhoon Profile –broken blue line). From top left to top right (TD, TS, C1, C2); bottom left to bottom right (C3, C4, C5) 68

Figure 64. SST profile forced at associated with different TC strength after 3 hours for a neutral feature as result of numerical experiments (Pre-Typhoon Profile – solid red line; Post

Typhoon Profile –broken blue line). From top left to top right (TD, TS, C1, C2); bottom left to bottom right (C3, C4, C5) 69

Figure 65. Temperature profile differences forced at wind stress at associated with different TC strength after 3 hours for a neutral feature as result of numerical experiments (Pre-Typhoon Profile – solid red line; Post Typhoon Profile –broken blue line). From top left to top right (TD, TS, C1, C2); bottom left to bottom right (C3, C4, C5) 69

Figure 66. SST profile forced at associated with different TC strength after 3 hours for a positive feature as result of numerical experiments (Pre-Typhoon Profile – solid red line; Post Typhoon Profile –broken blue line). From top left to top right (TD, TS, C1, C2); bottom left to bottom right (C3, C4, C5) 70

Figure 67. Temperature profile differences forced at wind stress at associated with different TC strength after 3 hours for a positive feature as result of numerical experiments (Pre-Typhoon Profile – solid red line; Post Typhoon Profile –broken blue line). From top left to top right (TD, TS, C1, C2); bottom left to bottom right (C3, C4, C5) 70

Figure 68. (a) Meridional Plot of D26 averaged along the 124-145°E region acquired using ARGO Float data from 2003 to 2012. Boxed highlighting NEC Bifurcation window (10-15°N) 71

CHAPTER 1

Introduction

A Tropical Cyclone is defined by the World Meteorological Organization (WMO) as "a synoptic-scale to meso-scale low-pressure system which derives its energy primarily from: (1) evaporation from the sea in the presence of high winds and low surface pressure; and (2) condensation in convective clouds concentrated near its center" (Holland, 1993). The National Oceanic and Atmospheric Administration (NOOA) defines tropical cyclones as "a warm-core, low pressure system without any "front" attached, that develops over the tropical or subtropical waters, and has an organized circulation".

Tropical cyclones are classified by form and intensity as they increase in size. These tropical cyclones undergo different stages as defined by Bowditch (2002) and the Philippine Atmospheric, Geophysical and Astronomical Services Administration (PAGASA) (http://kidlat.pagasa.dost.gov.ph/genmet/psws.html):

- A tropical disturbance is a discrete system of apparently organized convection, generally 100 to 300 miles in diameter, having a non-frontal migratory character, and having maintained its identity for 24 hours or more.
- A tropical depression has one or more closed isobars and some rotary circulation at the surface. It is a weak low pressure disturbance with a definite surface circulation having maximum wind speed of up to 63 kilometers per hour (kph) or approximately less than 25 mile per hour (mph).
- A tropical storm has closed isobars and a distinct rotary circulation. It is a moderate tropical cyclone with maximum wind speed of 64 to 118 kph (25 to 75 mph) and with closed isobars.
- When fully developed, a hurricane or typhoon has closed isobars, a strong and very pronounced rotary circulation. It becomes an intense tropical cyclone when maximum wind speed exceeds 118 kph.

Table 1. Saffir Simpson Scale for Hurricane Classification and associated Wind Speed, Pressure and Storm Surge Height

Saffir Simpson Scale Category	Wind Speed		Pressure	Storm Surge Height
	$m \cdot s^{-1}$	$km \cdot hr^{-1}$	mb	m
1	33-42	120-153	980+	1.0-1.7
2	43-49	154-177	965-979	1.8-2.6
3	50-58	178-209	945-964	2.7-3.8
4	59-69	210-249	920-944	3.9-5.6
5	70+	250+	919-	5.7+
Non-Hurricane (TS/TD)	< 33	<120	-	-

Typhoons or hurricanes are tropical cyclones with speed greater than 33 ms^{-1} and are categorized based on the Saffir-Simpson Hurricane Scale (SSHS) (Table 1). The potential storm surge height and damage level associated with the Saffir-Simpson Hurricane scale are illustrated in Figure 1.

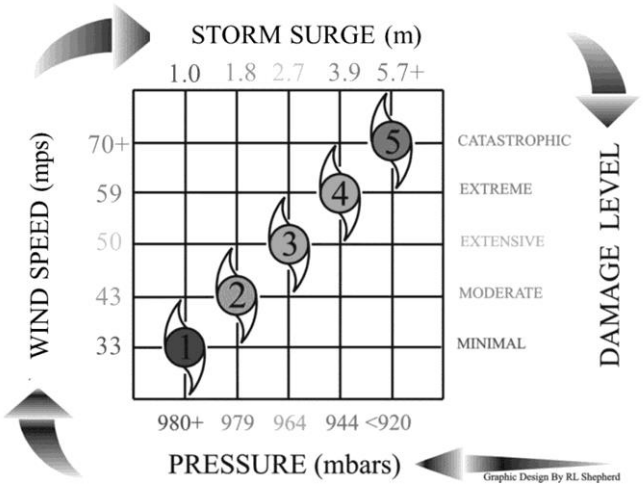

Figure 1. Saffir-Simpson Hurricane Scale with associated Wind Speed (mph), Pressure (mbars), Storm surge (ft) and Damage level (SOURCE: National Weather Service)

In the Philippines, PAGASA is tasked to monitor tropical cyclone occurrences along the Philippine area of responsibility (PAR) bounded by the dashed lines shown in Figure 2. The agency issues Public Storm Warning Signals (PSWS) depending on wind speeds likely to affect a certain region. A PSWS #1 is issued for winds of 30-60 kph for the next 36 hours; PSWS #2 for winds 60-100 kph in the next 24 hours; PSWS #3 for winds of 100 to 185 kph in the next 18 hours; and PSWS #4 for more than 185 kph in at least 12 hours.

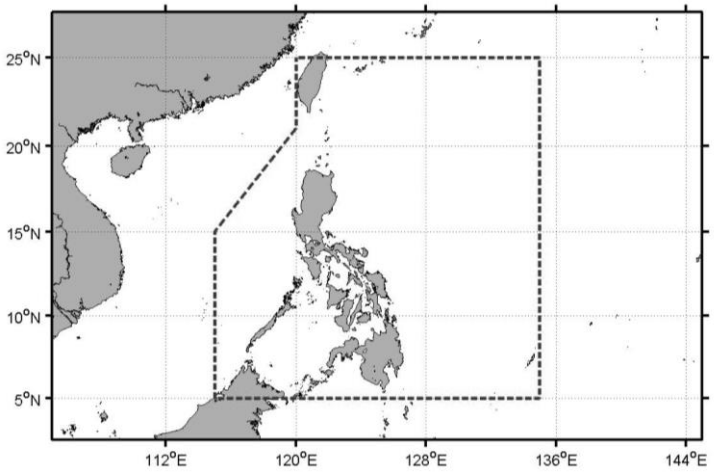

Figure 2. Philippine Area of Responsibility bounded by dotted red lines.

The Philippines is a region where most typhoons inflict damage on communities and their livelihood with a notable hazard risk on oceans and mortality risk on land (Peduzzi, et al 2012). Around 95% of the population is affected by tropical cyclones. Sixty three percent of the tropical cyclones formed in the Western North Pacific Region from 2003 to 2012 have entered the Philippine Area of Responsibility (PAR).

Data records as early as 1566-1934 show the peak typhoon season during the months of August to October (Ribera, 2005; Garcia-Herrera, 2007). A similar trend is observed from present day typhoons based on 2003-2012 data (Figure 3). Several CAT 5 typhoons occur on the same period. The peak of the typhoon season is during the southwest monsoon period - June to October (Williams et al, 1993) - where the SST is also at its annual peak (Botin et al, 2010).

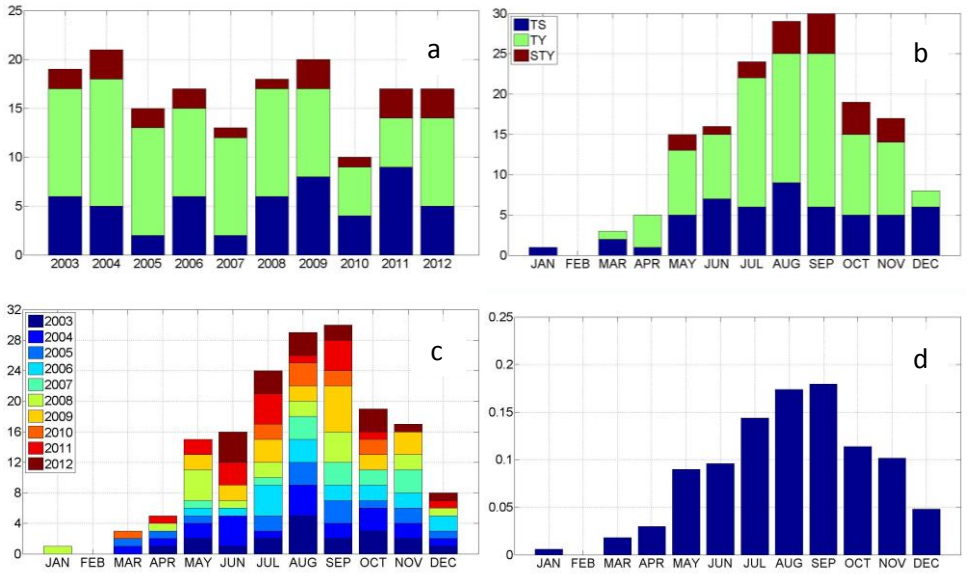

Figure 3. Frequency of Tropical Cyclones from 2003-2012 affecting the Philippine Area of Responsibility summarized according to year (a), and month (b). Lower plots show monthly frequency categorized by year (c) and Normalized monthly events over the total events from 2003-2012 (d).

Tropical Cyclogenesis

Figure 4 illustrates typhoon tracks and their origin (green dots) from 2003 to 2012 affecting the PAR overlaiN with mean sea surface temperature (SST). Formation occurs between 5-20°N latitude where the necessary latent heat and Coriolis force is strong enough (Aguado and Burt, 2010). An increase in sea surface temperature enhances the possibility of formation (Katsaros, 2009) and intensification (Goni et al, 2009) given necessary atmospheric

conditions. Formation of tropical cyclones is associated with warm regions with SST > 26°C. Dare and McBride (2011) added that this threshold temperature of 26.5°C, also called the Tropical Cyclone Heat Potential (Minett, 2009), maintained for a duration of at least 48 hours is needed for TCs to form. Intensification and the translation speed (the speed of transit) of TCs is strongly dependent on background climatological conditions such as the depth of the 26°C isotherm (D26) and Upper Ocean Heat Content (Lin et al, 2009).

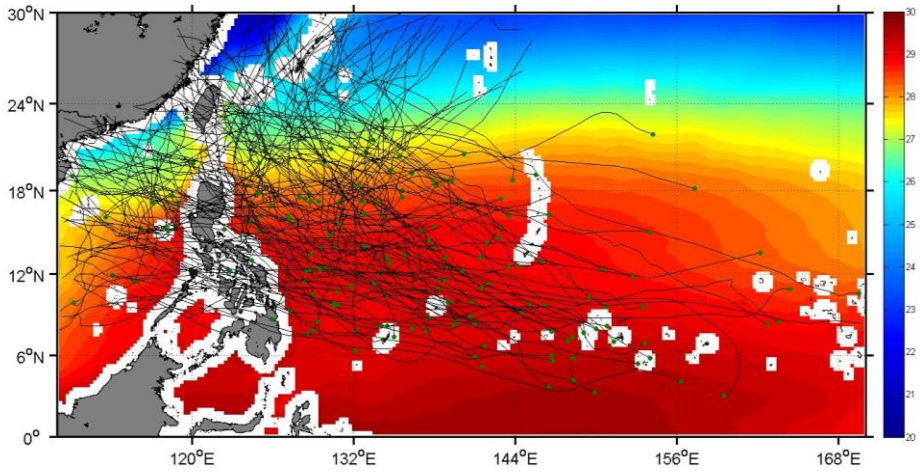

Figure 4. Regional map showing the tracks of tropical cyclones during the period 2003–2012, with green circles indicating where they formed. The background color is the satellite-derived mean sea surface temperature from 2003 to 2012.

Ocean Response to Tropical Cyclone

Oceanic response to tropical cyclones are generally associated with surface cooling and mixed layer deepening through several physical processes such as shear-driven entrainment mixing, surface convergence/divergence, surface and moisture fluxes and advection (Shay, 2009). Figure 5 illustrates these physical processes. Shay (2009) reported that around 60 to 85% can be attributed to shear driven mixing while around 5 to 15% through surface heat fluxes exchanges and also, around 5 to 15% through advection. Numerical experiments conducted by Vincent et al (2012) added that surface heat fluxes contributes around 50 to 80% of the cooling induced by weaker TCs as well as surface layer away from the TC track. On the other hand, mixing induced cooling explained around 30% for weaker TCs and 80% for the stronger TCs.

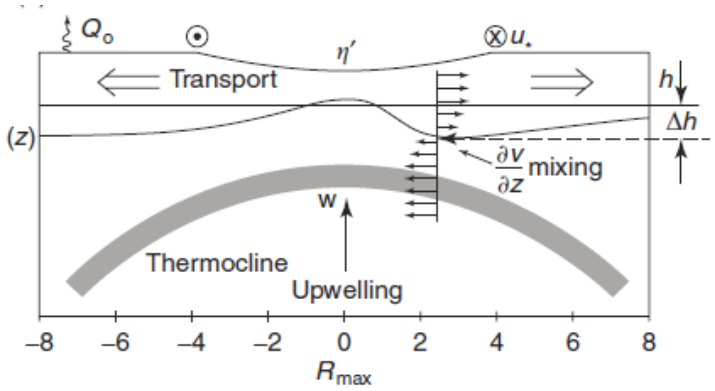

Figure 5. Cross-section schematic of the physical processes that alter the mixed layer depth (MLD) (h: light gray line) forced by Tropical Cyclone winds (u_*) such as shear-induced mixing ($\partial v/\partial z$=shear) and MLD changes (Dh: dark gray line), upwelling (w) due to transport (arrows) by currents away from the storm center relative to the surface depression (Z_0), and surface heat fluxes (Q_o) from the ocean to the atmosphere, all of which may contribute to ocean cooling during TC passage (Shay, 2001).

The effect of tropical cyclones on oceans is primarily wind-driven. Wind blowing over the ocean surface causes a tangential stress ("wind stress") at the air-sea interface pushing a vertical flux of horizontal momentum. General mechanism for momentum exchange includes Ekman transport causing surface divergence/convergence and wind-induced vertical current shears across the thermocline causing Upper Ocean mixing. Momentum exchange is characterized by the variations of winds speed with height and surface drag coefficient which can be a factor of wind speed and surface roughness (Shay, 2009). Momentum flux given by wind stress is shown using the following equation:

(Equation 1) $\tau_{wind} = \rho_{air} C_D U^2$

Where τ_{wind} is the momentum flux (Wind Stress);

ρ_{air} is the density of air; $\rho_{air} = 1.22\ \text{kg}\cdot\text{m}^{-3}$

C_D is the drag coefficient

U is the wind Speed

Ekman transport is always to the right of the direction of the wind in the northern hemisphere. In the presence of a typhoon, the wind moves in a cyclonic motion, forcing Ekman transport to move away from its core. This pushes water away causing surface divergence, which upwells water from below (Figure 6). Furthermore, as the typhoon moves during the other half of the cycle, ocean currents converge towards the track causing downwelling (Shay, 2009). Ekman Pumping Velocity (EPV) is the velocity of upwelling (Enriquez and Frienche, 1995) and is used to measure magnitude of upwelling.

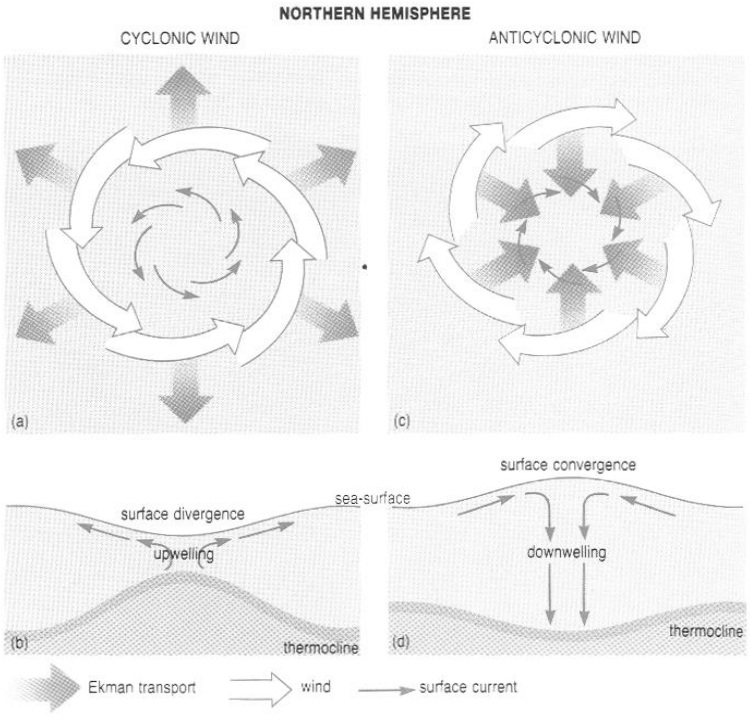

Figure 6. Effect of Winds in the Northern Hemisphere. (a) Cyclonic Wind on surface waters and (b) corresponding shape of the sea surface and thermocline; (c) Anticyclonic wind on surface waters and (d) corresponding shape of the sea surface and thermocline (from Collins, 2000)

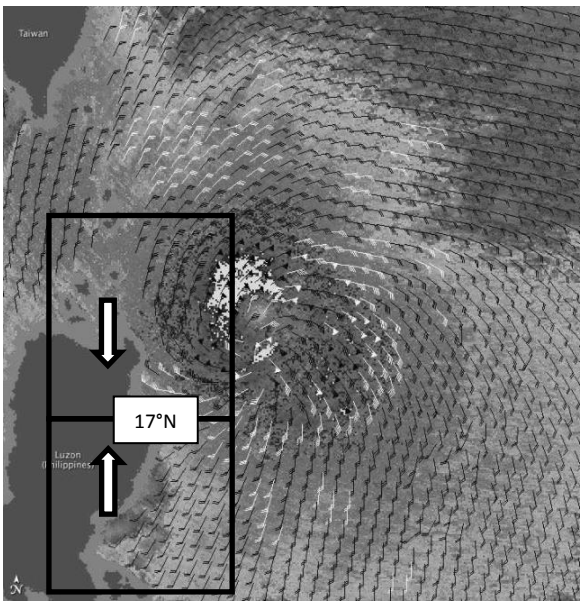

Figure 7. Wind Fields during the passage of Typhoon Lupet on October 22-23, 2009 passing through along the east coast of Luzon (http://earthobservatory.nasa.gov/NaturalHazards./vew.php?id=40882)

As typhoons approach the coast, wind orientation relative to the coast can result in Ekman transport divergence (upwelling) or convergence (downwelling) (Figure 7). The

landfall of storms can induce coastally trapped waves, such as Kelvin waves and may lead to upwelling events. An example is shown in Figure 7, along the east coast of Luzon (a western boundary). The passage of Typhoon Lupet (local name: Ramil) on October 22-23, 2009 caused a change in the direction of the wind - southward winds affecting the region north of 17°N while northward wind are observed south of 17°N. Varying wind direction along the coast due to typhoons can lead to a different response as a result of Ekman transport. At the northern hemisphere, a northward wind affecting a western boundary favors coastal upwelling while a southward wind favors coastal downwelling (Figure 8).

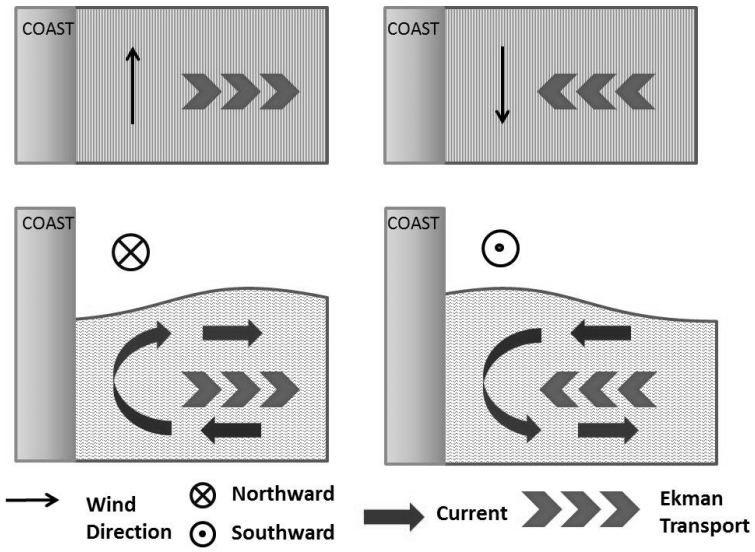

Figure 8. Ekman Transport along the Coast (along western boundary). (Left) wind blowing to the north, transport is away from the coast causing coastal upwelling (Right) wind blowing to the south, Transport towards the coast will cause coastal downwelling

SSH Response

Sea surface height anomaly can indicate Ekman layer divergence or convergence and is used to identify warm-core (positive SSHA) and cold-core eddies (negative SSHA). Studies have indicated that the passage of typhoons lead to a decrease in sea surface temperature due to formation of cold-core eddies in the Northwest Atlantic (Son et al, 2007; Babin et al, 2004; Shay et al, 2000; Hu and Muller-Karger, 2007), the Indian Ocean (Rao et al, 2006; Maneesha et al, 2011; Wang and Zhao, 2010); the Western North Pacific Region (Shang et al, 2008; Pan and San, 2013; Siswanto et al, 2008; Chen et al, 2012; and Lee and Park, 2011). Other post-storm effects include elevated values in Chl-a (Shiah, 2000; Vinayachandran and Matthew, 2003; Babin et al, 2004; Son et al, 2007; Shang et al, 2008; Hanshaw et al, 2008; Wang and Zhao, 2010; Yang et al, 2010; Chiang et al, 2011; Hung and Gong, 2011;Lee and Park, 2011; Chen et al, 2012; Zhao et al, 2013), primary production (Lin et al, 2003; Rao et al, 2006;

Siswanto, 2008) and nutrients (Fogel et al, 1999; Shiah, 2000; Son et al, 2007;Chen et al, 2009; Hung and Gong, 2011; Lee and Park, 2011) as an effect of local upwelling, entrainment or non-local advection. Changes in phytoplankton assemblages have been observed in several studies (Chang et al, 1996; Li et al, 2009; Chen et al, 2009). Figure 9 shows a schematic describing the link between plankton production and fishery productivity (Rao et al, 2006; Maneesha et al, 2011; Hung and Gong 2011).

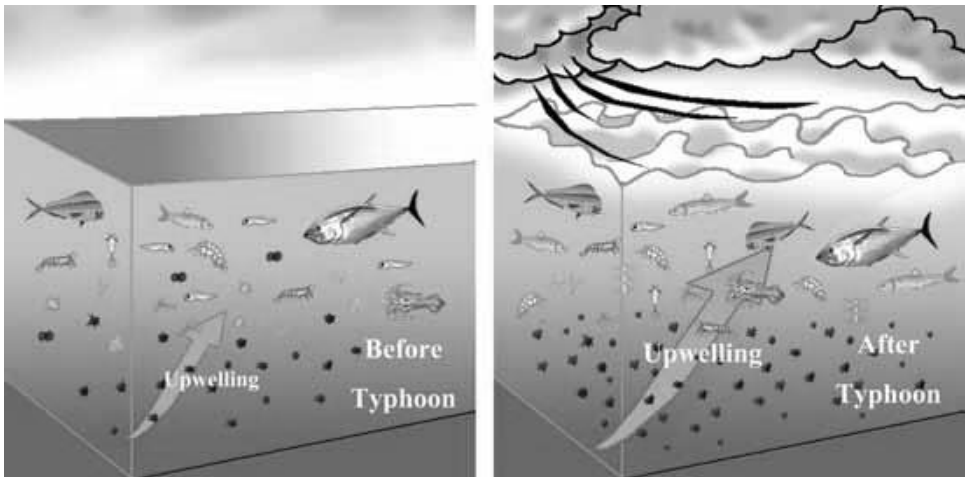

Figure 9. Biological responses (a) before and (b) after passage of Tropical Cyclones (Hung and Gong, 2011)

SST Response

The passage of tropical cyclones is associated with cooling events at the sea surface (Wada and Chan, 2008). Studies of individual TC's in the Western North Pacific (WNP) showed significant differences in maximum SST change and recovery time between the South China Sea (West Philippine Sea) and the Philippine Sea Basin (Chen et al, 2012; Yang et al, 2012). Factors such as TC's strength based on wind speed (intensity), translation speed or the speed of transit, and background climatological thermal structure are major factors affecting SST Response.

*(*Equation 2*)* $\Delta SST = Mixing + Heat\ Fluxes + Advection;$

SST Response due to passage of TC can be attributed to several physical processes such as mixing, input of heat fluxes and the role of advection ((*(*Equation 2). Shay (2009) quantified this parameters based on its contribution where around 60-85% can be attributed to mixing, 5-15% to heat fluxes and 5-15% on the role of advection. Furthermore, numerical experiments conducted by Vincent et al (2012) quantified the contribution of these major

parameters based on wind potential intensity (tropical cyclone strength) and its distance from the eye of the typhoon. Results showed that vertical mixing plays an important role in the cooling process at the center of the eye of the typhoon especially for strong TC while heat fluxes play a major role for weak TC and farther distance from the eye of the TC.

An analysis of SST response due to tropical cyclones based on temperature time series conducted in all major ocean basins made of (a) maximum change in temperature (ΔT_{max}) or the local minimum (Hart et al, 2007; Dare and McBride, 2010) and (b) recovery time in days which includes full recovery and *e*-folding period (Dare and McBride, 2010). These two parameters characterize the ocean's response to TCs (shown in Figure 10). Full recovery is defined as the time it takes to recover to climatological temperature from induced ΔT_{max}. The e-folding period is the time it takes to recover to ΔT_{max}/Actual temp ~= 2.718 since recovery assumes a logarithmic function.

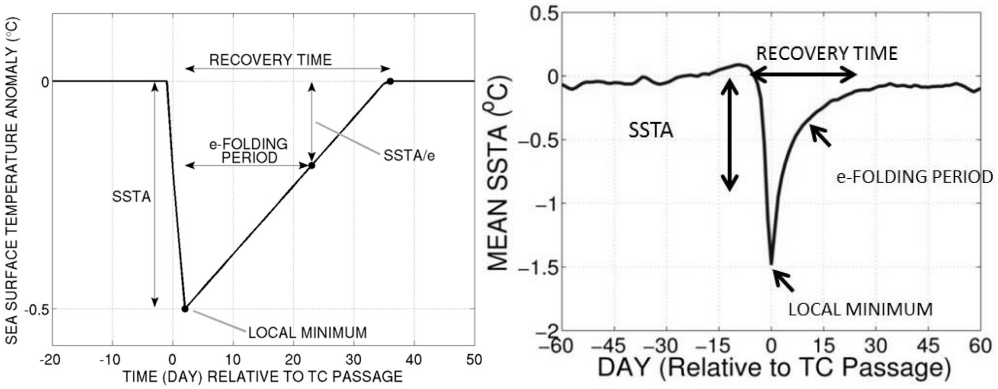

Figure 10. Schematic of the time series of SSTA in terms of full recovery time, and e-folding period as a response to TC passage adapted from Dare and McBride, 2011 (right) and actual data (left)

Other factors include parameters such as precipitation where around 10% of the heat loss from the ocean was attributed to the passage of Tropical Cyclones (Jacob and Koblinsky, 2007). Surface cooling can cause a reduction of air-sea flux and in turn reduction of peak winds (D'Asaro et al, 2007). Recovery is attributed to available heat flux and longer recovery is associated with amount of cloud cover which can hinder SST warming (Price et al, 2008).

Upper Structure in Relation to the passage of Typhoons

Oceanic subsurface parameters can be based on salinity and/or temperature. Upper ocean structure based on temperature includes parameters such as Mixed Layer Depth (MLD), Mixed Layer Temperature (MLT), depth of the 26°C isotherm (D26), upper ocean

heat content (UOHC) based on Tropical Cyclone Heat Potential (TCHP) derived as the depth-integrated temperature up to D26, and the depth averaged temperature up to 100m (T100). Barrier layers, associated with salinity stratification, have been both linked to typhoon intensification and induced cooling.

The thermal-structure are associated with surface parameters such as SST and SSH/SSHA. Positive features (SSHA>6 cm) are associated with deep mixed layer while negative features (SSHA<-6) are associated with shallow mixed layer (Figure 11a). TCHP is linearly correlated with T100 at high THCP (Vissa et al, 2008; Price et al, 2008). The introduction of T100 as a parameter reduces the damping effect of cool SST upon the passage of typhoon and making it a useful parameter to study thermal responses due to typhoons.

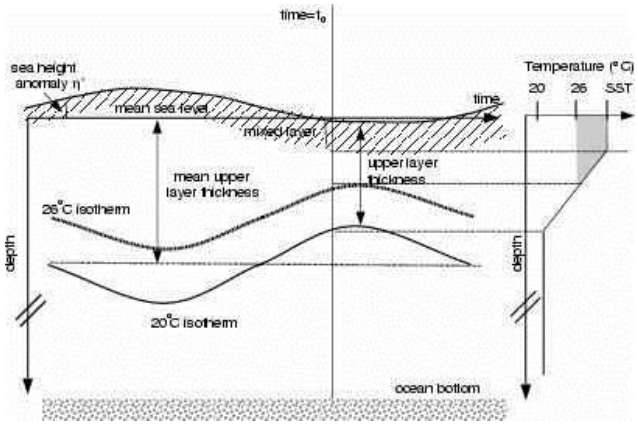

Figure 11. (a) Relationship of the Upper thermal structure associated with Sea surface height anomaly (SSHA) including the Mixed Layer Thickness and the Depth of 26°C and 20°C isotherm (D26 and D20, respectively) (http://www.aoml.noaa.gov/phod/cyclone/data/method.html)

SST cooling is expected to be more intense if the mixed layer is shallow and thermal stratification is strong (Chiang et al, 2011; Vincent et al, 2012). MLT and SST changes are dependent on initial MLD, which varies in latitude (Park et al, 2005; Zheng et al, 2008), and mesoscale oceanic features (Nam et al, 2012). Figure 12 shows a schematic of magnitude of sea surface cooling and typhoon intensification depending on background thermal layer where a thin oceanic mixed layer favors weakening of the hurricane while a deeper mixed layer favors hurricane intensification.

Figure 12. The three-dimensional schematic of the temperature distribution in the upper ocean shown above illustrates the impact of a hurricane passing over the ocean when the oceanic mixed layer is thin (left) and thick (right). In both cases, the hurricane propagates down and left over the warm sea surface (red), creating a cold wake behind the storm as colder water (blue) is brought towards the sea surface by the hurricane's wind stress. The thin oceanic mixed layer (left) favors formation of the cold wake making the hurricane weaker than a thick oceanic mixed layer (right). (Scrowcroft et al, 2011)

Mignot et al (2009) define barrier layers as the layer between the pycnocline and the thermocline associated with the MLD when the latter are different as a result of salinity stratification (Figure 13). Deepening of the mixed layer and the decay of barrier layer thickness, associated with deeper D26 was observed as results of the passage of a TC (Vissa et al, 2012). Conditions under barrier layer has an associated effect by reducing storm vertical mixing and SST cooling by 0.4 to 0.8 less compared to conditions with no barrier-layer (Wang et al, 2011).

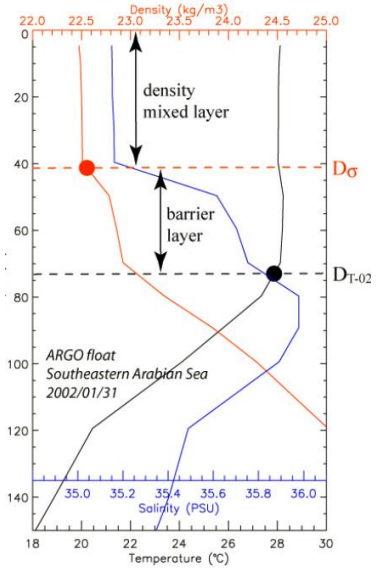

Figure 13. Structure of the barrier layer in association with the mixed layer depth (Mignot et al, 2009)

Tropical cyclone intensity driven by large-scale oceanic conditions displays the control of the oceanic sensitivity to atmospheric forcing (Lloyd and Vecchi, 2011). Intensification occurs when ocean stratification is weak and SST cooling is expected to be small while intensification is suppressed in regions where there is strong ocean stratification and SST cooling is higher. Intensification is related to regions with barrier-layer (Balagaru, 2012) and higher values of TCHP contained in mesoscale features particularly warm eddies (Goni et al, 2009). Intensification of tropical cyclones to category 5 occurs when the climatological warm layer is deep (D26 ~ 100-120 m) and upper-ocean heat content (UOHC) is 80–120 kJ cm^2 which restrains surface cooling (Lin et al, 2008).

Northwest Pacific Basin

The Northwest Pacific Basin is an entry point and a region for intensification and formation of an average of 27 tropical cyclones per year. Of these, 17 are considered as typhoons and 9 as intense typhoons (speed ≥ 50 m/s or Category 3-5 based on SSHS) (Aguado and Burt, 2010). Climate studies had indicated that El Nino is linked to more intense and longer-lived TCs in the North Western Pacific than La Nina (Camargo and Sobel, 2005). TC activity is enhanced as a result of the increase in mid-level atmospheric moisture during the boreal summer of El Nino (Lyon et al, 2008). The east of the Philippines is part of the gyre central region (10°-21° N, 121°-170°E) where the background climatological condition is suitable for Category 5 intensification (Lin et al, 2008).

TCHP is locally high in the western North Pacific and in turn, an associated increase in TC's activity in the region (Wada and Chan, 2008). The east of the Philippines is also associated with the Main Development Region (MDR) for typhoon formation and intensification. During the peak of the typhoon season (July to October), warming of TCHP and deepening of the D26 is observed from the MDR during peak of typhoon season from 1992 to 2011 (Figure 14) allowing the region more suitable for formation and intensification (Pun et al, 2013). Weakening of the western North Pacific subtropical high and strengthening of the Asian monsoon causes warm SST anomalies over the equatorial western and central Pacific, leading to an increase in number of tropical cyclones affecting the region near Taiwan from 1970 to 2006 (Tu et al, 2009).

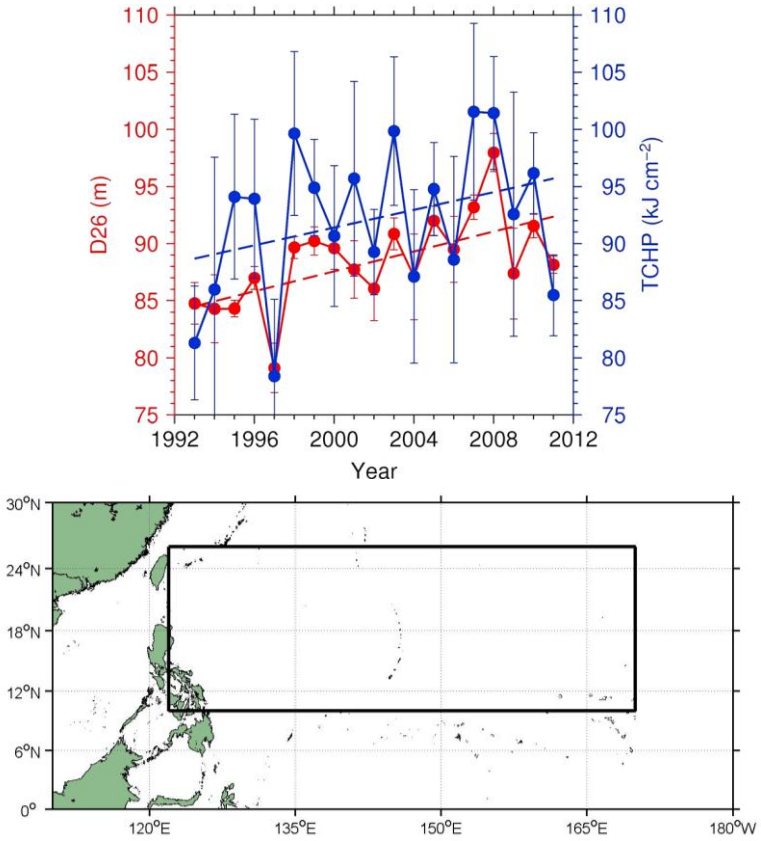

Figure 14. Main Development Region (MDR) for typhoon formation and intensification area average of the depth of 26°C isotherm (D26) and Tropical Cyclone Heat Potential (TCHP) during the peak of typhoon season (July-October) from 1993 to 2011 (left); Region enclosed in red rectangle (right) is the MDR (122°-170°E; 10°-26°N) (Pun et al, 2013).

Furthermore, the East of the Philippines is oceanographically a very dynamic region. Here the NEC bifurcates into the Kuroshio Current to the North and Mindanao Current to the South (Figure 15). Local monsoon winds also play an important mechanism governing seasonal variation (Yaremchuk and Qu, 2004; Chen and Wu, 2011; Jensen, 2011; Rudnick et al, 2011) and interannual variations of NEC (Qiu and Chen, 2010). The NEC bifurcation latitude varies seasonally from 14.8°N in July and 17.2°N in December based on historical temperature and salinity data (Qu and Lukas, 2003), and interannually with ENSO; with a northerly bifurcation latitude during EL Nino Events and southerly bifurcation latitude during La Nina events (Qiu and Chen, 2010; Qiu and Chen, 2012; Zhao et al, 2012). Variation of the NEC is related to the strength of the equatorial trade winds.

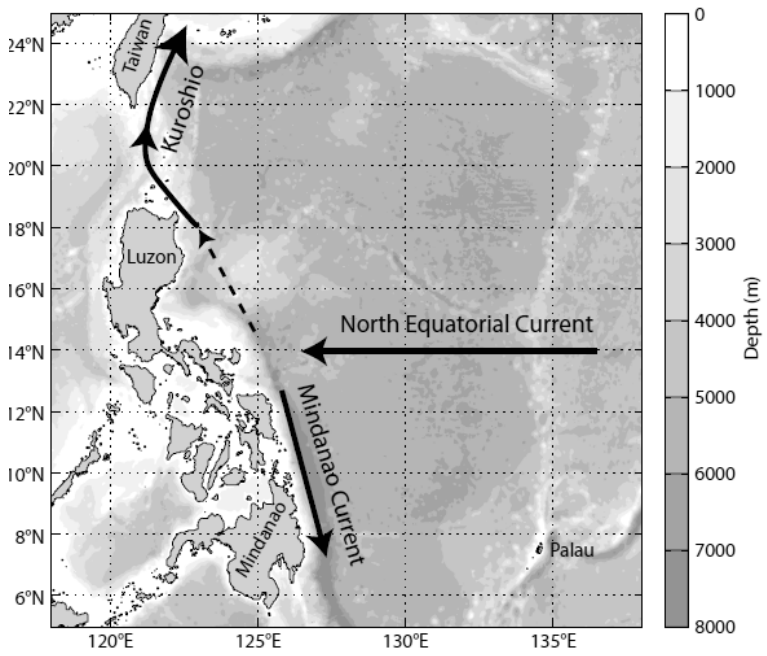

Figure 15. General Diagram illustrating bifurcation of the NEC into the Kuroshio Current to the North and Mindanao Current to the South (Rudnick et al, 2011)

Studying the climatological sea surface and upper ocean thermal structure will provide insights on the immediate response of tropical storms along the east of the Philippines. The variability of the NEC bifurcation latitude may alter the source waters of the Kuroshio and modify the sea surface temperature and structure field that can in turn alter the strength of the typhoons and upper ocean response.

Objectives of the Study

The primary objective of this study is to determine upper ocean response to tropical cyclones off Eastern Philippines. The specific objectives are

1. To determine the role of the background climatological condition on SST response associated with the passage of tropical cyclones.
2. To determine the role of migration of the NEC bifurcation latitude on SST response associated with tropical cyclones.

Datasets

The Tropical Cyclone best track data from 2003 to 2012 was downloaded from the Joint Typhoon Warning Center (JTWC) website (http://www.usno.navy.mil/NOOC/nmfc-ph/RSS/jtwc/best_tracks/). This record includes 6 hourly position (longitude and latitude), maximum wind and intensity in the Saffir-Simpson Hurricane Scale (SSHS) (Chu et al, 2002). The TCs were individually selected for the region affecting the Philippine Area of Responsibility (PAR) (Figure 16). This includes 167 out of the 265 tropical cyclones affecting the Western North Pacific (WNP) Region. Figure 17 shows the distribution of TCs affecting the WNP (a) and PAR (b). Tropical cyclone translation speed was computed by dividing the distance travelled by a tropical cyclone over a 6-hour period.

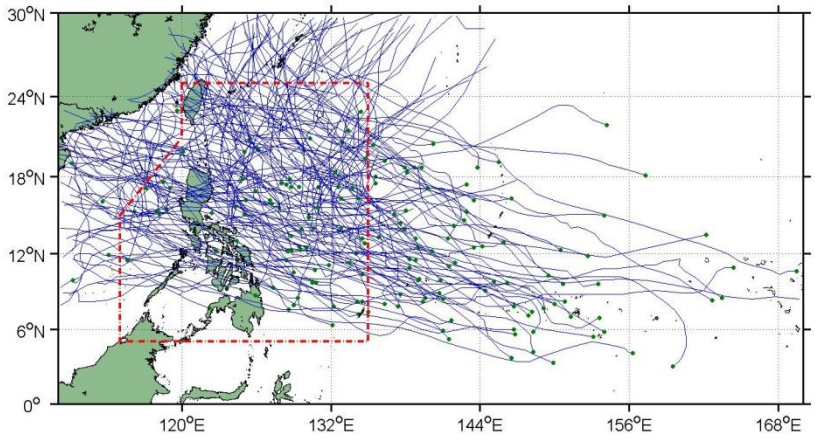

Figure 16. Tropical Cyclone Tracks affecting Philippine Area of Responsibility from 2003 to 2012.

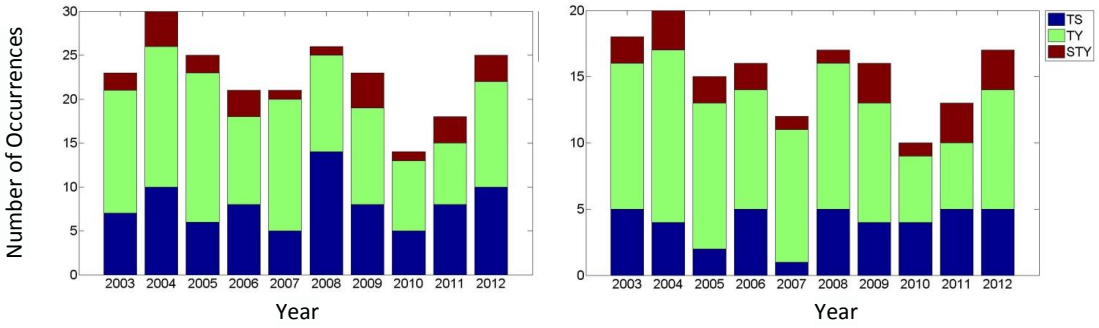

Figure 17. Number of Tropical Cyclone affecting (a) Western North Pacific Region (b) Philippine Area of Responsibility. TS includes Tropical Storm and Tropical Depression, TY includes typhoons from Cat 1-3 while STY includes typhoons from Cat 4-5 based on the Saffir-Simpson Hurricane Scale

Satellite-derived Sea Surface Temperature (SST), Sea Surface Height (SSH) and SSH Anomaly (SSHA) were extracted between 0-30°N and 110-170°E from 2003 to 2012. Details about these products are discussed below.

SST data used in this study is the merged product of the Tropical Rainfall Measuring Mission (TRMM) Microwave Imager (TMI) and Advanced Microwave Scanning Radiometer - EOS (AMSR-E). Data was downloaded from ftp://ftp.discover-earth.org/sst/daily/tmi_amsre/. TMI and AMSRE are widely used in tropical cyclone studies because of its capability to measure SST behind clouds. Spatial resolution is 0.25° by 0.25°with daily temporal resolution.

SSH and SSHA was downloaded from AVISO (http://ftp.aviso.oceanobs.com/). The altimeter products were produced by Ssalto/*Duacs* and distributed by *Aviso*, with support from *CNES* (http://www.aviso.oceanobs.com/duacs/). It includes data from different satellite missions such as Saral/AltiKa, Cryosat-2, OSTM/Jason-2, Jason-1, Topex/Poseidon, Envisat, GFO, ERS-1&2 and Geosat. Spatial resolution is 0.25° by 0.25° with 7-day temporal resolution.

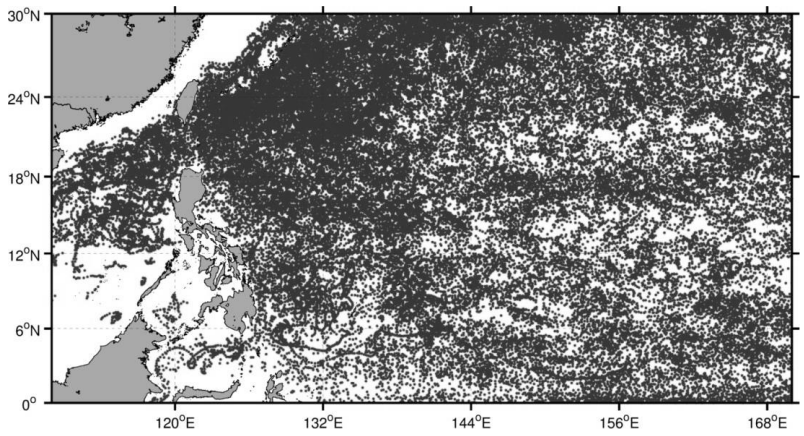

Figure 18. Spatial Distribution of Available ARGO Profiles from 2003 to 2012

Profiles from ARGO (http://www.argo.ucsd.edu/) were used to describe background climatological conditions. Argo Data were collected and made freely available by the International Argo Program and the national programs that contribute to it. (http://www.argo.ucsd.edu, http://argo.jcommops.org). The Argo Program is part of the Global Ocean Observing System. Figure 18 shows spatial distribution of available profiles from 2003 to 2012.

CHAPTER 2. Sea Surface Temperature Response to Tropical Cyclones off Eastern Philippines: Dependence on Background Thermal Structure

Introduction

The east of the Philippines belongs to the Western North Pacific (WNP) region of tropical cyclones (TC) and it serves as an entry point to an average of 15 TC per year including several super-typhoons. The main development region (10-26°N, 122-170°E) was identified in the region as very suitable for typhoon formation and intensification (Pun et al, 2013) due to background thermal climatological conditions.

The presence of TC along WNP is associated with cooling of the region (Wada and Chan, 2008) and plays an important role in regional and global climate. Oceanic cooling due to TC can be attributed as an effect of vertical mixing, divergence, air-sea flux exchanges and advection (Vincent et al, 2012). Oceanic cooling also occurs when there is an increase in meridional flux by cooling of warm region and warming of cool regions (Korty et al, 2008). An important parameter based SST response to tropical cyclones such as recovery time and local minima is necessary to understand and estimate the role of these fluxes.

SST response to tropical cyclones was studied by Dare and McBride (2011) and Vincent et al (2012) for all basins affected by tropical cyclones. A general trend associates longer recovery period, resulting from winds induced by tropical cyclones, with maximum cooling. However, SST response of tropical cyclones may vary depending on background climatological conditions including tropical cyclone strength (intensity), translation speed (Zhao et al, 2008) and background upper ocean structure (Chen et al, 2012; Yang et al, 2012).

Background upper ocean structure off the region east of the Philippines was classified into two major regions divided by 15°N latitude, where 15°N is associated with the maximum latitude of the NEC bifurcation window initially defined by Qiu and Chen (2010). These two regions are named the South Region (BS, Latitude <15°N) and North Region (BN, Latitude >15°N). Details about the structure of both regions are discussed in the next section.

Background Climatological Condition

Mean climatological SST (Figure 19, black dotted lines) at 121-170°E, 0-30°N shows maximum SST occurring during the month of June to October and minimum SST during the months of February to March. This semi-annual peak is related to local monsoon periods (Botin et al, 2010). The month of June to October coincides with the Southwest monsoon where a number of typhoons peak at the same period (Williams et al, 1993). A normalized distribution of the passage of tropical cyclones along the Philippine Area of responsibility is shown in Figure 20a. The peak of the typhoon Season is from June to November.

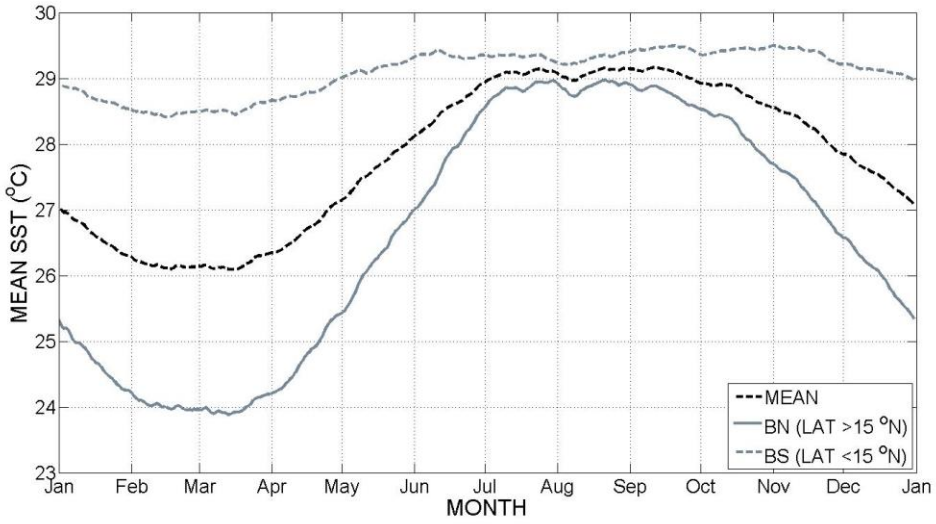

Figure 19. Climatological data based on (a) Sea Surface Temperature (SST) Mean Climatological for the entire region (black solid lines); at BN (LAT > 15°N) (gray broken line line); and at BS (LAT < 15°N) (gray solid line)

Two regions along 120-170°E longitude were defined as BN (15-30°N) and BS (0-15°N) based on background climatological conditions. Both regions show similar seasonal trend (Figure 19) but different seasonal SST ranges (1°C for BS and 5°C for BN). The SST represents the temperature of the top layer linked to the characteristics of the upper thermal structures of the ocean. Figure 20 shows average spatial variation of SST (b) from TMI-AMSRE and, mixed layer depth (MLD) (c) and temperature (MLT) (d) derived from ARGO float data from 2003 to 2012 occurring during the peak of the typhoon season.

Climatological mean of the mixed layer depth (MLD) and temperature (MLT) was derived from the gridded climatological dataset from the World Ocean Atlas 09 and available ARGO float data from 2003 to 2012. MLD is defined as the depth where there is a change of

1.0°C from the surface (Siswanto et al, 2008) while MLT is the depth average temperature from the surface up to the mixed layer depth. However, data from ARGO Profiles are limited in the upper 10 meters and a revised definition of the MLD will be used in this study adapted from the work of de Boyer Montegut et al (2004). Throughout the course of this chapter, MLD and MLD values will be based on the definition used by Wu and Chen (2012) where MLD (Argo) is the depth where the temperature has decreased by 0.2°C from the 10 meter value and MLT (Argo) is calculated by integrating the temperature from 10 meter depth to the base of the Mixed Layer.

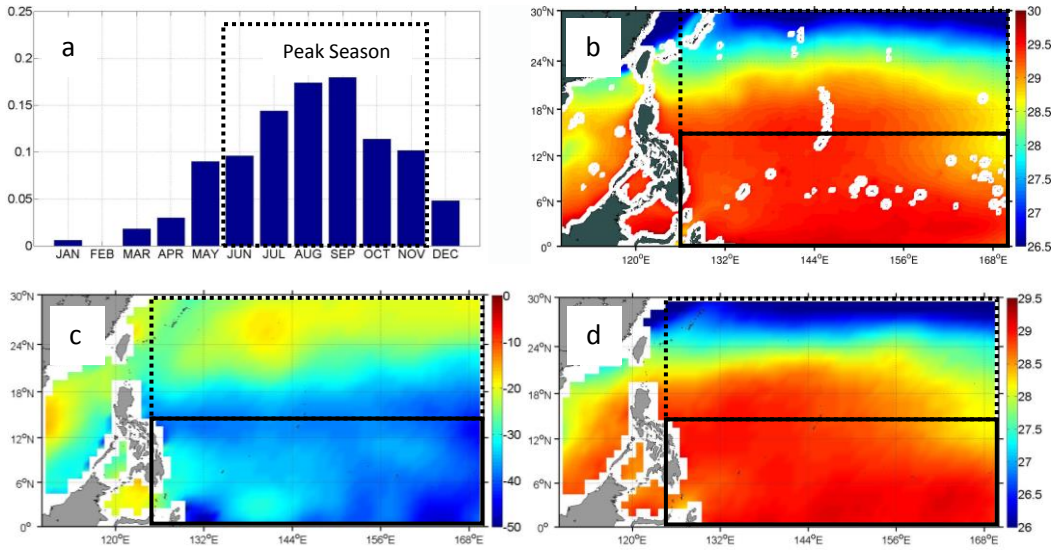

Figure 20. (a) Normalized distribution to the total number of occurrences of Tropical Cyclones affecting the Philippine Area of Responsibility – Typhoon peak season is enclosed in black broken line rectangular box; Climatological (b) Sea Surface Temperature (SST) (c) Mixed Layer Depth (MLD) (d) Mixed Layer Temperature (MLT) averaged during the peak of the typhoon season (June to October)

Table 2. Mean and standard deviation of Upper Ocean Thermal Parameters (T100 in °C, MLT in °C, MLD in meters, and D26 in meters) using annual, typhoon season (June to November) and outside the typhoon season (December to May) along the region bounded by 0-30°N, 120-150°E, and at BN (15-30°N) and BS (0-15°N) based on ARGO float data from 2003-2012.

	ANNUAL				TYPHOON				NON-TYPH			
	T100	MLT	D26	MLD	T100	MLT	D26	MLD	T100	MLT	D26	MLD
ALL	26.0 ±2.8	27.3 ±2.7	-65 ±52	-52 ±30	26.7 ±2.3	28.5 ±1.4	-75 ±44	-44 ±23	25.2 ±3.0	25.9 ±3.0	-55 ±57	-62 ±35
BN	24.8 ±2.6	26.3 ±2.8	-44 ±46	-49 ±32	25.8 ±2.2	28.1 ±1.5	-58 ±40	-37 ±20	23.8 ±2.6	24.5 ±2.7	-29 ±47	-60 ±38
BS	28.4 ±0.9	29.1 ±0.7	108 ±35	-61 ±24	28.6 ±0.7	29.4 ±0.4	-107 ±34	-55 ±19	28.2 ±1.0	28.8 ±0.7	-108 ±37	-67 ±27

The mixed layer thermal structure gives an idea of the stratification. A shallow MLD is associated with weaker stratification link to gentle gradient of the thermocline than with

deeper MLD. During the typhoon season, mean MLD (MLT) is shallower (cooler) in BN than BS (Figure 20;

Table 2). However, outside the typhoon season, MLD is almost the same (>60m) but MLT is cooler at BN (23°C) than at BS (28°C). A general upper thermal structure based on MLD and MLT were described using an associated averaged profile for typhoon and non-typhoon season are shown in Figure 20a for BS and Figure 20b for BN.

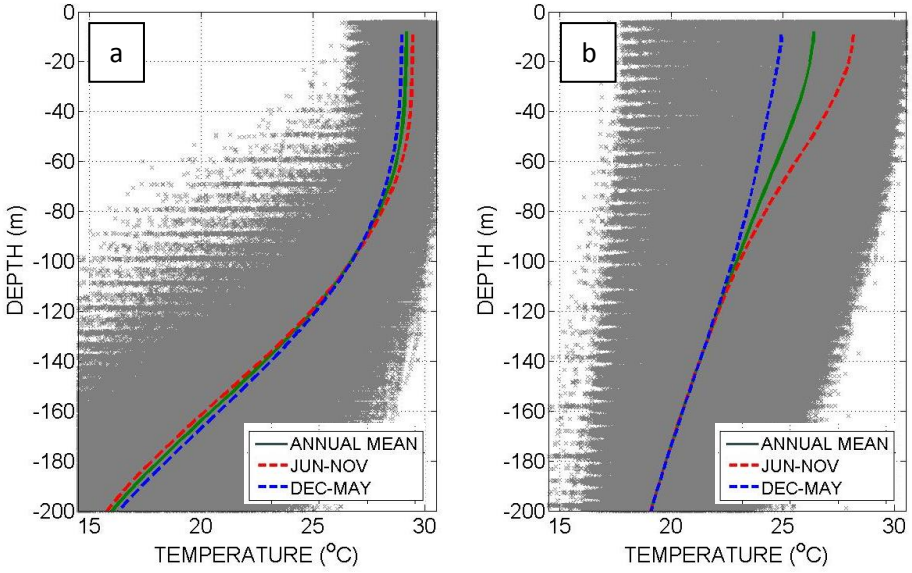

Figure 21. Mean temperature Profile derived from ARGO Float Data from 2003 to 2012 associated with (e) BS Region and (f) BN Region. Identified regions are BN (Latitude > 15°N), enclosed in a black broken line rectangular box and BS (Latitude < 15°N), enclosed in solid black line rectangular box.

A similar trend for the seasonal depth-averaged temperature in the top 100m (T100) and 26°C isotherm depth (D26) was observed from the ARGO float data. Average T100 at BS (BN) was 28.64°C ± 0.71°C (25.79°C ± 2.18°C) during the typhoon season (Table 2). On the other hand, D26 at BS is deeper throughout the year with an average depth of at least 100m. However, D26 is shallower outside the typhoon season at BN where SST is below 26°C and deepest during the typhoon season with an average depth of 58±40 meters. Meridional plots of D26 and T100 from 0-30°N Latitude are shown in Figure 22. Generally, the BS region, D26 is <-100m and T100 between 28-30°C especially at the NEC Bifurcation window (10-15°N) (Qiu and Chen, 2010) except when the Mindanao dome is Active (2003-2005). The NEC displayed a strong advection role in setting up the background climatological upper ocean structure. On the other hand, BN has a shallower D26 and both parameters vary largely seasonally (Table 2).

Since both regions displayed a distinctive characteristic based on thermal structure during the peak of the typhoon season, it is interesting to look on oceanic response of tropical cyclones in both regions. This chapter aims to determine upper ocean SST response to tropical cyclones from 2003 to 2012 off Eastern Philippines and its dependence on background thermal structure.

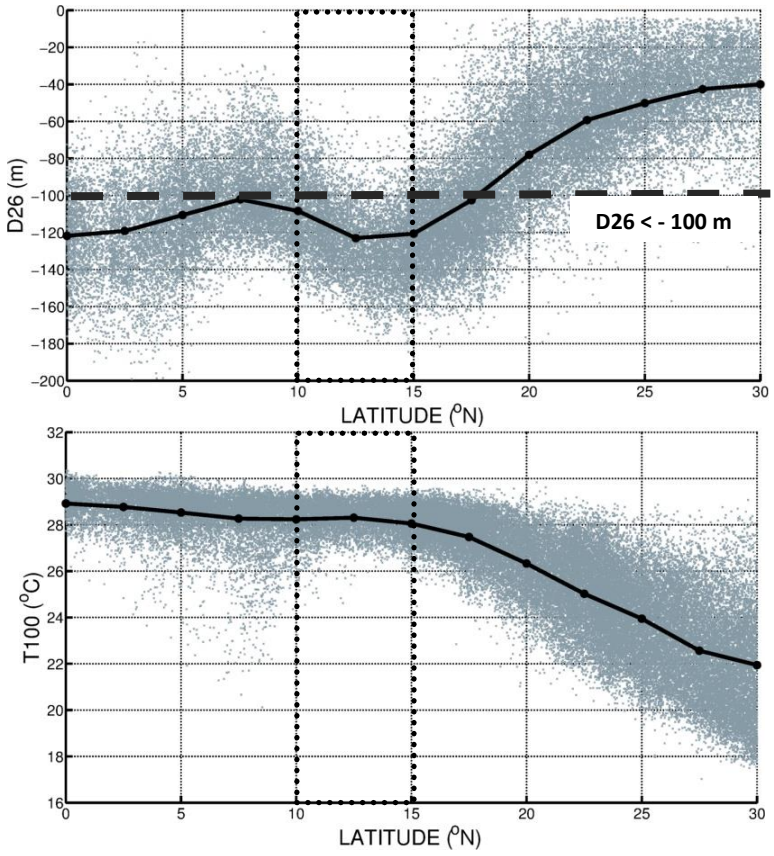

Figure 22. Meridional Plot of (top) Depth of 26°C Isotherm (D26); and (bottom) Depth Averaged Temperature up to 100m (T100) from 0° to 30°N Latitude derived from ARGO Float data. Dotted box is the Bifurcation window, 10-15°N (Qiu and Chen, 2010); dashed line showing boundary below and above -100m D26 isotherm (top)

Methodology

SST Response

Daily sea surface temperature (SST) dataset used in this study is the merged product of Tropical Rainfall Measuring Mission (TRMM) Microwave Imager (TMI) and Advance Microwave Scanning Radiometer – EOS (AMSR-E) from 2003 to 2012 (ftp://ftp.discover-earth.org/sst/daily/tmi_amsre/). Spatial resolution of the data set is 0.25 x 0.25°. The climatological dataset is constructed by averaging daily SST values at each grid point from 2003-2012. SST Anomaly (SSTA) is derived by subtracting daily SST from the climatological SST.

Tropical cyclone (TC) best track data of typhoons affecting the Philippine Area of Responsibility was extracted from the JTWC Western North Pacific basin dataset from 2003-2012. The dataset includes 6- hourly positions of the TC.

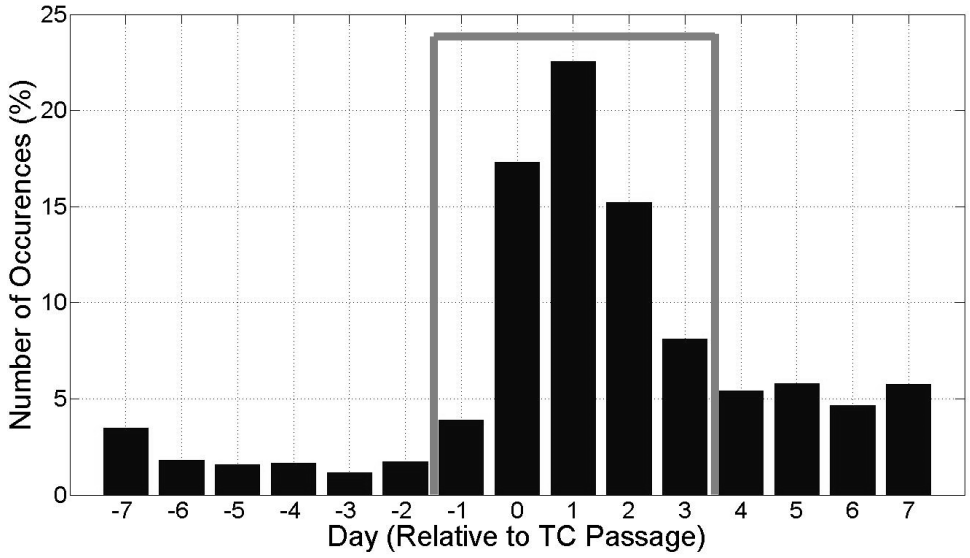

Figure 23. Number of occurrence the day of local SSTA minima relative to TC passage, compiled from 3426 Data Points from TCs affecting the Philippine Area of Responsibility from 2003 to 2012; Highlighted in red box is the events considered in the study

For each TC track point, the SSTA is extracted 60 days before and 60 days after relative to its passage. SSTA minima were then selected within ±7 days from TC passage. Figure 23 shows around 23% of SSTA minima occurring at day 1. Significant occurrence before (after) the passage can be attributed to a TC affecting a wider region, which can inflict significant SSTA change even after it reaches (passes) another TC track point. Only data points having

an immediate response to a TC on the SST from Day -1 to Day 3 was selected (comprises 67% of all data points).

However, since local minima occur at different days relative to TC passage, the SSTA time series was then adjusted by shifting the occurrence of the local minima to occur at day 1. This adjustment was used to set the supposedly local minimum occurring at a common reference day and limits the underestimation of the mean time series affecting the region (Dare and McBride, 2011) and relative recovery period. SST Response affecting eastern region of the Philippines (120°-170°E; 0°-30°N) were considered in this study.

Numerical Modeling

A 1-dimensional mixed layer model using the General Ocean Turbulence Model (GOTM, Umlauf et al. 2005, http://www.gotm.net/) was used to investigate the SST response based on varying storm intensities and forcing duration affecting BN and BS region. GOTM is used for the hydrodynamic and thermodynamic process related to vertical mixing which uses one dimensional version of transport equations of momentum, salt and heat. Transport equation used for the turbulence submodel was adapted from Cheng et al (2002), a second-order turbulence model that is used to simulate planetary boundary layer (PBL).

The model requires temperature profiles as input background condition and momentum flux (wind stress) for surface forcing. A constant mean value of the shortwave radiation affecting the region was also added as input of the model (Q_{sw} =200 $W \cdot m \cdot s^{-2}$) derived from NCEP reanalysis data from 2003 to 2012 during the months of June to November (http://www.esrl.noaa.gov/psd/data/gridded/data.ncep.reanalysis.surfaceflux.html). Initial mean profiles from June to November (Figure 21a,b) for both BN and BS regions were used as background temperature profiles while a constant momentum flux associated with the wind was computed using (Equation 1.

Wind stress representing different tropical cyclone intensity was considered and their equivalent wind speeds representing different TC Strength are shown in Table 3. Drag coefficient used in the simulation was adapted from laboratory experiments conducted by Takagaki et al (2012) using the universal relationship between energy and significant frequency of wind waves normalized by the roughness length. Simulation using constant wind

stress was conducted using an incremental time step of 1 minute and outputs every 1 hour for the duration of 12 hours.

Table 3. Input Momentum Flux or Wind Stress (τ_{wind}) representing different TC scales based on the Saffir-Simpson Hurricane Scale (SSHS)

SSHS Scale	U (ms^{-1})	U_{sample} (ms^{-1})	ρ_{air} (kgm^{-3})	C_D (Takagaki et al, 2012)	τ_{wind} (Nm^{-2})
TD	0-17	12.0	1.22	0.00170	0.3
TS	18-32	26.0	1.22	0.00220	1.8
C1	33-42	37.8	1.22	0.00255	4.4
C2	43-49	46.1	1.22	0.00255	6.6
C3	50-58	54.1	1.22	0.00255	9.1
C4	58-70	64.2	1.22	0.00255	12.8
C5	> 70	75.2	1.22	0.00255	17.6

Duration of wind forcing is a representation of the TC translation speed where lower (higher) magnitude is associated with longer (shorter) duration of wind forcing. The relationship of the translation speed over the TC's radius of maximum winds was derived based on the assumption that the TC affects the same area over the TC's span and the duration of its movement (Translation speed). Representation of different translation speed into equivalent wind forcing duration is shown in Figure 24. For slow moving typhoons with translation speed of 0 to $4m \cdot s^{-1}$, the duration of wind forcing ranges from 3 to 9 hours, moderate moving (4 to $8m \cdot s^{-1}$) extend the duration from 1 to 6 hours and fast moving (>$8m \cdot s^{-1}$) with less than 3 hours of wind duration. This relationship will be then used in comparing numerical experiments results with observations.

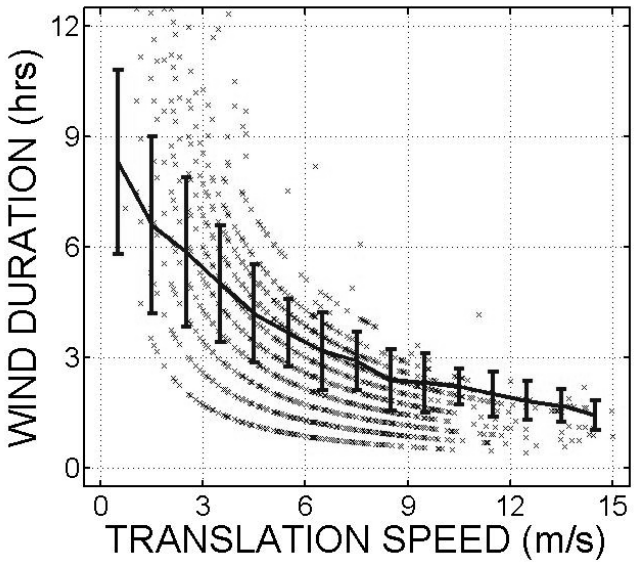

Figure 24. Relationship between Translation speeds versus wind duration derived from TC track data translation speed and radius of maximum wind. Line graph show mean values; Error bar are standard deviations.

Results

SST Response

The mean SSTA minima of -1.22°C due to TC cooling is lower than the mean SSTA minima of -0.49°C derived from a global dataset (Dare and McBride, 2011) (Figure 25a; Table 4) and the adjusted mean SSTA (-1.47°C) at the region is lower than the global mean of -0.91 (Figure 25b; Table 4). Mean local minimum induced by TCs at the east of the Philippines is slightly lower than on the entire WNP region affected by TC affecting PAR and lower than of SCS region (Table 4) The apparent difference in local minima which is below the mean value (based the global dataset, Table 4) can be attributed to the passage of strong and slow-moving tropical cyclones affecting the Western North Pacific region and background thermal structure of the ocean. General implications will be discussed in the next sections of this chapter.

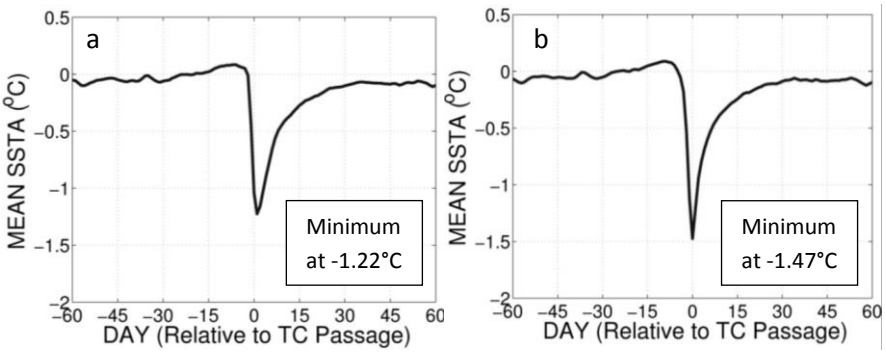

Figure 25. Mean SSTA Time Series for dataset with local minima occurring from Day -1 to Day 3 using (b) actual time series (c) adjusted local minima of the time series to Day 1.

Table 4. Mean Local Minima (°C) induced by Tropical Cyclones

	Raw	Adjusted
Global Dataset (Dare and McBride, 2011)	-0.49	-0.91
Global Dataset (Area-averaged) (Vincent et al, 2012)	~-1.00	-
WNP (Area-Averaged) (Hart et al, 2007)	-0.2 to - 0.5	-
Computed in this work		
WNP Tropical Cyclones affecting PAR	-1.22	-1.47
East of Philippines	-1.18	-1.42
BN (Lat > 15°N)	-1.50	-1.75
BS (Lat < 15°N)	-0.63	-0.84
South China Sea	-1.41	-1.71

Higher change in SST (local minimum SSTA) is associated with longer recovery time (Hart et al, 2007; Dare and McBride, 2011). Relationship of local minimum SSTA versus

recovery time and e-folding period for the dataset affecting East of Philippines shows similar trends to the global dataset (Figure 26) except for the slightly faster recovery time and e-folding period. Since e-folding period tend to be less variable after -2°C local minima (Figure 26d), only full recovery period will be used in the next set of analysis.

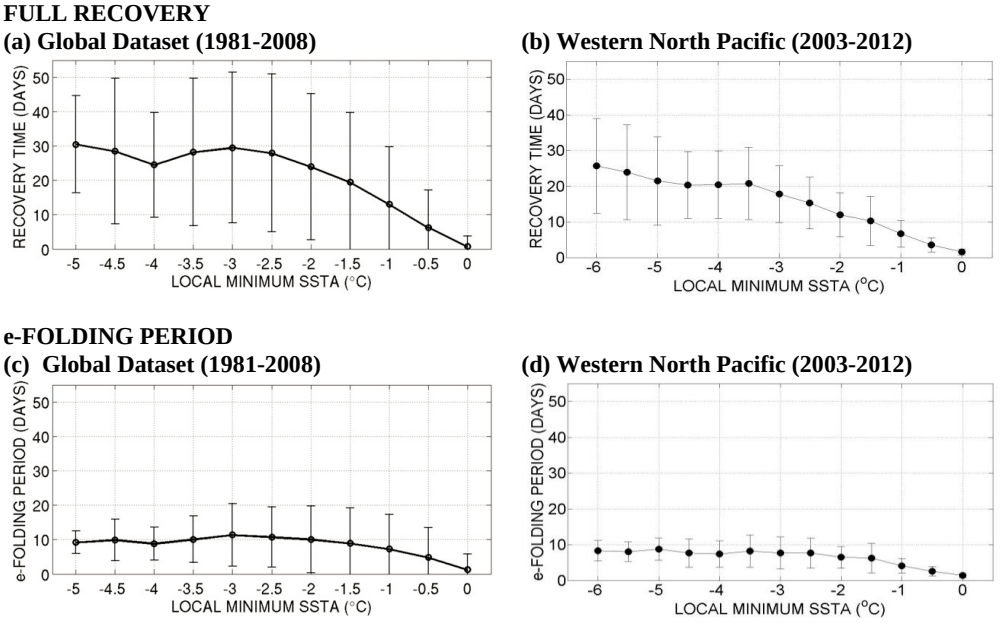

Figure 26. Mean and standard deviation for Local Minimum SSTA versus Recovery Time at 0.5°C increment for (a) Global dataset (Dare and McBride, 2011) (b) East of the Philippines; Mean and standard deviation for Local Minimum versus e-Folding Period at 0.5°C increment for (c) Global Dataset (Dare and McBride, 2011) (d) East of the Philippines.

With respect to TC translation speed, local minimum SSTA is higher and recovery period longer when translation speed is slow (0-5 m/s) and at minimum for fast (>10 m/s) moving TCs (Figure 27). On the other hand, strong tropical cyclones (STYP, C4 and C5) induced maximum local minimum and longer recovery period and minimum for tropical storms and depression (Figure 28).

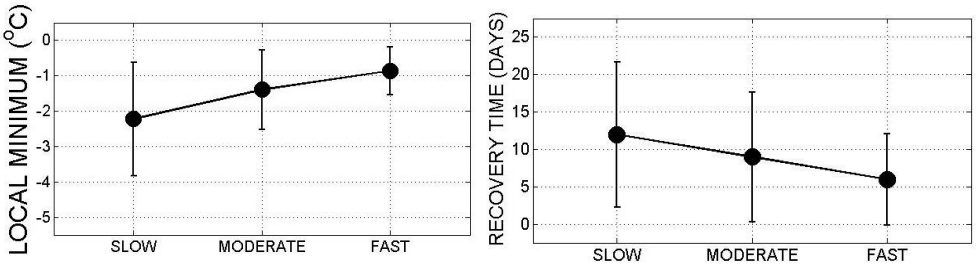

Figure 27.Relationship between varying TC translation speed on local minima SSTA and recovery period. Translation Speed expressed as slow (0-5 ms^{-1}); Moderate (5-10 ms^{-1}) and Fast (>10 ms^{-1}).

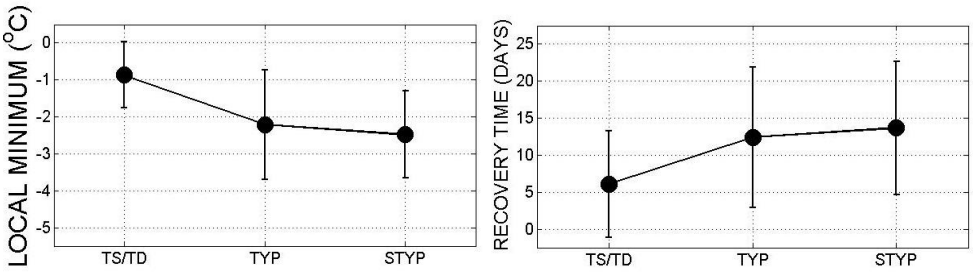

Figure 28. Relationship between varying TC Strength on local minima SSTA and recovery period. TC Strength labeled as TS/TD for tropical storms and depression; TYP for Cat 1 to 3 and STYP for Cat 4 to 5.

Numerical Experiments

The result of the numerical experiments showed that for both BN and BS, maximum cooling is associated with strongest winds and longest wind duration (Figure 29). Figure 30 (top) shows pre and post storm profiles showing the result of vertical mixing for a given TC strength (category 3). Results on other different TC strength are shown in supplementary figures (BN Region - Figure 56 ; BS Region - Figure 58). Bigger change in SST is obtained for the BN region given that this region has a relatively shallow mixed layer (~37 meters, Table 2) making it easier to change the SST significantly at a shorter period of time even at weaker TC induced winds. On the other hand, the BS region has a relatively deep mixed layer and D26 making it more resistant to changes especially during short wind durations. The difference between SSTA response between BN and BS regions ranges up to 1.5°C (Figure 31). At least 1°C difference between both regions is associated with a stronger TC's (at least Category 4 TC) at faster wind forcing and a longer wind forcing associated with weaker TCs (at most a Category 2 TC).

Parametric changes include deepening of the MLD and D26 alongside with the warming of the upper T100 and cooling of the MLT (Table 5). Temperature response is associated to cooling above and warming below the mixed layer depth (Figure 30, bottom).

Table 5. Pre and post typhoon parameters (T100, MLT, D26 and MLD) for both BN and BS Region.

	T100 (°C)		MLT (°C)		D26 (m)		MLD (m)	
Region	PRE	POST	PRE	POST	PRE	POST	PRE	POST
BN	25.8	26.1 ↑	28.1	27.0 ↓	-58	-68 ↓	-37	-44 ↓
BS	28.6	28.8 ↑	29.4	29.0 ↓	-107	-108 ↓	-55	-64 ↓

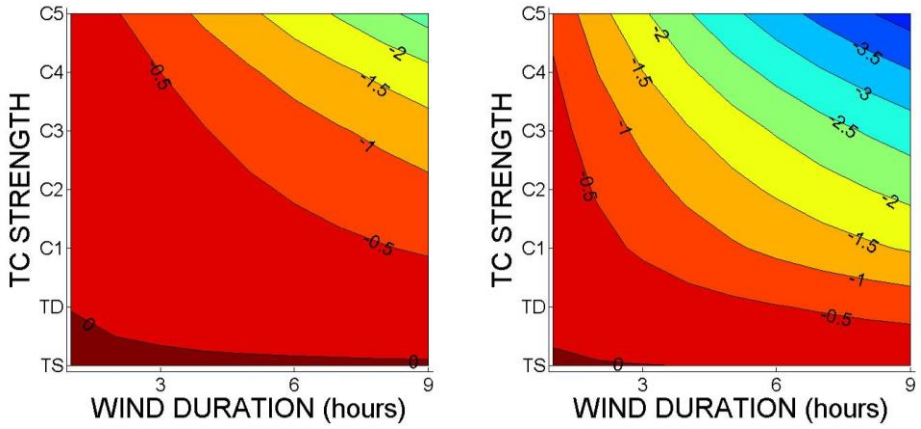

Figure 29. SSTA response (local minimum) derived from numerical experiments by varying TC strength and wind duration forcing time for (left) BN; and (right) BS region.

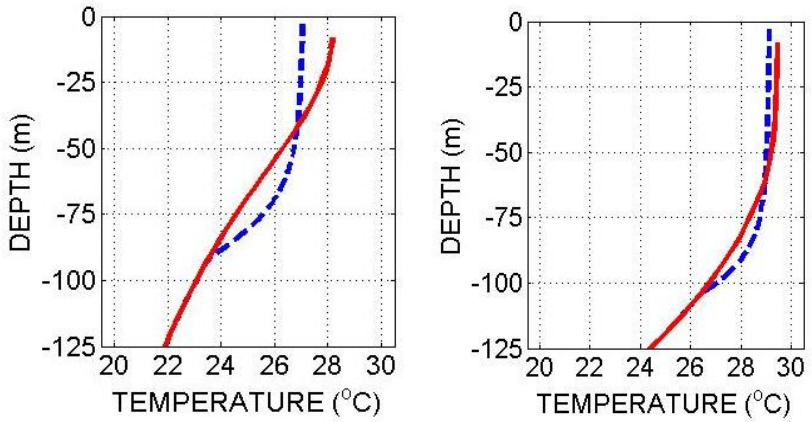

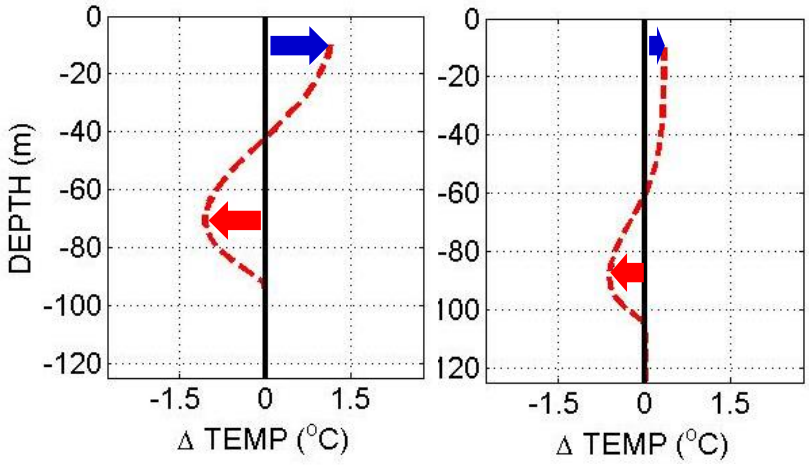

Figure 30. Temperature profile during a pre- and post-TC condition (top) and temperature profile changes (bottom) of a simulated Category 3 typhoon after 3 hours of wind forcing at (left) BN; and (right) BS region.

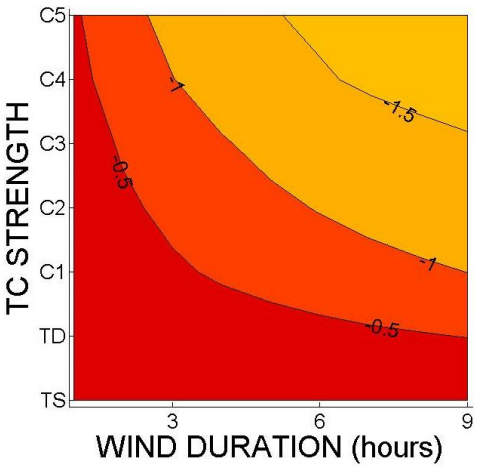

Figure 31. Difference on SST Response on BS region subtracted from the SST response on the BN region derived from numerical experiments

The results of the model showed how the local minima changes with variable wind speeds and wind durations associated with general background thermal structure of BN and BS. In the next section local minima and recovery response based on actual data are compared between the two regions.

SST Response in the BN and BS Region

Scatter plot of the SSTA Response based on local minimum and recovery period are shown in Figure 32, integrating factors such as TC Strength and translation speed. Both regions shows maximum SST changes and longer recovery period during strong TC Strength and slow translation speed. Maximum mean SSTA change is upto 2°C for BS while BN region 3°C. Minimum SSTA changes and shorter recovery period occurs with fast moving TC

and weaker TC strength. Minimum mean SSTA changes is recorded to be at 0.5°C for BS while for BN region, 1°C.

Mean SST response and standard deviation (errorbars) for induced local minimum and associated recovery period in both regions are shown in Figure 33. Recovery is faster in BS (where local minimum SSTA is lower) compared to BN. These differences are also well observed at different translation speed classes. These results are consistent with numerical modelling results where slow translation speed is related to longer duration of wind forcing affecting a higher change in local minimum SSTA as well as with TC Strength (Figure 60, Supplementary Figures).

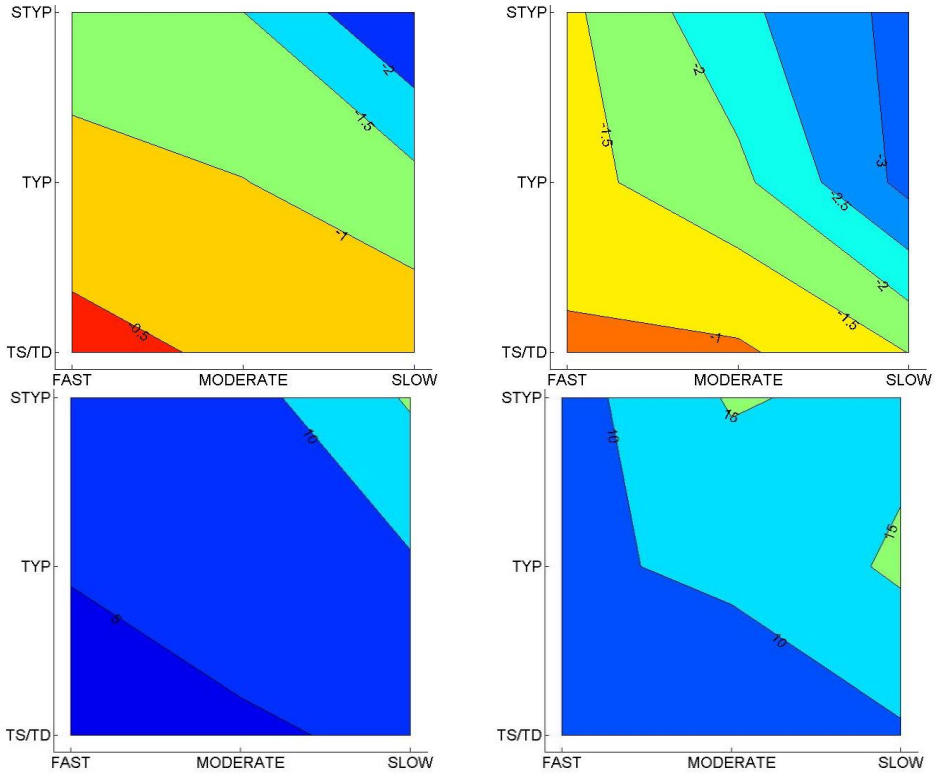

Figure 32. SSTA response (local minimum) (top) and Recovery Period (bottom) from observations at varying translation speed and TC strength for BS (left) and BN (right) region. Translation Speed are considered slow for 0-4 ms^{-1}; Moderate for 4-8 ms^{-1} and Fast for >8 ms^{-1}; TC Strength is TS/TD for Tropical Storms and Depression, TYP for CAT 1 to 3 and STYP for CAT 4 to 5

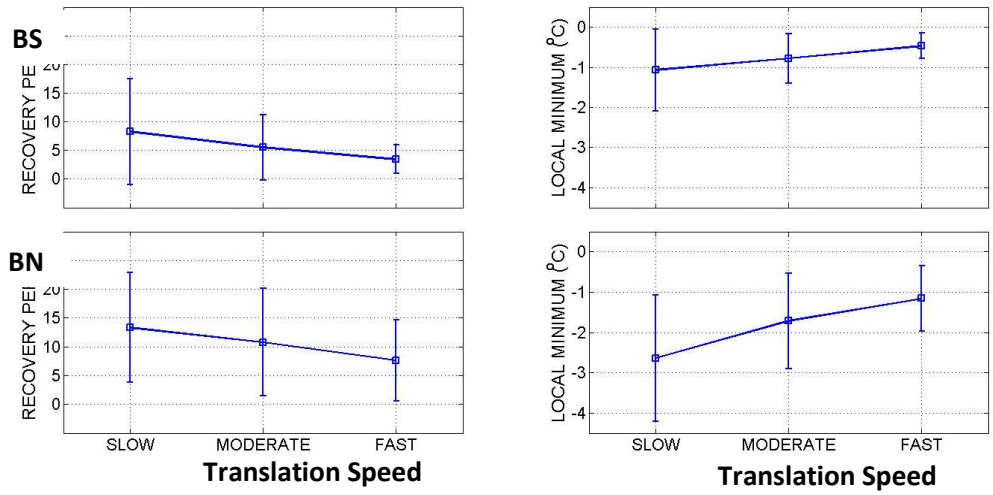

Figure 33. Relationship between translation speed on local minima and recovery period for BS (top) and BN (bottom) region. Translation Speed are considered slow for 0-4 ms^{-1}; Moderate for 4-8 ms^{-1} and Fast for >8 ms^{-1}

Cases of TC events are higher in the BN region than in the BS region (Figure 34). This is consistent with Pun et al. (2012) where they considered the region as the Main Development Region (MDR, 10-26°N, 122-170°E) for TC formation and intensification. Even though MDR overlaps with both BN and BS region, results show a lot of occurrences of typhoons (Cat 1 to 5) in the BN region (Figure 34a,c) favoring more intensification to occur than on the BS region (Figure 34c,d) which favors formation since TS and TD are the early stages of TC. In terms of translation speed classes, both regions shows similar trend on percentage occurrences (Figure 34d).

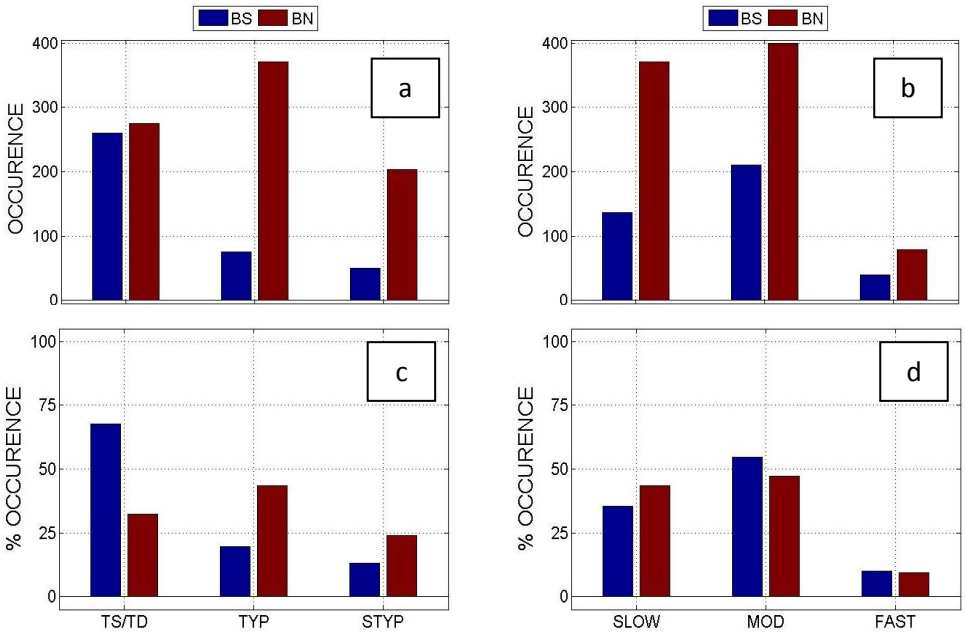

Figure 34. Actual number of occurrence of events (a, b) and percentage occurrence (c, d) based on TC strength (a, c) and based on translation speed (b, d) in both BS (blue) and BS (red) region.

In terms of the percentage occurrences, around 57% incurred an SSTA of less than 1°C in the BS region, majority of which are induced by tropical storms, depressions and fast moving TC (Figure 35, top) in contrast to the BN region where only 25% of occurrences have SSTA of < 1°C (Figure 35, bottom). On the other hand, around 70% of fast recovery period (<5 days) are attributed to cases in the BS compared to 29% in the BN Region (Figure 36).

Generally, BN is associated with a shallow MLD and greater variability in SST and MLT while BS is associated with a deep MLD and nearly uniform SST and MLT. Since tropical cyclone winds affect the upper layer of the ocean up to the Ekman depth, the BN layer is more susceptible to extreme changes as an immediate response to the passage of tropical cyclones as shown by more cases of SSTA > 1°C and longer recovery period (>5 days).

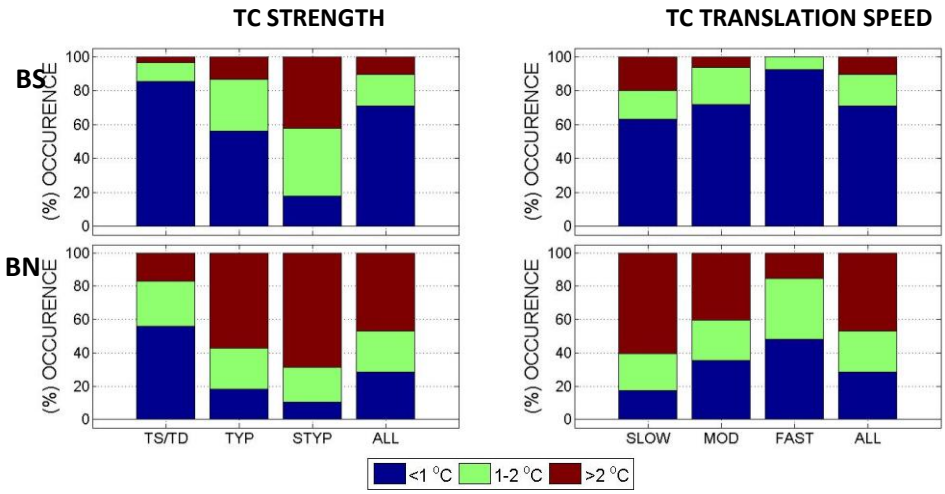

Figure 35. Number of Occurrence for local minimum SSTA classes with respect to TC Strength (Left) and translation Speed (Right) for regions, BS (Top) and BN (Bottom); Strength is TS/TD for Tropical Storms and Depression, TYP for CAT 1 to 3 and STYP for CAT 4 to 5; Translation Speed is SLOW for 0-5 m/s, MOD for 5-10 m/s and FAST for > 15 m/s.

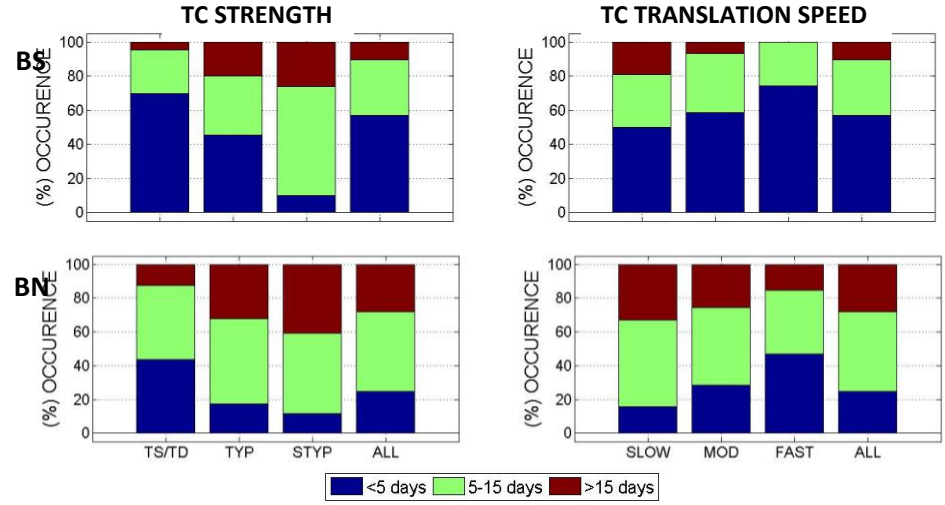

Figure 36. Number of Occurrence for recovery period classes with respect to TC Strength (Left) and translation Speed (Right) for regions, BS (Top) and BN (Bottom); Strength is TS/TD for Tropical Storms and Depression, TYP for CAT 1 to 3 and STYP for CAT 4 to 5; Translation Speed is SLOW for 0-5 m/s, MOD for 5-10 m/s and FAST for > 15 m/s.

Discussion

Increased cooling and longer recovery times are associated with decreased translation speed and increased typhoon intensity (Price et al, 1981; Lin et al, 2009; Dare and McBride, 2011) and background thermal structure (Scrowcroft et al, 2011).

Maximum SST cooling has been reported to be dependent on the TC strength (Morey et al, 2006; Korty et al, 2008). Slow moving typhoons are major contributors to induced maximum cooling of up to 10°C (Zhao et al, 2008; Siswanto et al, 2008) although affecting a smaller region. On the other hand, small changes in SSTA are related to fast TC translation speed (Yang et al, 2010). Cases of maximum cooling with fast translation are related to the tropical cyclone's intensity or wind speed (Babin et al, 2004; Zhao et al, 2008). The size of the typhoon also serves as major contributor, affecting a wider area. Both TC translation speed and strength are consistent with the results of the numerical experiments and actual SST response.

Numerical experiments results showed at 3 hours wind duration, a maximum change of SSTA is expected to be at 0.5°C at all TC Strength at BS while at BN, at least 0.5°C is expected even at C1 TC strength. Larger SST response experienced in the BN region is related to shallow MLD and strong thermal gradient (Prasad and Hogan, 2007) in turn inducing maximum cooling as an effect of shoaling of the mixed layer (Bond et al, 2011). Cooling due to shallow MLD has been reported in several TC events (Park et al, 2005) and individual events (Morey et al, 2006; Chen et al, 2012). Moreover, Lin et al (2008) added that in regions with a shallow mixed layer (BN), more cases were reported to have maximum cooling >1°C even at fast translations speed and low TC strength than on regions (BS) with a deep MLD and D26 where SST cooling is restrained.

Table 6. Comparison of Maximum SSTA changes based on Numerical Experiments and Observation Data in degree Celsius for Both BN and BS region

Translation Speed (ms^{-1})		**Numerical experiments (°C)**		**Observation Data (°C)**			
Class	**Range**	**BS**	**BN**	**BS**		**BN**	
Slow	3 to 9	-2.5	-3.5	-2.58	±0.97	-3.17	±1.10
Moderate	1 to 6	-1.5	-2.5	-1.46	±0.80	-2.38	±1.12
Fast	< 3	-0.5	-1.5	N/A[+]	N/A[+]	-1.39	±0.50
[+] SSTA cooling induced no difference for fast moving typhoons at the BS region							

Table 6 shows the comparison of the induced maximum SSTA (local minima) changes on both BS and BN region conducted in numerical experiments and the observed data. Results show a similar trend based on maximum value conducted in numerical experiments and the mean value derived from observed data for both BN and BS region. However, no SSTA cooling changes were observed in the BS region for fast moving TCs even if there were several occurrences in the region. This shows that heat fluxes, aside from deep mixed layer, may play a possible role in cooling process. Vincent et al (2012) reported that around 50% of the cooling can be attributed to heat fluxes for weaker TC's and possible for fast moving TC's. Although the numerical experiments conducted only include the influence of heat fluxes and wind-induced vertical mixing, the results show a good correspondence on actual observed data. Shay (2009) reported that around 60-85% of the cooling process can be attributed to vertical mixing while heat fluxes contribute around 5-15%. Moreover, numerical experiment conducted by Vincent et al (2012) shows vertical mixing accounts for around 30% of the cooling for weaker TCs while 80% for stronger TCs. This shows that physical processes such as Ekman divergence/convergence and advection plays a minor role in the cooling process thus one-dimensional model can be a useful tool in estimating SSTA response.

Standard deviation can be attributed to initial background climatological condition used in numerical experiments where both regions where generalized into major regions where in reality, temperature profiles are varied based on different background oceanic features. This variation will be discussed in Chapter 3.

SST response with latitude shows the general trend based on the extension and differences encompassing both BN and BS regions. Mean SSTA changes and recovery appears to be increasing from 5° to 22.5°N Latitude and decreasing after 22.5°N Latitude (Figure 37). The increasing trend can be attributed to inertial motion influences with respect to latitude given the same MLD where inertial motions due to TC wind plays a greater contribution to the mixing process with increasing latitude. On the other hand, there is no occurrence between 0° and 5° due to the fact that TC does not form on this region because of zero to low Coriolis force. On the other hand, the increasing trend can be attributed to the shallow mixed layer and colder upper ocean temperature (T100 and MLT) making it more vulnerable to induced extreme temperature changes (Figure 38) while minimum SSTA changes below 15°N are associated with regions with deeper D26 (>100m) that can restrain sea surface cooling (Lin et al, 2008). The decreasing trend after 22.5°N can be attributed to colder upper ocean background temperature. The region from 10°-15° N Latitude shows a

deeper D26 associated with the NEC bifurcation window and is associated with a minimal SST change and fast recovery period.

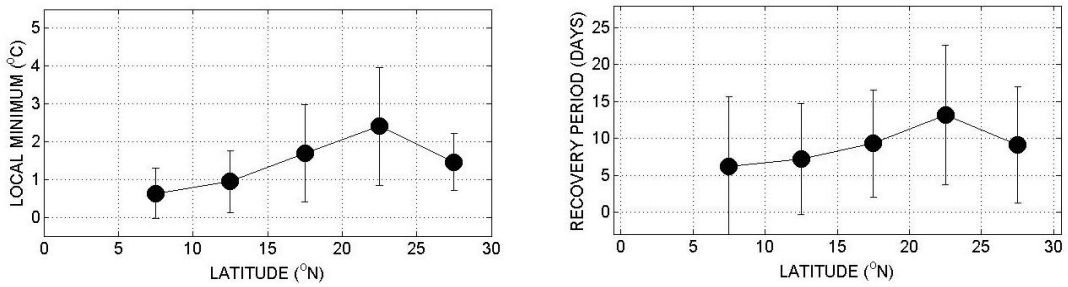

Figure 37. Meridional variation of Local Minimum (°C) (left) and Recovery Period (days) (right) at an increments of 0° from 0 to 30°N at 5° increment. Error bars are standard deviation.

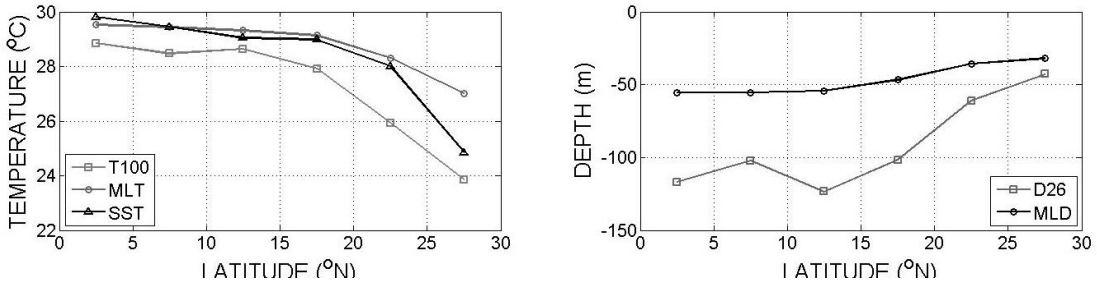

Figure 38. Meridional Climatological Background Conditions from 2003 to 2012 during the peak of the Typhoon Season (June to November) based on Temperature (T100, MLT and SST) (left) and Depth (D26 and MLD) (right) at an increments of 5° from 0 to 30°N.

Variation of SSTA response (local minimum) can be observed seasonally by looking on the mean monthly response as shown on Figure 39. Intense cooling and varied response was observed at the BN region compared to the BS region. Although varied response on the BN region can be associated to the background conditions even during the peak of the typhoon season (June to November), maximum SSTA response was observed during the months of October to November (monsoonal transition period) which can be associated to a shallower MLD and D26 and colder T100 and MLT (Figure 40, green line). However, non-typhoon season can be associated to both weaker and lesser occurrence of tropical cyclones and colder and deeper background conditions. On the other hand, SSTA response at BS region is steadily at almost the same level which can be associated with an almost near-constant background conditions based on MLD, D26, MLT and T100 (Figure 40, blue line).

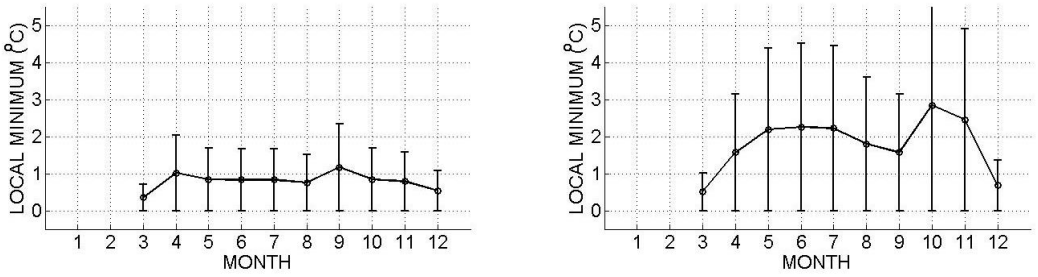

Figure 39. Monthly variation of Local Minimum (°C) on BS (left) and BN (right) Error bars are standard deviation.

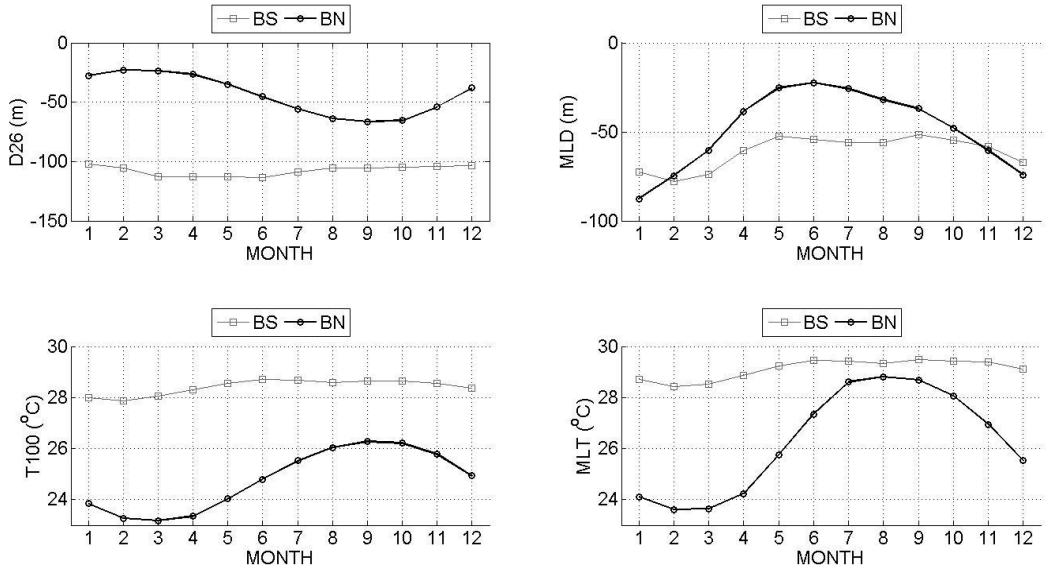

Figure 40. Monthly variation of D26 (m) (top-left); MLD (m) (top-right); T100 (°C) (bottom-left) and MLT (°C) (bottom-right) for both the BS (gray) and BN (black) region.

SST Response on off Eastern Philippines (EP) is suppressed due to background thermal structure. Current work on Yang et al (2012) about the passage of a binary typhoon on both South China Sea (SCS) and EP induced maximum cooling for both regions but SST cooling is much higher in the SCS than in EP even wind strength due to TC is stronger in the EP. The background thermal structure of the SCS is susceptible to SST cooling than the EP where it has relatively warm and deep thermal structure driven by the North Equatorial Current (NEC).

In this work, BN showed higher SST cooling which is possibly associated with a shallower and colder background conditions than the BS. The warm North Equatorial Current (NEC), which bifurcates into the Kuroshio and Mindanao current, plays an important role in changing the upper ocean characteristics off Eastern Philippines. The NEC influences the upper ocean response to tropical cyclones mainly through horizontal advection by setting up the background climatological condition. The BS region, at around 10-15°N, where the NEC

bifurcation latitude is estimated to be the located may plays a possible major role in the formation and intensification of major typhoons around the region.

Summary and Conclusion

The SST response of tropical cyclones off Eastern Philippines from 2003 to 2012 was determined to understand the dependence on upper ocean thermal structure. Two general regions were identified, BN (> 15°N) and BS (<15°N) differentiated by their mean background thermal structure parameterized as mean SST, MLD, MLT, T100 and D26. The BN region, characterized with a shallow MLD and D26 and colder SST, T100 and MLT showed higher seasonal variability; while BS region with deeper MLD and D26 (>100m), and warmer SST, T100 and MLT were more consistent throughout the year. The BS region is associated with the NEC bifurcation window where the deeper D26 contributes to warmer waters in the region.

Numerical experiments were conducted to simulate SSTA response for both regions as a result of vertical mixing while actual SSTA response was extracted from available satellite data (TMI-AMSIRE where induced local minimum SSTA and recovery period was derived). Results show a good correspondence with respect to SSTA response of both regions with vertical mixing, playing a major role in surface cooling.

The BN region tends to be more susceptible to oceanic cooling with at most 2°C (0.5°C) observed and computed difference in local minimum for slow (fast) moving and strong (weak) TC than the BS region. The results suggest the possible role of the NEC contributing warm waters as a result of horizontal ocean-ocean thermal exchange through advection. In general, results indicate that background climatological thermal structure of the ocean plays an important role in the oceanic cooling as a result of the passage of tropical cyclones.

CHAPTER 3. Sea Surface Temperature Response to Tropical Cyclones off Eastern Philippines: Dependence on Oceanic Features

Introduction

The east of the Philippines serves as an entry point to at least 15 tropical cyclones every year. The ocean is dynamic where the North Equatorial Current (NEC) bifurcates into the Kuroshio Current to the north and Mindanao Current to the south. The displacement and intensity of NEC bifurcation in the region varies seasonally (Yaremchuk and Qu, 2004; Chen and Wu, 2011) and interannually (Qiu and Chen, 2010) driven by local monsoons and ENSO. The variability of the NEC bifurcation latitude may alter the source waters of the Kuroshio and modify the intensity of permanent oceanic features (Zhao et al, 2012) such as the temperature field and consequently the strength of the typhoons and upper ocean response.

The main development region (MDR) for typhoon formation and intensification is located east of the Philippines (10-26°N, 122-170°E) (Pun et al, 2013). The region has been identified with a warming and deepening of the D26 from 1993 to 2011 associated with the increase in number of warm features and decrease of cold features. A possible direct link can be associated with the migration of the NEC Bifurcation latitude. Oceanic features are affecting the magnitude of sea surface cooling induced by the passage of tropical cyclones (Wada and Usui, 2010). Studies on individual tropical cyclones showed a direct link of maximum SST cooling associated with cold features (D'Asaro, 2007; Shang et al, 2008; Yang et al, 2010; Chiang et al, 2011) and reduced SST cooling in relation to warm features (Lin et al, 2008; Ulhorn and Shay, 2012; Wu and Chen, 2012).

This chapter aims to determine the association of SST response to tropical cyclones on oceanic features and the migration of the NEC Bifurcation Latitude.

Methodology

SST Response

Daily sea surface temperature (SST) dataset used in this study is the merged product of Tropical Rainfall Measuring Mission (TRMM) Microwave Imager (TMI) and Advance Microwave Scanning Radiometer – EOS (AMSR-E) from 2003 to 2012. Spatial Resolution of the data set is 0.25 x 0.25°. Climatological dataset is constructed by averaging daily SST values at each grid point from 2003-2012 and subtracting from the daily SST to form the SST Anomaly (SSTA).

Tropical cyclone (TC) best track data downloaded from JTWC was sampled from the Western North Pacific basin dataset from 2003-2012. Only typhoons affecting the Philippine Area of Responsibility (PAR) were considered. Dataset includes 6 hourly positions of each TC. SST responses based on local minimum SSTA and recovery period were extracted from the time series of each point position of the TC. Recovery period is defined as the time it takes for the SST change induced by tropical cyclones to recover back to climatological condition.

SST responses were then clustered according to different oceanic features. These features will be discussed in the next section.

Oceanic Features

Oceanic features will be based on sea surface height anomaly (SSHA) information, positive features are areas with SSHA > 6cm, neutral features with -6cm < SSHA < 6cm and and negative features SSHA <-6cm. Altimetry data including SSHA and SSH was downloaded from French Archiving, Validation and Interpretation of Satellite Oceanographic (AVISO). It includes data from different satellite missions such as Saral/AltiKa, Cryosat-2, OSTM/Jason-2, Jason-1, Topex/Poseidon, Envisat, GFO, ERS-1&2 and Geosat. Spatial resolution is 0.25° by 0.25° with 7 days temporal resolution.

Mean temperature profiles during the peak of the typhoon period for different oceanic features are shown in Figure 41. Negative features are associated with shallow mixed layer and D26 while deep mixed layer and D26 are associated with the positive features. Mean profiles during the typhoon season (June to November) will be used as initial profiles used in

numerical experiments to understand the effect of tropical cyclones strength and duration of sustained winds affecting the same region. With respect to SST Level, cold features are often associated with coldest SST than positive features (Figure 41).

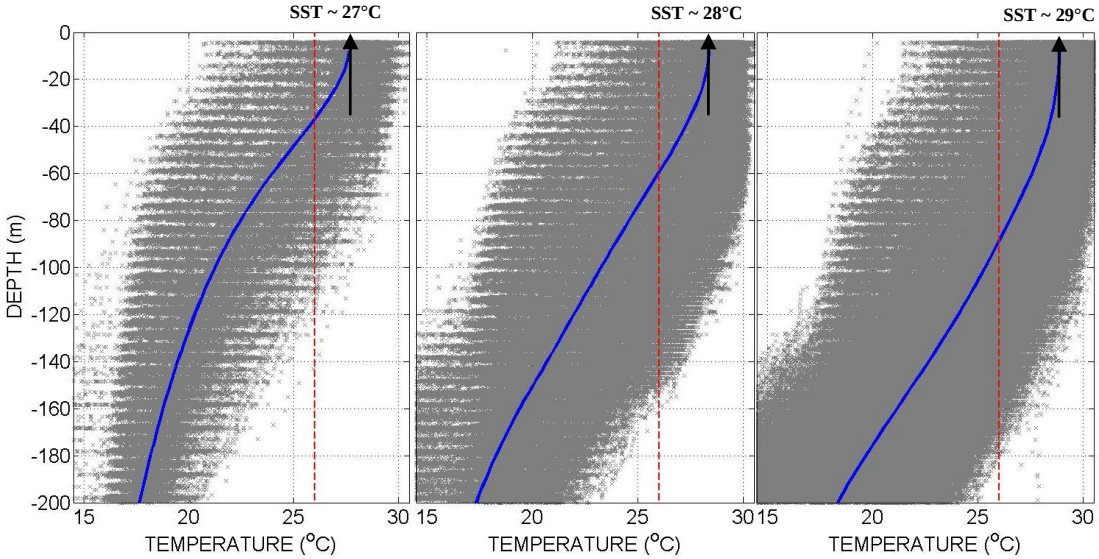

Figure 41. Mean Temperature Profile using ARGO Profiles from 2003 to 2012 at different Oceanic Feature (a) Negative Features (SSHA < -6cm) (b) Neutral Feature (SSHA>-6 cm and SSHA <6 cm) and (c) Positive Features (SSHA > 6cm); Also highlighted red dashed line showing the depth of 26°C isotherm (D26). Black arrow indicating estimated value of SST.

Numerical Modeling

A numerical experiment was conducted with similar scheme used in chapter 2. Background temperature profiles used are means for different oceanic features representing positive, neutral and negative features. These profiles are shown in Figure 41 showing the increasing D26 from negative to positive feature.

NEC Bifurcation Latitude

A Proxy (Y_p) for NEC Bifurcation Latitude from 2003 to 2012 was estimated using Sea Surface Height Anomaly (SSHA) data given by the formula:

$$Y_p(t) = 11.9 - 0.13 \times h'(t)$$ (Equation 2, adapted from Bo and Chiu (2010))

where

$Y_p(t)$ is the Bifurcation Latitude proxy

$h'(t)$ is the weekly SSHA value (in cm) averaged in 12°-14°N and 127°-130°E box

Background climatological conditions of tropical cyclones are based on upper ocean subsurface parameters such as D26 (depth of 26°C isotherm) and T100 (vertically averaged temperature up to 100m). These were computed from available ARGO temperature profiles from 2003 to 2012. D26 and T100 (used as proxy for upper ocean heat content by Price (2009) and Vissa et al (2008) have been used as metrics for typhoon intensification (Lin et al, 2008; Lin et al, 2009). Mean values of these parameters are used to support analysis of the result of the upper ocean response and the migration of the NEC bifurcation latitude.

Results

Numerical Experiments

Results from numerical experiments show variation of SSTA response on different oceanic features (negative, neutral and positive) as a result of vertical mixing are shown Figure 42 (top). Negative features associated with shallow D26 have the highest maximum cooling based on tropical cyclone strength and duration of wind forcing affecting the same region. On the other hand, positive features associated with deeper D26 induced the lowest SST change at varying tropical cyclone's intensity and temporal forcing.

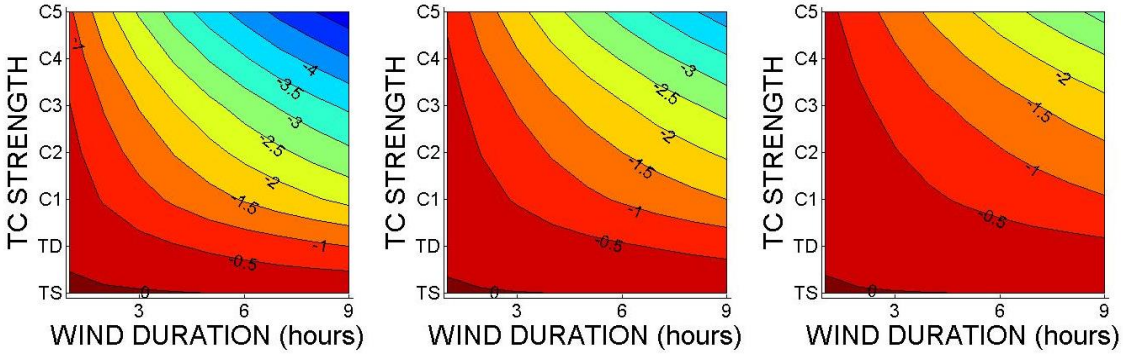

Figure 42. SSTA response (local minimum) from numerical experiments by varying TC strength and wind duration forcing time at different oceanic features (left) negative; (middle) neutral and (right) positive.

Temperature profiles for different scenarios shows deepening of the D26 after the passage of a Category 3 tropical cyclone after 3 hours (Figure 43-top) represented by solid green line (pre-typhoon) to green broken line (post typhoon). Temperature profiles for different strength of TC are shown in the Appendix – Supplemental Figures (Negative Features - Figure 62; Neutral Features - Figure 64; Positive Features - Figure 66). Also Figure 43-bottom shows the difference of the temperature profiles before and after a passage of a TC at varying oceanic features showing cooling at above the pre-typhoon mixed layer depth and warming underneath. However, highest cooling with negative features is associated with a shallow background condition with a higher capability to mix colder water up to its mixing depth than with conditions associated with positive features.

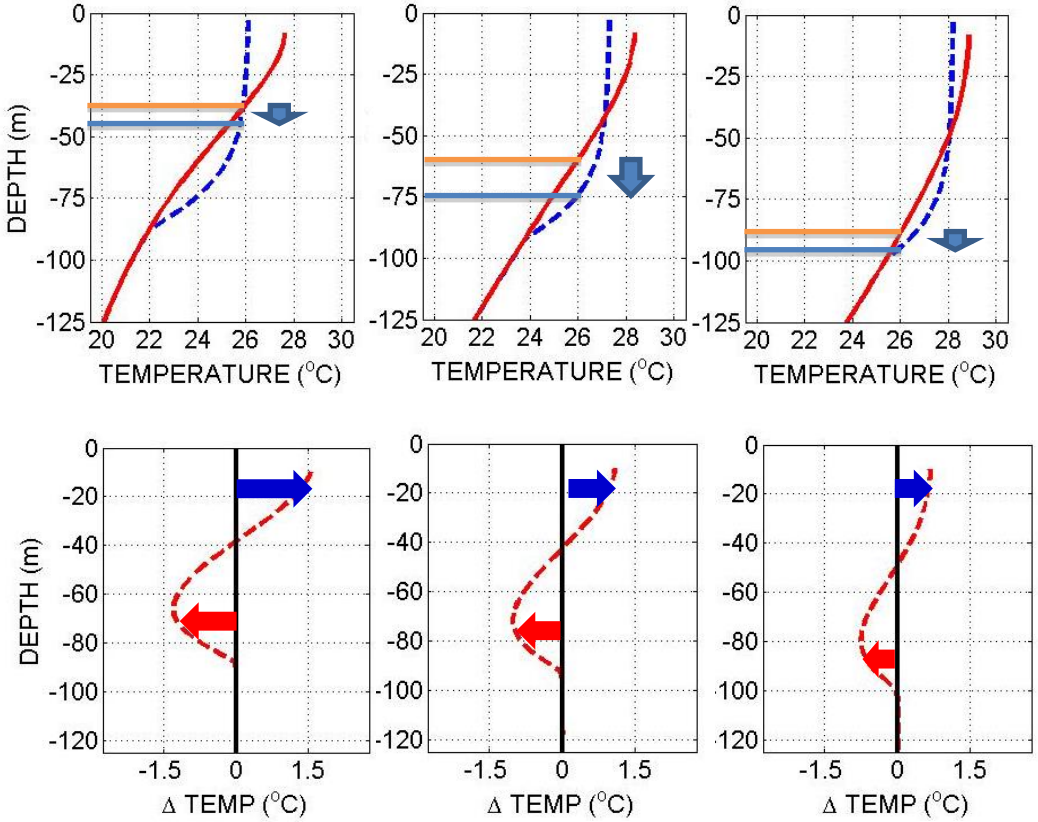

Figure 43. Temperature profile of pre and post-TC condition (top) and temperature profile changes (bottom) of a simulated Category 3 typhoon after 3 hours of wind forcing different background profiles on (left) negative features; (middle) neutral features and (right) positive features. Light red solid line and light blue solid line indicating pre and post-storm D26, respectively.

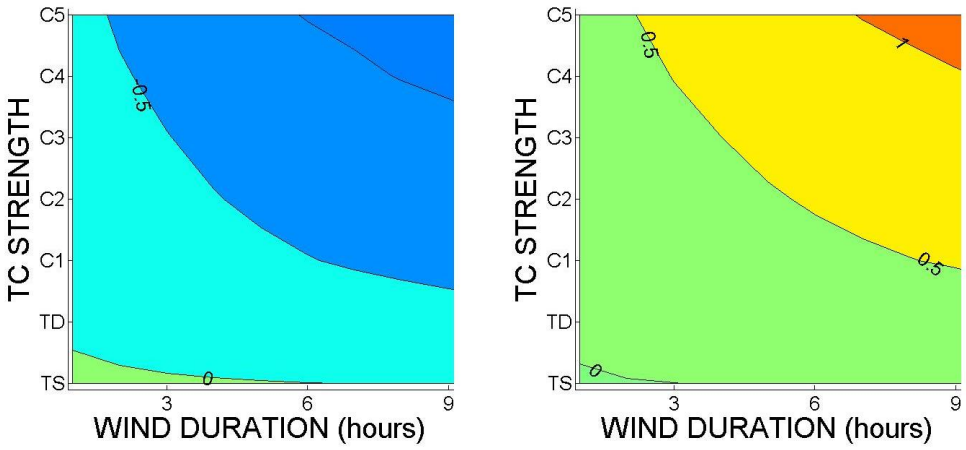

Figure 44. Difference on SSTA Response on negative (SSHA <-6cm) (left) and positive (SSHA >6cm) (right) features relative to SSTA response occurring in neutral (SSHA >-6cm and SSHA <6cm) features derived from numerical experiments

Moreover, difference on SSTA response on positive features (Figure 44, left) with respect to SSTA response on neutral features is greater than 0.5 °C for a C4 within 3 hours, C2 within 6 hours and C1 with at least 0 hours. On the other hand, difference in SSTA

response in negative features is less than 0.5 for a C3 TC within 3 hours and C1 with at least 6 hours with respect to the SSTA response on neutral features.

The results of the numerical experiment showed initial expected response at different oceanic features at varying TC intensity and wind duration. On the next section, SST response based on SSTA local minimum and recovery period that was derived from observation data will be presented.

SST Response: dependence on oceanic features

Scatter plot of the SST Response based on local minimum and recovery period are shown in Figure 45, integrating factors such as TC Strength and translation speed. Both regions shows maximum SST changes and longer recovery period during strong TC Strength and slow translation speed. Maximum mean SSTA change is up to 3.5°C on negative features, and 2.5°C for both neutral and positive features. Minimum SSTA changes and shorter recovery period occurs with fast moving TC and weaker TC strength. Minimum mean SSTA change is 0.5°C for positive features and 1°C for both neutral and negative features. Fastest recovery occurs generally on all positive features.

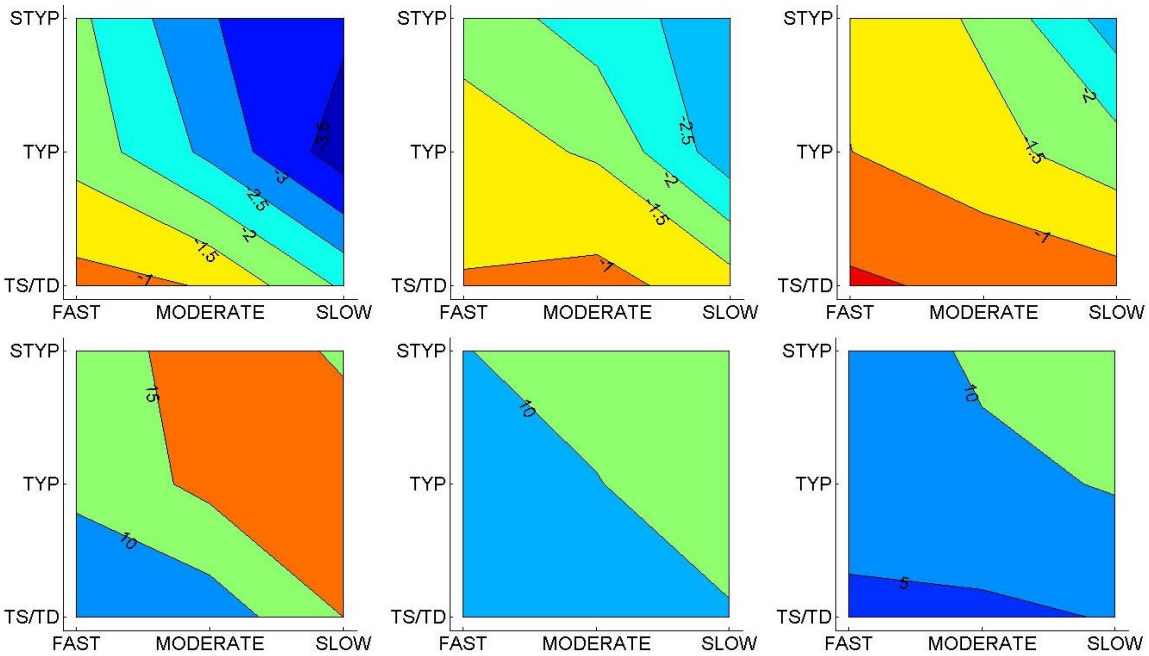

Figure 45. SSTA response (local minimum) (top) and Recovery Period (bottom) from observations at varying translation speed and TC strength for different oceanic features – Negative Features (Left); Neutral Features (Center) and Positive Features (Right). Translation Speed are considered slow for 0-4 ms^{-1}; Moderate for 4-8 ms^{-1} and Fast for >8 ms^{-1}; TC Strength is TS/TD for Tropical Storms and Depression, TYP for CAT 1 to 3 and STYP for CAT 4 to 5

Low translation speed of tropical cyclones and maximum wind speed is a major factor to induce maximum cooling (Price et al, 1981; Lin et al, 2009; Dare and McBride, 2011). Mean SSTA response based on local minimum shown in Figure 46 (left) favors maximum cooling for positive features (red) at varying TC Strength (top) and translation speed (bottom) and minimum cooling was observed on negative features (blue). Mean recovery period as shown Figure 46 (right) shows the same trend. Results are consistent with the results of the numerical experiments shown in the previous section.

Figure 47 (top) also shows the relationship of TC translation speed and strength for features, POS+ (SSHA >18cm) and NEG+ (SSHA<-18cm). This indicates that the more negative the feature the more it favors cooling while a more positive SSHA suppresses cooling.

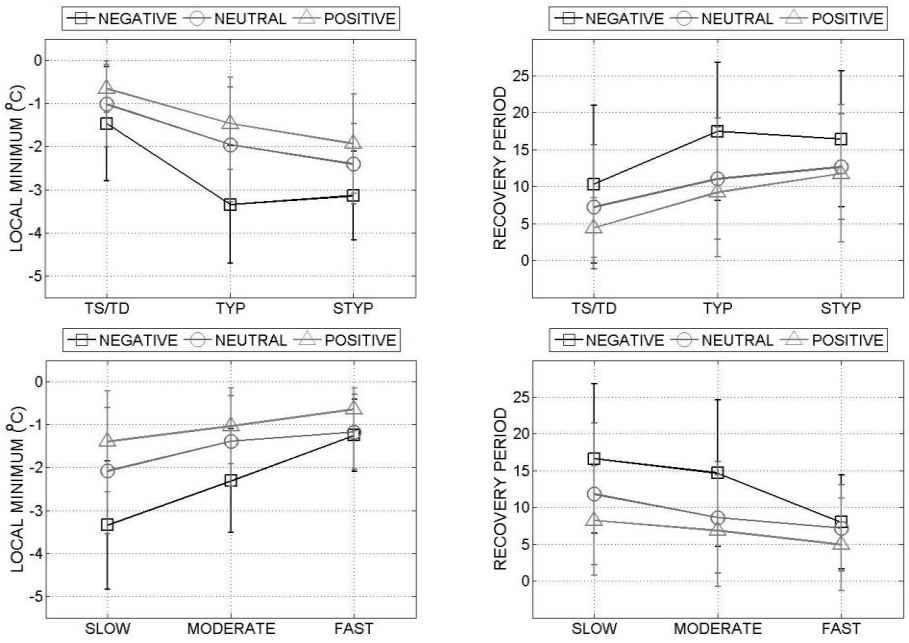

Figure 46. Relationship between translation speed on local minimum (°C) (left) and recovery period (days) (right) for different oceanic feature [positive (Δ), neutral (O) and blue (□) features] at varying TC Strength (top) and translation speed (bottom) derived from observation data. Error bars are standard deviation.[TC Strength: TS/TD – Tropical Storms/Depression; TYP – CAT 1 to 3; STYP – CAT 4 to 5.Translation Speed: SLOW – 0-4ms^{-1}; MODERATE – 4-8ms^{-1}; FAST - >8ms^{-1}]

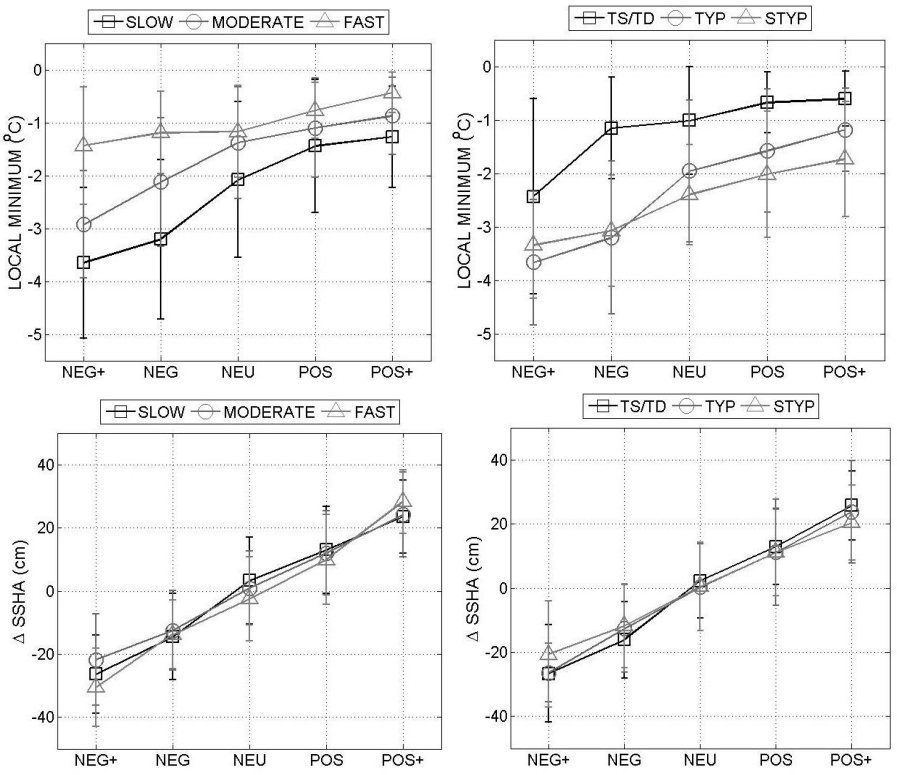

Figure 47. Mean and standard deviation of the local minimum (°C) (top) and ΔSSHA (cm) (bottom) for different oceanic features [NEG+, SSHA <-18cm; NEG, SSHA >-18cm & SSHA <-6cm; NEU, SSHA >-6cm & SSHA <6cm; POS, SSHA >6cm & SSHA <18cm; POS+, SSHA >18cm] derived from observation data. Error bars are standard deviation. [TC Strength: TS/TD – Tropical Storms/Depression; TYP – CAT 1 to 3; STYP – CAT 4 to 5.Translation Speed: SLOW – 0-4ms^{-1}; MODERATE – 4-8ms^{-1}; FAST - >8ms^{-1}]

Pre-TC and post-TC changes on SSHA are shown in Figure 47 (bottom). For negative features (SSHA <-6cm), a change in mean SSHA of less than zero resulting to an increase in mean SSHA while for positive features (SSHA >6cm), a decrease in mean SSHA was observed. Results may play a role on the possible effect of TC on the formation on divergent and convergent zones as a result of the moving anticyclonic wind on different oceanic features.

Migration of the NEC Bifurcation Latitude

The NEC bifurcation latitude varies along 10-15°N window with notable northerly bifurcation from 2003-2004, 2005 and southerly bifurcation from 2008-2009 (Figure 48) during the 2003 to 2012 season. Mean upper ocean parameters (D26 and T100) derived along the NEC bifurcation latitude window, 10-15°N (adapted from Bo and Chiu, 2010) correlates negatively (R_{D26}= -0.91; R_{T100} = -0.78) with the bifurcation latitude (Yp) (Figure 49).

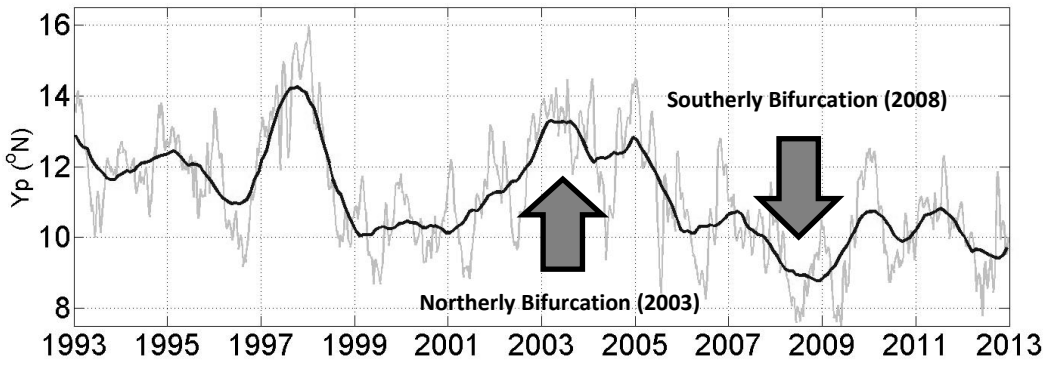

Figure 48. NEC Bifurcation Latitude (Yp) derived from satellite-derived SSHA from 1993 to 2013

A northerly bifurcation is associated with negative SSHA off the coast of Eastern Philippines while a southerly bifurcation is connected with positive SSHA. Annual SSHA for 2003 and 2008 (Figure 50) corresponds to Yp = 13.7503 and Yp = 10.4333 associated with nearly the SSH contour value of 105cm visually identified as the bifurcation point (Qiu and Chen, 2010; Zhao et al, 2012). SSHA is negatively correlated (r^2>0.5) with the bifurcation latitude (Yp) at the region 6° to 18°N (Figure 51 left) meaning when bifurcation is southerly, negative features are favored to increase and vice versa. D26 shows deepening while T100 warming as bifurcation latitude decreases (Figure 51, right). Relationship between D26 and T100 versus the bifurcation latitude for different regions of high correlation are shown in Figure 68 (Supplementary Figures)

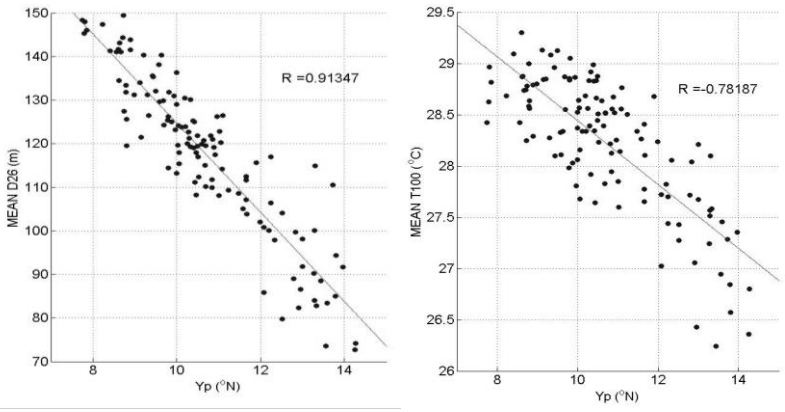

Figure 49. (left) Monthly Mean D26 along the NEC Bifurcation window (10-15°N) with the bifurcation latitude (R=0.91347) and (right) Monthly Mean T100 along the NEC Bifurcation window with the bifurcation latitude (R=-78187)

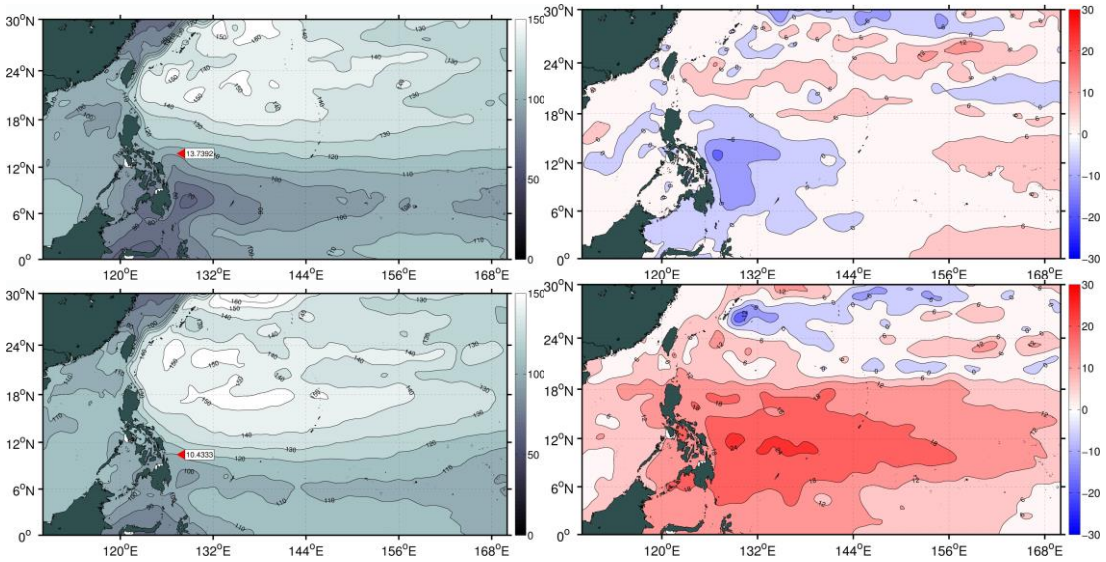

Figure 50. Northerly Bifurcation (2003): (a) Annual Sea Surface Height with Yp = 13.7503°N (b) Annual Sea Surface Height Anomaly associated with cold core eddies near the coast; Southerly Bifurcation (2008): (c) Annual Sea Surface Height with Yp = 10.43333 (d) Annual Sea Surface Height Anomaly associated with warm core eddies near the coast. Values are in cm.

Statistically, changes in the number of oceanic features shown in Figure 52 shows negative correlation (r=-0.82) for positive features (Figure 52 top, left) with respect to bifurcation latitude. On the other hand, the number of positive (Figure 52 bottom, left) and neutral features (Figure 52 top, right) are positively correlated with the bifurcation latitude with r_{pos}=0.72 and r_{neu} =0.58, respectively. Although the values are not highly correlated (with respect to r-squared), the sum on the number of positive and neutral features show high correlation with r^2=0.68.

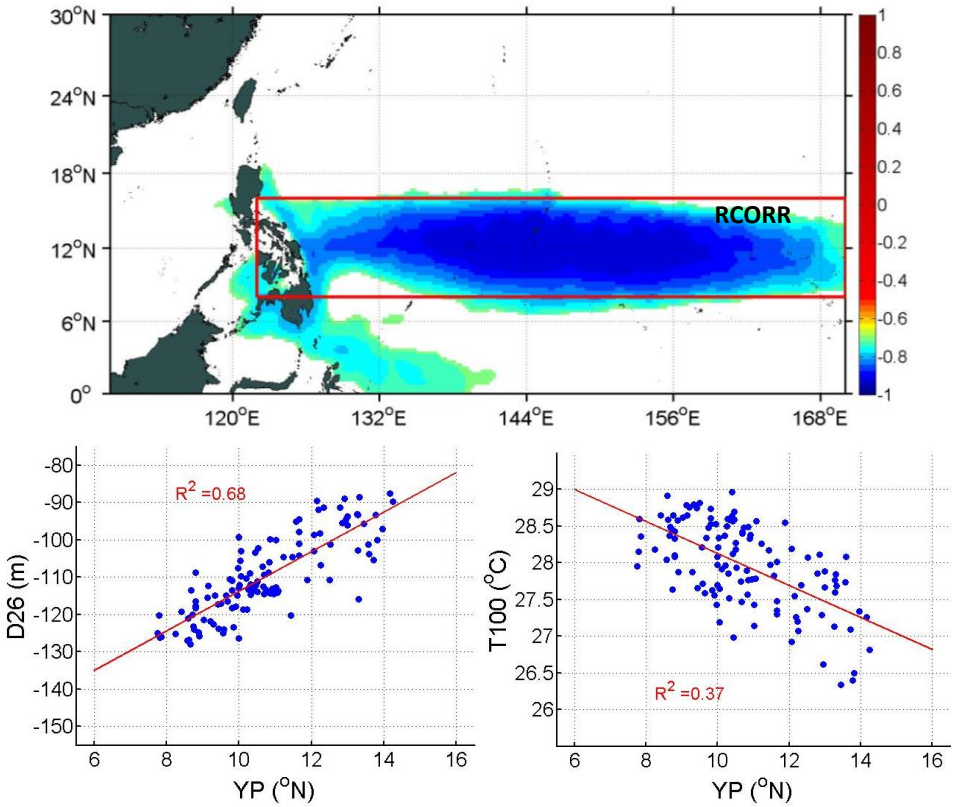

Figure 51. Spatial distribution of the correlation coefficient (r) [top left] and squared correlation coefficient (r^2) [bottom left] of the bifurcation latitude (Yp) versus SSHA derived from 1993 to 2012 satellite altimetry data; On the enclosed box labeled as the RCORR region (Latitude: 6 °N to 18°N and Longitude: 125°E to 170°E) where monthly mean D26 [top right] and T100 [bottom right] derived from ARGO float data from 2003 to 2012 showing correlation of R_{D26}=0.82 and R_{T100}=-0.61 with the bifurcation latitude (Yp).

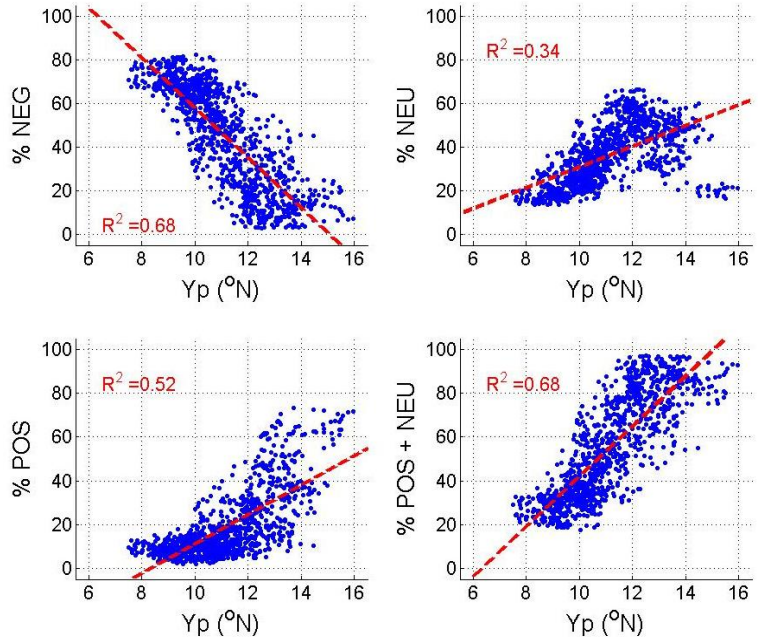

Figure 52. Correlation between bifurcation latitude (Yp) and the percentage of occurrence of negative (top left), neutral (top right), positive (bottom left) and positive+neutral (bottom right) oceanic features along 6-18°N, 125-170°E.

The upper ocean characteristics (particularly SSHA and D26) clearly change with the bifurcation latitude shift northward and southward. In the next section, SST response within Latitude: 6 °N to 18°N and Longitude: 125°E to 170°E region will be discussed with a northward bifurcation (Yp > 11°N) and a southward bifurcation (Yp < 11°N).

SST Response with the NEC Bifurcation

Mean SSTA response with respect to recovery period shows the same trend for both a northerly (YP>11) and southerly bifurcation (YP<=11) for the whole dataset (Figure 53, left). However, at 6° to 18°N region (Figure 53, right), a southerly bifurcation induced longer recovery period at local minimum at -2.5°C or lesser although still not statistically significant because of the wide range of the standard deviation (error bar).

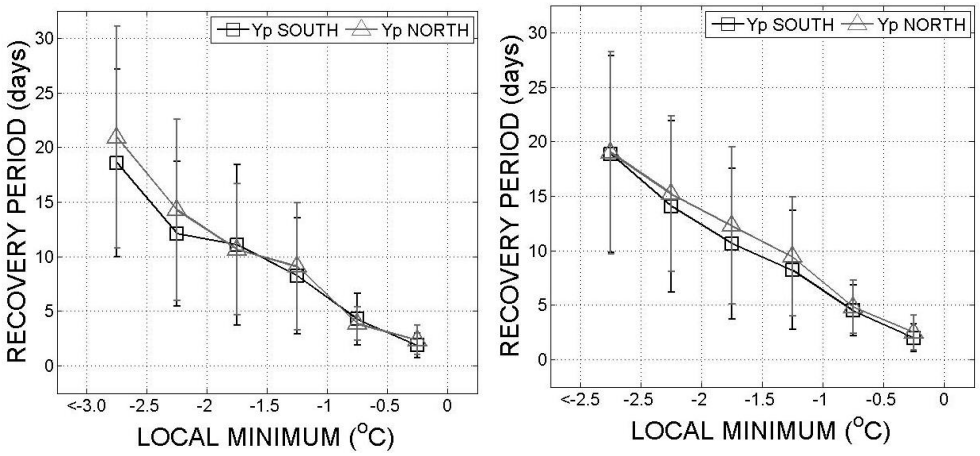

Figure 53. Mean SSTA Response versus recovery period based on actual data during events with Bifurcation latitude (Yp) > 11°N (North, Δ) and < 11°N (South, □) in 6°-18°N (left) and 0°-30°N (right); Error bars are standard deviations.

In terms on the number of occurrence in the RCORR region, around 40% of slow moving TC (translation speed – 0 to 4 ms^{-1}) (Figure 54 top, left) are associated with a northerly bifurcation compared to 3% for a southerly bifurcation. Moderate moving TC is is associated with a 90% occurrence during a southerly bifurcation compared to 60% during a northerly bifurcation. However, in the entire region slow moving TC is around 35% occurrence during a southerly bifurcation compared to at least 10% during a northerly bifurcation (Figure 54 top, right). There is not much difference in percentage occurrence in the MDR region (Figure 54 top, center).

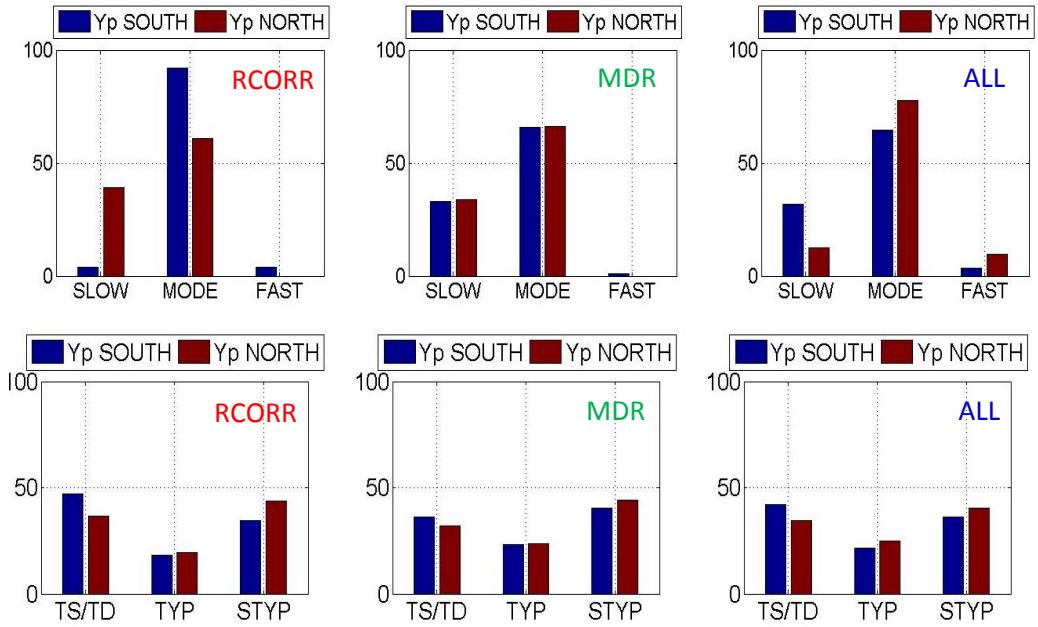

Figure 54. Percentage number of occurrences of different TC Translation Speed (top) and Strength (bottom) classes for RCORR (left); MDR (center) and entire dataset (right) during a northerly bifurcation (YP > 11°N, red) and southerly bifurcation (YP <=11°N, blue). TC Strength: TS/TD – Tropical Storms/Depression; TYP – CAT 1 to 3; STYP – CAT 4 to 5.Translation Speed: SLOW – 0-4ms^{-1}; MODERATE – 4-8ms^{-1}; FAST - >8ms^{-1}.

With respect to TC strength, a higher percentage of strong typhoons (Category 4 and 5) (Figure 54 bottom) are associated also with the northerly bifurcation for all three predefined regions (RCORR, MDR and ALL) while a number of tropical storms and depression are associated with a southerly bifurcation.

Although there is no significant difference on SST Response during a southerly and northerly shift, the differences in the percentage number of occurrence of different translation speed and TC strength classes may play an important role in balancing air-sea interaction response due to varying conditions as a result in the variation of the NEC bifurcation latitude at a given favorable atmospheric conditions.

Discussion

Oceanic cooling due to TC can be attributed the effect of vertical mixing, divergence, air-sea flux exchanges and advection (Vincent et al, 2012). Sea surface cooling has been reported to be a result of a lowering of SSH due to surface divergence causing upwelling (Chen et al, 2012) and an increase of SSH due to reduced atmospheric pressure (Rao et al, 2006). However, at the center of a TC, vertical mixing plays a major role in the SSTA response (Vincent et al, 2012). The highest change in local minima was observed in negative features while minimum change was observed in positive features. Both scenarios can be more pronounced as a result of high energy input such as strong winds. Cold features favor ML shallowing upon the passage of typhoons while warm features favor ML deepening (Wu and Chen, 2012).

Sea surface cooling in oceanic features has been reported in individual events such as enhancement in the presence of negative features (associated with SSHA <-6 cm) (D'Asaro, 2007; Shang et al, 2008; Yang et al, 2010; Chiang et al, 2011; Nam et al, 2011) while positive features serves as insulation to minimize sea surface cooling due to high Upper Ocean Heat Content and deeper D26 (Lin et al, 2008; Nam et al, 2011;Ulhorn and Shay, 2012; Wu et al, 2012). Some report neutral features induced maximum cooling as a factor of slow translation speed (Siswanto et al, 2008).

Specific events such as the passage of binary typhoons affecting east of the Philippines (EP) and the South China Sea (SCS) simultaneously induced a maximum change of 7°C and 2°C, respectively, even though TC's translation speed of the typhoons are slow (< 4 m/s) (Yang et al, 2012). The difference on the change in temperature can be differentiated based on the background climatological condition – EP is under a positive feature (SSHA>6cm) while SCS is under neutral condition (SSHA<6cm and SSHA>-6cm). Change in temperature was induced by long forcing time of strong wind stress curls (TC's translation speed < 4 m/s).

Results in this chapter shows the same response as a result of numerical experiments and actual SST response observed from 2003 to 2012 favoring maximum cooling for negative features and suppressed cooling on positive features. Table 7 shows the comparison of SSTA (local minimum) response in both numerical experiments and observation data for different oceanic features. Results show comparable trend with respect to trend showing slow moving TC contribute to the highest SSTA response than fast moving TCs. Although results in

Chapter 2 shows that vertical mixing acts as a major physical process providing greater SSTA cooling, results in this chapter shows that the mean value based on observation data is lower than the results in numerical experiments. This error can be attributed to background temperature profiles generalized based on pre-typhoon SSHA condition despite expected latitudinal differences based on the results conducted in Chapter 2.

Table 7. Comparison of Maximum SSTA changes based on Numerical Experiments and Observation Data in degree Celsius for different oceanic features (Negative, Neutral and Positive)

Translation Speed (ms^{-1})		Numerical experiments (°C)			Observation Data (°C)					
Class	Range	NEG	NEU	POS	NEG		NEU		POS	
Slow	3 to 9	-4.5	-3.5	-2.5	-3.34	±1.49	-2.08	±1.47	-1.39	±1.18
Moderate	1 to 6	-3.5	-2.5	-1.5	-2.31	±1.21	-1.38	±1.06	-1.03	±0.88
Fast	< 3	-2.0	-1.5	-1.0	-1.25	±0.84	-1.17	±0.87	-0.64	±0.5

On the other hand, major region where there is a high correlation with the bifurcation latitude was identified at 6°N to 18°N Latitude and 125° to 170°E Longitude. A southward shift favors an increase of positive features while a northward shift favors increase in neutral and negative features also favoring changes in upper ocean D26 (deeper when bifurcation is southward) and T100 (warmer when bifurcation is southward). Warming based on upper ocean heat content (UOHC) and deepening of D26 was reported across the Main Development Region (MDR) for typhoon formation and intensification [110°-170°E; 10°-22°N]. This trend is associated with a decrease of positive and neutral features and an increase of negative features of the MDR (Pun et al, 2013). A possible lead in the changes in the numbers of features can be linked to the migration of the NEC. Varied response can be attributed to seasonal variation of the NEC (Figure 55). A northward shift is associated during the months of November and December while southward shift occurring the months of June to September. Monthly difference on SSTA response was discussed on Chapter 2.

However, changes in the features in this region were able to restrain cooling making both events with a northerly and southerly bifurcation not significantly different on SST response. Moreover, numerical experiments conducted by Lin et al (2009) showed that positive features identified in the gyre central region (10°-21°N, 121°-170°E), where background climatological D26 is deep (~105-120 m), is able to restrain surface cooling compared to the positive features in Pacific South Eddy Zone (21°-26°N, 127°-170°E) and Kuroshio (21°-30°N, 121°-170°E) where background climatological D26 is shallower (~ 60m).

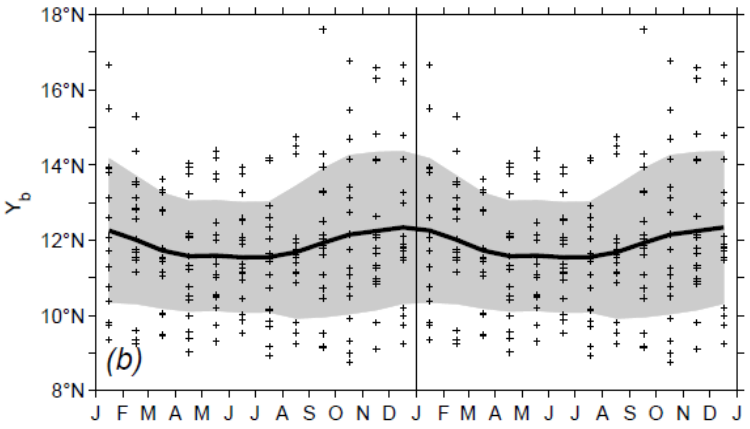

Figure 55. Seasonal trend of the NEC Bifurcation Latitude adapted from Qiu and Chen, 2010

In terms on the number of occurrences, slower translations speed is associated with a southward bifurcation and the presence of more positive features. Given a positive feature, maximum induced SSTA changes is less with around 0.5° to 1.5°C with increasing TC strength and a wind forcing duration of 6 hours (based on numerical experiments). In contrast to a northerly bifurcation where it favors an increase in the number of neutral and positive features favoring fast moving TC with 0.5°C to 3°C induced cooling during duration of 6 hours wind forcing (based on numerical experiments).

Moreover, during southerly bifurcation, TC strength is an important factor in inducing maximum cooling at higher translation speeds (> 5m/s); while during northerly bifurcation a significant number of tropical cyclones, including tropical depression and storms, have very low translation speeds, which induced maximum cooling. The presence of tropical cyclones with lower translation speed is associated with deep D26 and higher UOHC (Lin et al, 2009).

Changes in the TC characteristic and behavior may be an important link between ocean and atmosphere in maintaining balance on the transfer of energy between the atmosphere and ocean as a result in the shift of the NEC bifurcation latitude.

Summary and Conclusion

SST response based on SST recovery time and local minimum induced by tropical cyclones affecting the Western North Pacific Region from 2003-2012 has been conducted to understand the role of different oceanic features and its response to the shifting of the NEC bifurcation latitude. Results show highest local minimum, alongside longest SST recovery, are associated with negative features due to turbulent mixing as an effect of a shallow D26 while lowest local minimum, alongside fastest recovery are associated with positive features as effect of entrainment serving as insulation. Both responses are enhanced by increasing force induced by winds and slow TC translation speed.

A region where there is a high correlation with the bifurcation latitude is located at 6°N to 18°N latitude and 125° to 170°E longitude showing changes in oceanic features alongside with D26 and T100 favoring increase in positive features during a southward shift allowing deepening of D26 and warming of T100 on the region and vice versa.

The migration of the NEC led to varying oceanic features along the east region of the Philippines. Northerly bifurcation is associated with more negative features (less warm) than a southerly bifurcation. Although there is no difference on the SST Response during northerly and southerly bifurcation period, changes where observed on the number of TC characteristics such as TC translation speed and strength during a bifurcation shifts.

CHAPTER 4. Synthesis

The east of the Philippines is a dynamic region where it serves as an entry point of at least 65% of tropical cyclones including super-typhoons affecting the Western North Pacific Region. The ocean varies in oceanic properties and structure through variation in strength of easterly trade winds driving shifts in the location of the North Equatorial Current (NEC) changing seasonally and interannually by monsoons and ENSO, respectively.

The passage of tropical cyclones at the western north pacific region places an important role to the climate of the Philippines and the rest of East Asia. This can be attributed to different interactions between the atmosphere, the ocean and the land. In this thesis, the interaction of the atmosphere to the ocean was investigated by looking into SST responses due to the passage of tropical cyclones through numerical experiments and observation data and its dependence on upper ocean thermal structure (chapter 2) and varying oceanic features (chapter 3). Oceanic parameters such as the mixed layer depth (MLD) and temperature (MLT), depth average temperature up to 100 m (T100) and depth of 26°C isotherm (D26) will serve as a point of comparison for the conditions of the different regions discussed in both chapters.

In chapter 2, the dependence of the upper thermal structure was examined. This was conducted by looking into two general regions, namely BN with latitude 15° to 30°N and BS with latitude 0° to 15°N. The BN region is associated with colder waters with shallow mean MLD and D26 (< 80 m) and with strong variations seasonally while the BS region is warmer with deeper mean MLD and D26 (> 100m) with less variation seasonally. Both numerical and observation data showed that greater cooling and longer recovery is associated with BN region while SST cooling and shorter recovery is suppressed in the BS region even at varying TC strength and translation speed. SST changes in the BS region displays a possible influence of the NEC in the oceanic control through advection of warm waters. Results also indicated that wind-induced upper ocean vertical mixing plays a major role for the surface cooling.

In chapter 3, the role of oceanic features based on satellite derived altimetry was conducted by investigating different oceanic features and as a results of the variation of the NEC bifurcation latitude. Three features where generalized namely positive (SSHA > 6cm), neutral (SSHA < 6 cm and SSHA > -6cm) and negative features (SSHA < -6cm). Generally, positive features are associated with deepest D26 and warmest and negative features with the

shallowest D26. As a result, SST response conducted in both numerical experiments and observations favors maximum induced cooling and longer recovery for negative features while minimum cooling and shorter recovery was observed for positive features. Changes in the number of oceanic features showed a strong correlation with the shifting of the NEC bifurcation latitude along with the oceanic parameters (T100 and D26). Warming and deepening resulted during a southward shift and vice versa. With respect to SST response, there is no significance difference. However, an increase in the percentage of slow moving typhoons and strong typhoons were observed during a northward shift while an increase in moderate moving and the number of tropical storms and depression during a southward shift.

In general, SST response is dependent on oceanic features related to a background upper ocean thermal structure, which varies with latitude, seasonally and interannually. Variations in magnitude and direction may play an important role in the relative strength of tropical cyclones and associated sea surface response. This shows that the ocean plays a role in manipulating control of the atmosphere given favorable atmospheric conditions.

Moving forward, quantification of different fluxes involving air-ocean, ocean-air and ocean-ocean will be an important step to understand the oceanic and atmospheric control. Other factors including interannual variations of the behavior of tropical cyclones and at the same time variation of the large and mesoscale circulations propagating along the eastern Philippines including planetary kelvin waves and the NEC should be considered. Furthermore, this complexity of the eastern Philippines may play an important role in the formation of a destructive storm, i.e. Supertyphoon Haiyan (Local Name: Yolanda).

REFERENCES

Aguado E, Burt JE. 2010. "Understanding Weather and Climate" (5th edition). Prentice Hall PTR.

Babin SM, Carton JA, Dickey T, Wiggert J. 2004. Satellite evidence of hurricane-induced phytoplankton blooms in an oceanic desert. Journal of Geophysical Research 109: 1–21.

Balaguru, K, Chang, P, Saravanan, R, Leung, LR, Xu, Z, Li, M, Hsieh, J-S. 2012. Ocean barrier layers' effect on tropical cyclone intensification. Proceedings of the National Academy of Sciences of the United States of America, 109(36), 14343–7. doi:10.1073/pnas.1201364109

Bond N, Cronin M, Sabine C. 2011. Upper ocean response to Typhoon Choi-Wan as measured by the Kuroshio Extension Observatory mooring. Journal of Geophysical Research 116: 1–8.

Botin ZT, David LT, del Rosario RCH, Parrott L. 2010. Spatio-Temporal Complexity analysis of the Sea Surface Temperature in the Philippines. Ocean Science 6: 933–947.

Bowditch N. 2002. "The American Practical Navigator" – Chapter 35, Tropical Cyclones. United States. National Imagery and Mapping Agency. Paradise Cay Publications

Camargo, S, Sobel, A. 2005. Western North Pacific tropical cyclone intensity and ENSO. Journal of Climate, 2996–3006.

Chang, J., Chung, C., & Gong, G. 1996. Influences of cyclones on chlorophyll a concentration and Synechococcus abundance in a subtropical western Pacific coastal ecosystem. Marine Ecology Progress Series, 140, 199–205.

Chen, Y., Chen, H., Jan, S., & Tuo, S. 2009. Phytoplankton productivity enhancement and assemblage change in the upstream Kuroshio after typhoons. Marine Ecology Progress Series, 385, 111–126. doi:10.3354/meps08053

Chen X, Pan D, He X, Bai Y, Wang D. 2012. Upper ocean responses to category 5 typhoon Megi in the western north Pacific. Acta Oceanologica Sinica 31: 51–58.

Chen, Z, Wu, L. 2011. Dynamics of the seasonal variation of the North Equatorial Current bifurcation. Journal of Geophysical Research, 116(C2), C02018. doi:10.1029/2010JC006664

Chiang T-L, Wu C-R, Oey L-Y. 2011. Typhoon Kai-Tak: An Ocean's Perfect Storm. Journal of Physical Oceanography 41: 221–233.

Collins A. 2001. Ocean Circulation. The Open University, 2nd edition, 286pp., ButterworthHeinemann.

D'Asaro EA., Sanford TB, Niiler PP, Terrill EJ. 2007. Cold wake of Hurricane Frances. Geophysical Research Letters 34: 2–7.

Dare RA, & McBride JL. 2011. The Threshold Sea Surface Temperature Condition for Tropical Cyclogenesis. *Journal of Climate*, *24*(17), 4570–4576. doi:10.1175/JCLI-D-10-05006.1

Dare RA & McBride JL. 2011. Sea Surface Temperature Response to Tropical Cyclones. *Monthly Weather Review*, *139*(12), 3798–3808. doi:10.1175/MWR-D-10-05019.1

De Boyer Montégut, C., Madec, G., Fischer, A. S., Lazar, A., & Iudicone, D. 2004. Mixed layer depth over the global ocean: An examination of profile data and a profile-based climatology. *Journal of Geophysical Research*, *109*(C12), 1–20.

Enriquez A, Friehe C. 1995. Effects of wind stress and wind stress curl variability on coastal upwelling. Journal of Physical Oceanography .

Fogel, M. L., Aguilar, C., Cuhel, R., Hollander, D. J., Willey, J. D., & Paerl, H. W. 1999. Biological and isotopic changes in coastal waters induced by Hurricane Gordon. Limnology and Oceanography, 44(6), 1359–1369. doi:10.4319/lo.1999.44.6.1359

García-Herrera R, Ribera P, Hernández E, Gimeno L. 2007. Northwest Pacific typhoons documented by the Philippine Jesuits, 1566–1900. Journal of Geophysical Research 112: 1–12.

Goni, G., DeMaria, M., Knaff, J., Sampson, C., Ginis, I., Bringas, F., Mavume, A., Lauer, C., Lin, I-I., Ali, M.M., Sandery, P., Ramos-Buarque, S., Kang, K., Mehra, A., Chassignet, E., Halliwell, G. (2009). Applications of Ocean Measurements to tropical cyclone intensity Forecasting. Oceanography, 22(3), 190–197.

Hanshaw, M. N., Lozier, M. S., Palter, J. B. 2008. Integrated impact of tropical cyclones on sea surface chlorophyll in the North Atlantic. Geophysical Research Letters, 35(1), 1–6. doi:10.1029/2007GL031862

Hart, R. E., Maue, R. N., Watson, M. C. 2007. Estimating Local Memory of Tropical Cyclones through MPI Anomaly Evolution. Monthly Weather Review, 135(12), 3990–4005. doi:10.1175/2007MWR2038.1

Holland GJ .1993. "Ready Reckoner" - Chapter 9, Global Guide to Tropical Cyclone Forecasting, WMO/TC-No. 560, Report No. TCP-31, World Meteorological Organization; Geneva, Switzerland.

Hu C, Muller-Karger FE. 2007. Response of sea surface properties to Hurricane Dennis in the eastern Gulf of Mexico. Geophysical Research Letters 34: 1–5.

Hung, C., & Gong, G. 2011. Biogeochemical responses in the southern East China Sea after typhoons. Oceanography-Oceanography Society, 24(4), 42–51.

Jacob SD, Koblinsky CJ. 2007. Effects of Precipitation on the Upper-Ocean Response to a Hurricane. Monthly Weather Review 135: 2207–2225. 29

Jensen, TG. 2011. Bifurcation of the Pacific North Equatorial Current in a wind-driven model: response to climatological winds. Ocean Dynamics, 61(9), 1329–1344. doi:10.1007/s10236-011-0427-2

Katsaros, K. 2001. Evaporation and Humidity. In J. H. Steele, K. K. Turekian, & S. A. Thorpe (Eds.), Encyclopedia of Ocean Sciences (2nd Editio., pp. 324–331). Oxford: Academic Press.

Korty RL, Emanuel K a., Scott JR. 2008. Tropical Cyclone–Induced Upper-Ocean Mixing and Climate: Application to Equable Climates. Journal of Climate 21: 638–654.

Lee, C, & Park, M-O. 2011. Time series changes in sea-surface temperature, chlorophyll a, nutrients, and sea-wind in the East/Japan Sea on the left- and right-hand sides of typhoon shanshan's track. Ocean Science Journal, 45(4), 253–265. doi:10.1007/s12601-010-0023-2

Li, G, Wu, Y, & Gao, K. 2009. Effects of Typhoon Kaemi on coastal phytoplankton assemblages in the South China Sea, with special reference to the effects of solar UV radiation. Journal of Geophysical Research, 114(G4), 1–9. doi:10.1029/2008JG000896 Lin I, Liu WT, Wu C-C, Wong GTF, Hu C, Chen Z, Liang W-D, Yang Y, Liu K-K. 2003. New evidence for enhanced ocean primary production triggered by tropical cyclone. Geophysical Research Letters 30: 10–13.

Lin I-I, Wu C-C, Pun I-F, Ko D-S. 2008. Upper-Ocean Thermal Structure and the Western North Pacific Category 5 Typhoons. Part I: Ocean Features and the Category 5 Typhoons' Intensification. Monthly Weather Review 136: 3288–3306.

Lin I-I, Pun I-F, Wu C-C. 2009. Upper-Ocean Thermal Structure and the Western North Pacific Category 5 Typhoons. Part II: Dependence on Translation Speed. Monthly Weather Review 137: 3744–3757.

Lloyd I, Vecchi G. 2011. Observational evidence for oceanic controls on hurricane intensity. Journal of Climate 1138–1153.

Lyon, B, Camargo, SJ. 2008. The seasonally-varying influence of ENSO on rainfall and tropical cyclone activity in the Philippines. Climate Dynamics, 32(1), 125–141. doi:10.1007/s00382-008-0380-z

Maneesha, K., Sarma, V. V. S. S., Reddy, N. P. C., Sadhuram, Y., Murty, T. V. R., Sarma, V. V, & Kumar, M. D. (2011). Meso-scale atmospheric events promote phytoplankton blooms in the coastal Bay of Bengal. Journal of Earth System Science, 120(4), 773–782.

Mignot, J, Montégut, CB, Tomczak, M. 2009. On the porosity of barrier layers. Ocean Science, 379–387.

Minnett, P. J.2009. Upper Ocean Heat and Freshwater Budgets. In J. H. Steele, K. K. Turekian, & S. A. Thorpe (Eds.), Encyclopedia of Ocean Sciences (2nd Editio., pp. 163–174). Oxford: Academic Press.

Morey SL, Bourassa M a., Dukhovskoy DS, O'Brien JJ. 2006. Modeling studies of the upper ocean response to a tropical cyclone. Ocean Dynamics 56: 594–606.

Nam S, Kim D, Moon WM. 2011. Observed impact of mesoscale circulation on oceanic response to Typhoon Man-Yi (2007). Ocean Dynamics 62: 1–12.

Pan, J., & Sun, Y. 2013. Estimate of Ocean Mixed Layer Deepening after a Typhoon Passage over the South China Sea by Using Satellite Data. Journal of Physical Oceanography, 43(3), 498–506. doi:10.1175/JPO-D-12-01.1

Park J, Park K, Kim K, Youn Y. 2005. Statistical analysis of upper ocean temperature response to typhoons from ARGO floats and satellite data. Proceedings. 2005 IEEE International Geoscience and Remote Sensing Symposium, 2005. IGARSS '05. 4: 2564–2567.

Peduzzi P, Chatenoux B, Dao H, De Bono a., Herold C, Kossin J, Mouton F, Nordbeck O. 2012. Global trends in tropical cyclone risk. Nature Climate Change.

Prasad TG, Hogan PJ. 2007. Upper-ocean response to Hurricane Ivan in a 1/25° nested Gulf of Mexico HYCOM. Journal of Geophysical Research 112: 1–18.

Price J. 1981. Upper ocean response to a hurricane. Journal of Physical Oceanography 11: 153–175.

Price, J, Morzel, J, Niiler, P. 2008. Warming of SST in the cool wake of a moving hurricane. Journal of Geophysical Research: 113(C7), C07010. doi:10.1029/2007JC004393

Pun, I-F, Lin, I-I, Lo, M-H. 2013. Recent increase in high tropical cyclone heat potential area in the Western North Pacific Ocean. Geophysical Research Letters, 40(April),. doi:10.1002/grl.50548

Qiu B, Chen S. 2010. Interannual-to-Decadal Variability in the Bifurcation of the North Equatorial Current off the Philippines. Journal of Physical Oceanography 40: 2525–2538.

Qiu B, Chen S. 2012. Multidecadal Sea Level and Gyre Circulation Variability in the Northwestern Tropical Pacific Ocean. Journal of Physical Oceanography 42: 193–206.

Qu T, Lukas R. 2003. The Bifurcation of the North Equatorial Current in the Pacific*. Journal of Physical Oceanography 33: 5–18.

Rao K, Smitha A, Ali M. 2006. cyclone induced productivity in south-western Bay of Bengal during November-December 2000 using MODIS (SST and chlorophyll-a) and altimeter sea surface height. Indian Journal of Marine Sciences 35: 153–160.

Ribera P, García-Herrera R, Gimeno L, Hernández E. 2005. Typhoons in the Philippine Islands, 1901-1934. Climate Research 29: 85–90.

Rudnick, D. L., Jan, S., Centurioni, L., Lee, C. M., Wang, J., Lee, D. K., Wang, J, Lee, DK, Tseng, RS, Kim, YY, Chen, CS. 2011. Seasonal and mesoscale variability of the Kuroshio near its origin. Oceanography, 24(4), 52–63.

Scowcroft, G., Ginis, I., Knowlton, C., Yablonsky, R., and Morin, H., 2011. *Hurricanes: Science and Society*. University of Rhode Island, 16 pp.

Shang S, Li L, Sun F, Wu J, Hu C, Chen D, Ning X, Qiu Y, Zhang C, Shang S. 2008. Changes of temperature and bio-optical properties in the South China Sea in response to Typhoon Lingling, 2001. Geophysical Research Letters 35: 1–6.

Shay, L., Goni, G., & Black, P. 2000. Effects of a warm oceanic feature on Hurricane Opal. Monthly Weather Review, 128, 1366–1383.

Shay, LK. 2001. Upper Ocean Structure: Response to Strong Forcing Events. In: Encyclopedia of Ocean Sciences, ed. R. A. Weller, S. A. Thorpe, J. Steele, Academic Press International, London, UK, 3100-3114.

Shay, LK. 2009. Upper Ocean Structure: Response to Strong Forcing Events. In: Encyclopedia of Ocean Sciences, 2nd Edition, Ed. J. Steele, S. A. Thope, K. Turekian, and R. A. Weller, Elsevier Press International, Oxford, UK, 4619-4637, DOI:10.1016/B978-012374473-9.00628-7.

Shiah, F.-K., Chung, S.-W., Kao, S.-J., Gong, G.-C., & Liu, K.-K. (2000). Biological and hydrographical responses to tropical cyclones (typhoons) in the continental shelf of the Taiwan Strait. Continental Shelf Research, 20(15), 2029–2044. doi:10.1016/S0278-4343(00)00055-8

Siswanto, E., Ishizaka, J., Morimoto, A., Tanaka, K., Okamura, K., Kristijono, A., & Saino, T. 2008. Ocean physical and biogeochemical responses to the passage of Typhoon Meari in the East China Sea observed from Argo float and multiplatform satellites. Geophysical Research Letters, 35(15), L15604. doi:10.1029/2008GL035040

Son, S., Platt, T., Fuentes-Yaco, C., Bouman, H., Devred, E., Wu, Y., & Sathyendranath, S. 2007. Possible biogeochemical response to the passage of Hurricane Fabian observed by satellites. Journal of Plankton Research, 29(8), 687–697. doi:10.1093/plankt/fbm050

Takagaki, N., S. Komori, N. Suzuki, K. Iwano, T. Kuramoto, S. Shimada, R. Kurose, and K. Takahashi (2012), Strong correlation between the drag coefficient and the shape of the wind sea spectrum over a broad range of wind speeds, Geophys. Res. Lett., 39, L23604, doi:10.1029/2012GL053988.

Tu, J-Y, Chou, C, Chu, P-S. 2009. The Abrupt Shift of Typhoon Activity in the Vicinity of Taiwan and Its Association with Western North Pacific–East Asian Climate Change. Journal of Climate, 22(13), 3617–3628. doi:10.1175/2009JCLI2411.1

Uhlhorn EW, Shay LK. 2012. Loop Current Mixed Layer Energy Response to Hurricane Lili (2002). Part I: Observations. Journal of Physical Oceanography 42: 400–419.

Umlauf, L., Bolding, K., and Burchard, H. (2005): GOTM – scientific documentation: version 3.2, Meereswissenschaftliche Berichte, 63, 231 pp. http://www.gotm.net/pages/documentation/manual/pdf/a4.pdf

Vinayachandran, PN, Matthew, S. 2003. Phytoplankton bloom in the Bay of Bengal during the northeast monsoon and its intensification by cyclones. Geophysical Research Letters, 30(11), 1999–2002. doi:10.1029/2002GL016717

Vincent, EM, Lengaigne, M, Madec, G, Vialard, J, Samson, G, Jourdain, NC, Menkes, CE, Jullien, S. 2012. Processes setting the characteristics of sea surface cooling induced by tropical cyclones. Journal of Geophysical Research, 117(C2), 1–18. doi:10.1029/2011JC007396

Vissa, NK, Satyanarayana, AN, & Prasad Kumar, B. 2012. Response of Upper Ocean during passage of MALA cyclone utilizing ARGO data. International Journal of Applied Earth Observation and Geoinformation, 14(1), 149–159. doi:10.1016/j.jag.2011.08.015

Wada, A, Chan, J. 2008. Relationship between typhoon activity and upper ocean heat content. Geophysical Research Letters, 35(17), 1–6. doi:10.1029/2008GL035129

Wada A, Usui N. 2010. Impacts of Oceanic Preexisting Conditions on Predictions of Typhoon Hai-Tang in 2005. Advances in Meteorology 2010: 1–15.

Wang D, Zhao H. 2008. Estimation of Phytoplankton Responses to Hurricane Gonu over the Arabian Sea Based on Ocean Color Data. Sensors 8: 4878–4893.

Wang X, Han G, Qi Y, Li W. 2011. Impact of barrier layer on typhoon-induced sea surface cooling. Dynamics of Atmospheres and Oceans 52: 367–385.

Williams F, Jung G, Englebretson R. 1993. Forecasters Handbook for the Philippine Islands and Surrounding Waters.

Wu Q, Chen D. 2012. Typhoon-Induced Variability of the Oceanic Surface Mixed Layer Observed by Argo Floats in the Western North Pacific Ocean. Atmosphere-Ocean 37–41.

Yang, Y-J, Sun, L, Liu, Q, Xian, T, Fu, Y-F. 2010. The biophysical responses of the upper ocean to the typhoons Namtheun and Malou in 2004. International Journal of Remote Sensing, 31(17-18), 4559–4568. doi:10.1080/01431161.2010.485140

Yang, Y.-J., Sun, L., Duan, A.-M., Li, Y.-B., Fu, Y.-F., Yan, Y.-F., Wang, Z-Q., Xian, T. 2012. Impacts of the binary typhoons on upper ocean environments in November 2007. Journal of Applied Remote Sensing, 6(1), 063583. doi:10.1117/1.JRS.6.063583

Yaremchuk M, Qu T. 2004. Seasonal Variability of the Large-Scale Currents near the Coast of the Philippines*. Journal of physical oceanography 844–855.

Zhao H, Tang D, Wang Y. 2008. Comparison of phytoplankton blooms triggered by two typhoons with different intensities and translation speeds in the South China Sea. Marine Ecology Progress Series 365: 57–65.

Zhao, H., Han, G., Zhang, S., & Wang, D. 2013. Two phytoplankton blooms near Luzon Strait generated by lingering Typhoon Parma. Journal of Geophysical Research: Biogeosciences, 118(2), 412–421. doi:10.1002/jgrg.20041

APPENDIX

Supplementary Figures – Chapter 2

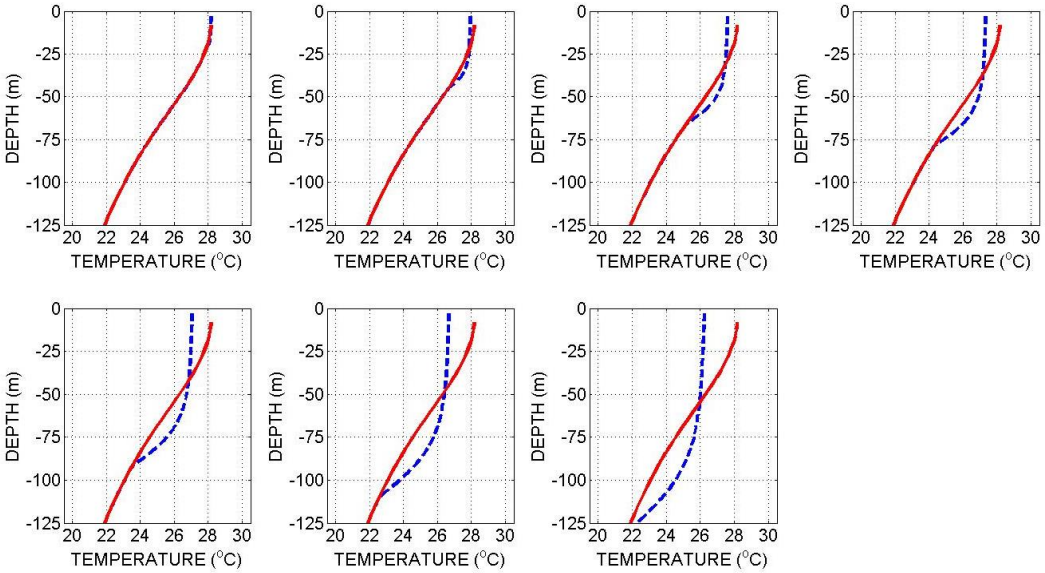

Figure 56. Temperature profile forced at wind stress at associated with different TC strength after 3 hours at BN as result of numerical experiments (Pre-Typhoon Profile – solid red line; Post Typhoon Profile – broken blue line). From top left to top right (TD, TS, C1, C2); bottom left to bottom right (C3, C4, C5)

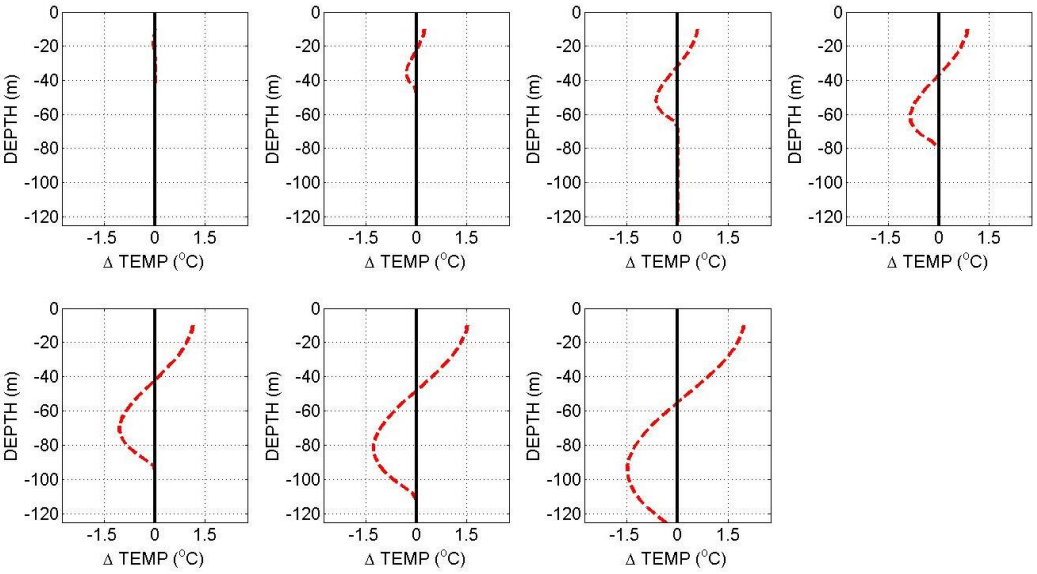

Figure 57. Temperature profile differences forced at wind stress at associated with different TC strength after 3 hours at BN as result of numerical experiments (Pre-Typhoon Profile – solid red line; Post Typhoon Profile –broken blue line). From top left to top right (TD, TS, C1, C2); bottom left to bottom right (C3, C4, C5)

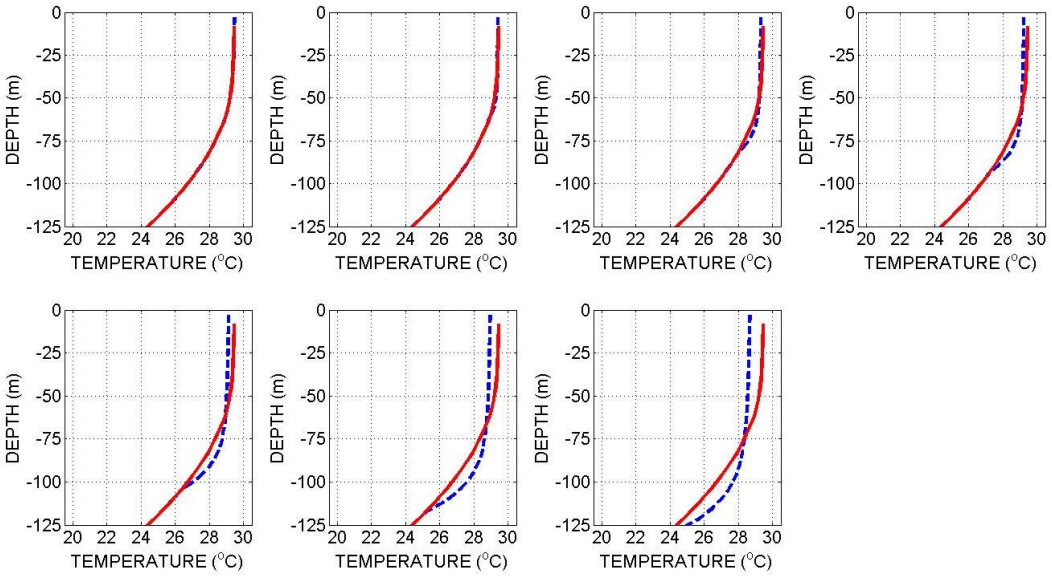

Figure 58. SST profile forced at wind stress associated with different TC strength after 3 hours at BS as result of numerical experiments (Pre-Typhoon Profile – solid red line; Post Typhoon Profile –broken blue line). From top left to top right (TD, TS, C1, C2); bottom left to bottom right (C3, C4, C5)

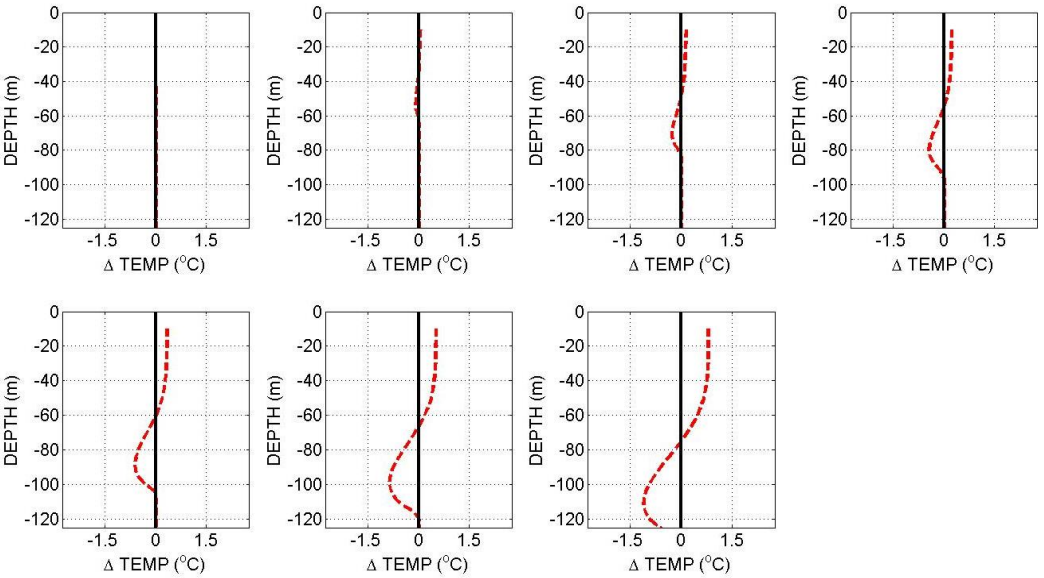

Figure 59. Temperature profile differences forced at wind stress at associated with different TC strength after 3 hours at BS as result of numerical experiments (Pre-Typhoon Profile – solid red line; Post Typhoon Profile –broken blue line). From top left to top right (TD, TS, C1, C2); bottom left to bottom right (C3, C4, C5)

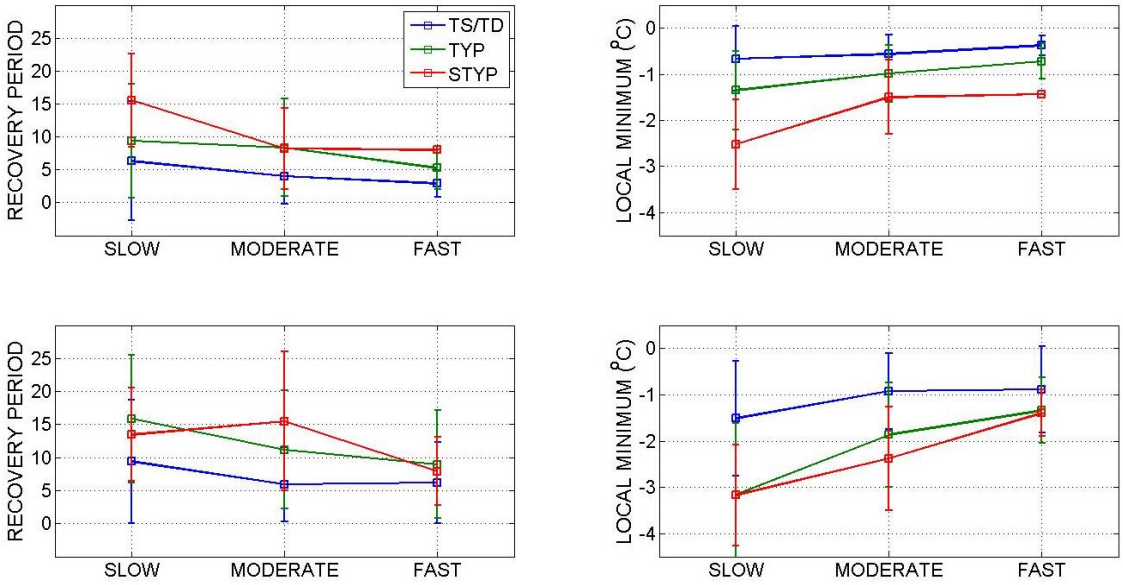

Figure 60. Relationship between translation speed on local minima and recovery period for BS (top) and BN (bottom) region at varying TC Strength; Color bar denotes TC Strength is classified as TS/TD (blue) for Tropical Storms and Depression, TYP (green) for CAT 1 to 3 and STYP (red) for CAT 4 to 5; Translation Speed are considered slow for 0-5 m/s; Moderate for 5-10 m/s and Fast for >10 m/s;

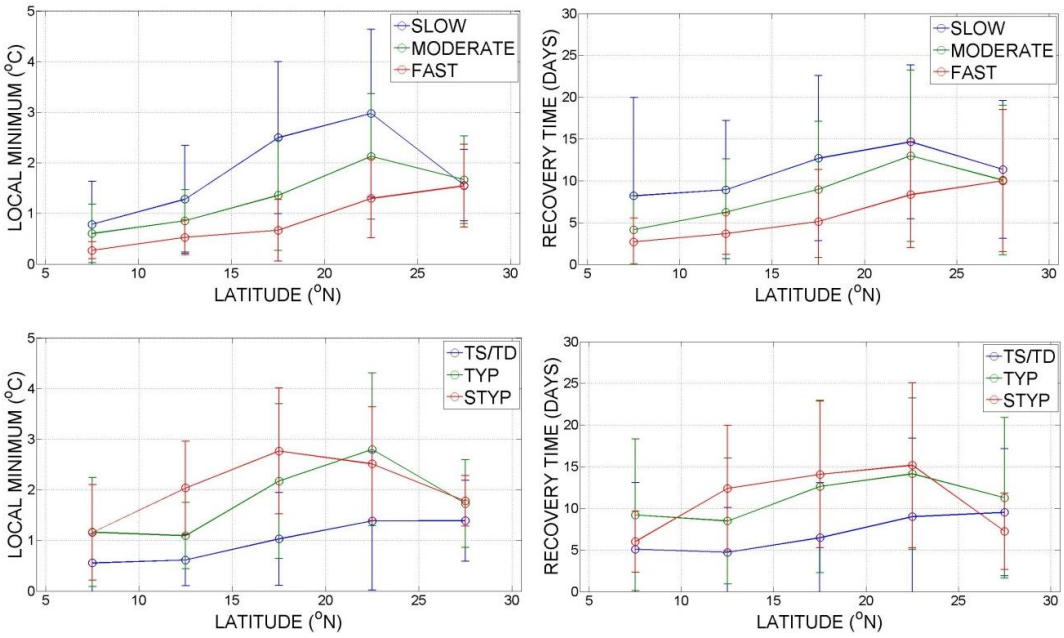

Figure 61. Meridional variations of mean and standard variation of (c) Local Minimum and (d) Recovery Time based on Translation Speed [Slow (blue) – Translation Speed < 4 m/s; Moderate (green) – Translation Speed > 4 & <8 m/s; Fast (red) – Translation Speed > 8 m/s]; Meridional variation of (c) Local Minimum and (d) Recovery Time for different typhoon intensities based on Saffir-Simpson Hurricane Scale (SSHS) [TS/TD (blue) – Tropical Storms and Depression; TYP (green) – Category 1 to Category 3; STYP (red) – Category 4 and 5]

Supplementary Figures – Chapter 3

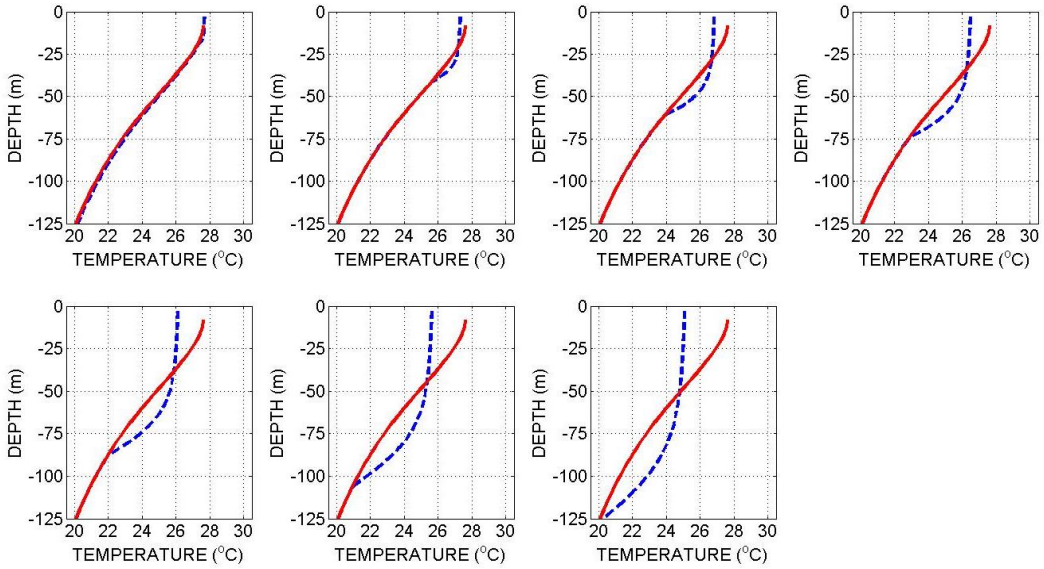

Figure 62. SST profile forced at associated with different TC strength after 3 hours for a negative feature as result of numerical experiments (Pre-Typhoon Profile – solid red line; Post Typhoon Profile –broken blue line). From top left to top right (TD, TS, C1, C2); bottom left to bottom right (C3, C4, C5)

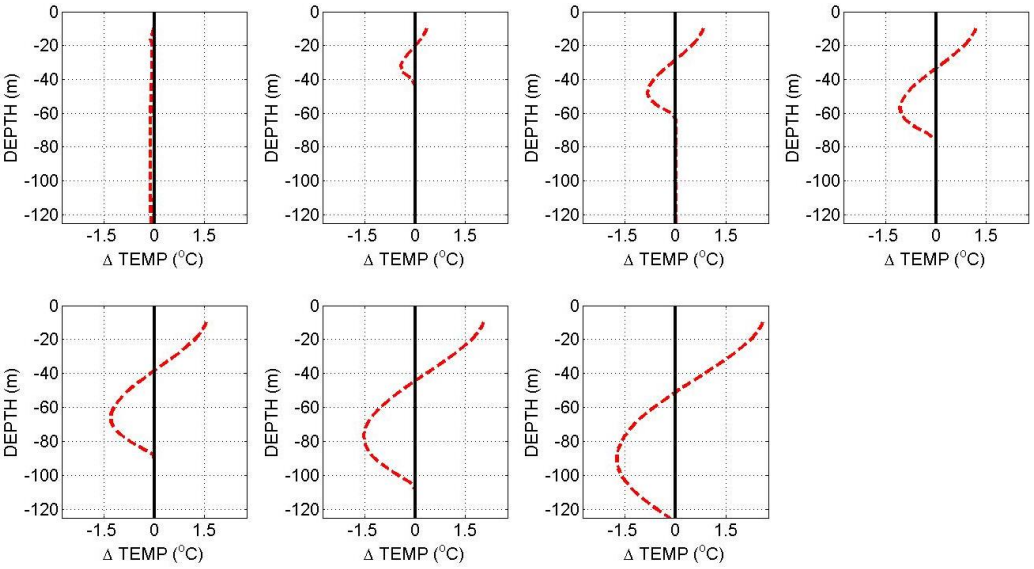

Figure 63. Temperature profile differences forced at wind stress at associated with different TC strength after 3 hours for a negative feature as result of numerical experiments (Pre-Typhoon Profile – solid red line; Post Typhoon Profile –broken blue line). From top left to top right (TD, TS, C1, C2); bottom left to bottom right (C3, C4, C5)

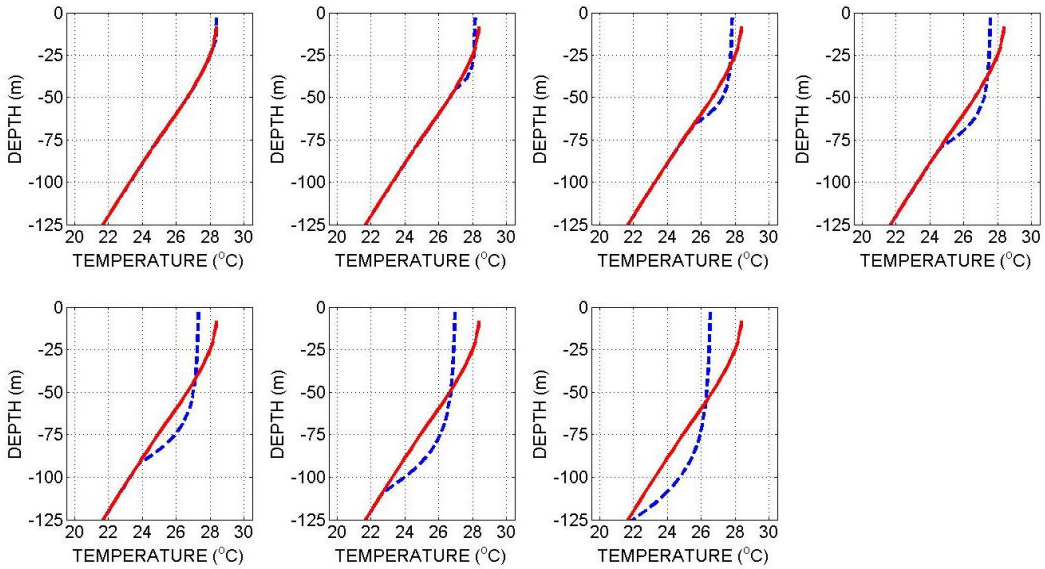

Figure 64. SST profile forced at associated with different TC strength after 3 hours for a neutral feature as result of numerical experiments (Pre-Typhoon Profile – solid red line; Post Typhoon Profile –broken blue line). From top left to top right (TD, TS, C1, C2); bottom left to bottom right (C3, C4, C5)

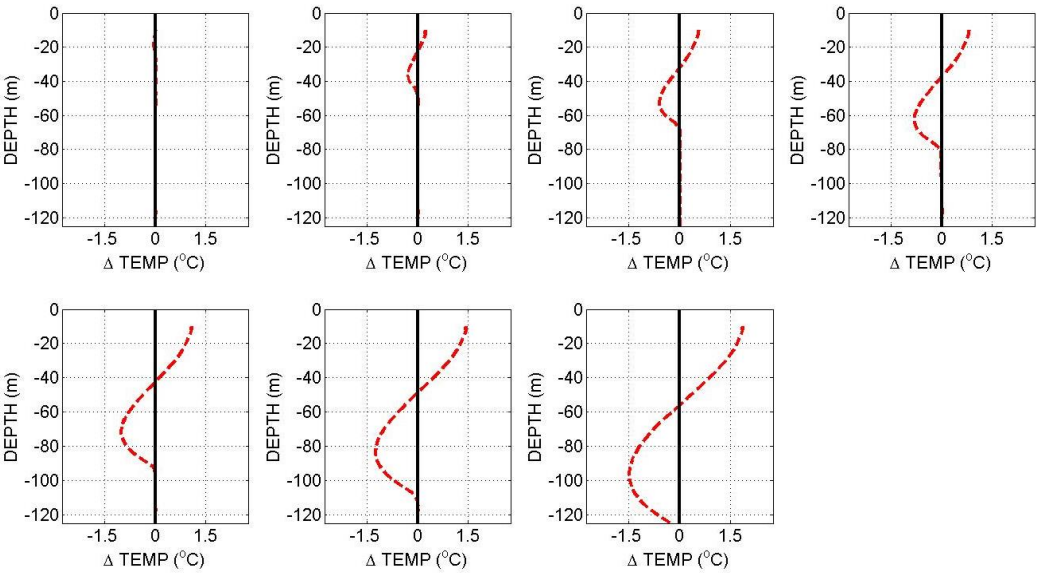

Figure 65. Temperature profile differences forced at wind stress at associated with different TC strength after 3 hours for a neutral feature as result of numerical experiments (Pre-Typhoon Profile – solid red line; Post Typhoon Profile –broken blue line). From top left to top right (TD, TS, C1, C2); bottom left to bottom right (C3, C4, C5)

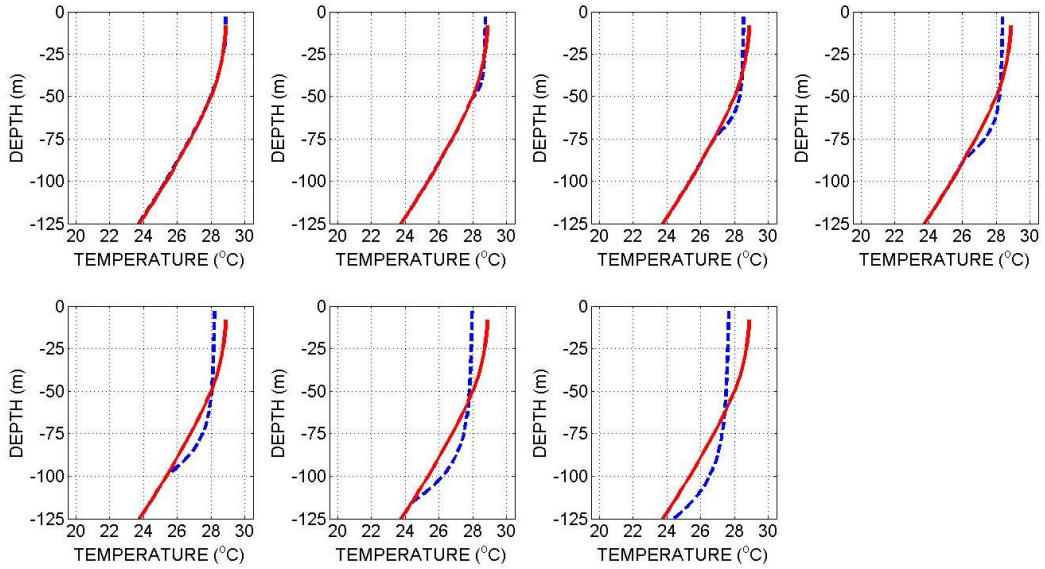

Figure 66. SST profile forced at associated with different TC strength after 3 hours for a positive feature as result of numerical experiments (Pre-Typhoon Profile – solid red line; Post Typhoon Profile –broken blue line). From top left to top right (TD, TS, C1, C2); bottom left to bottom right (C3, C4, C5)

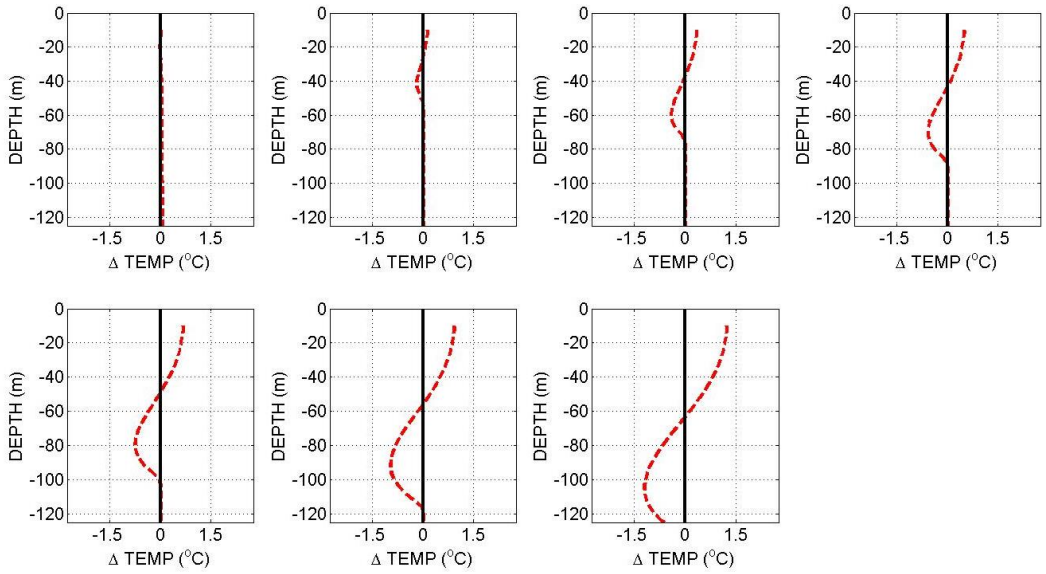

Figure 67. Temperature profile differences forced at wind stress at associated with different TC strength after 3 hours for a positive feature as result of numerical experiments (Pre-Typhoon Profile – solid red line; Post Typhoon Profile –broken blue line). From top left to top right (TD, TS, C1, C2); bottom left to bottom right (C3, C4, C5)

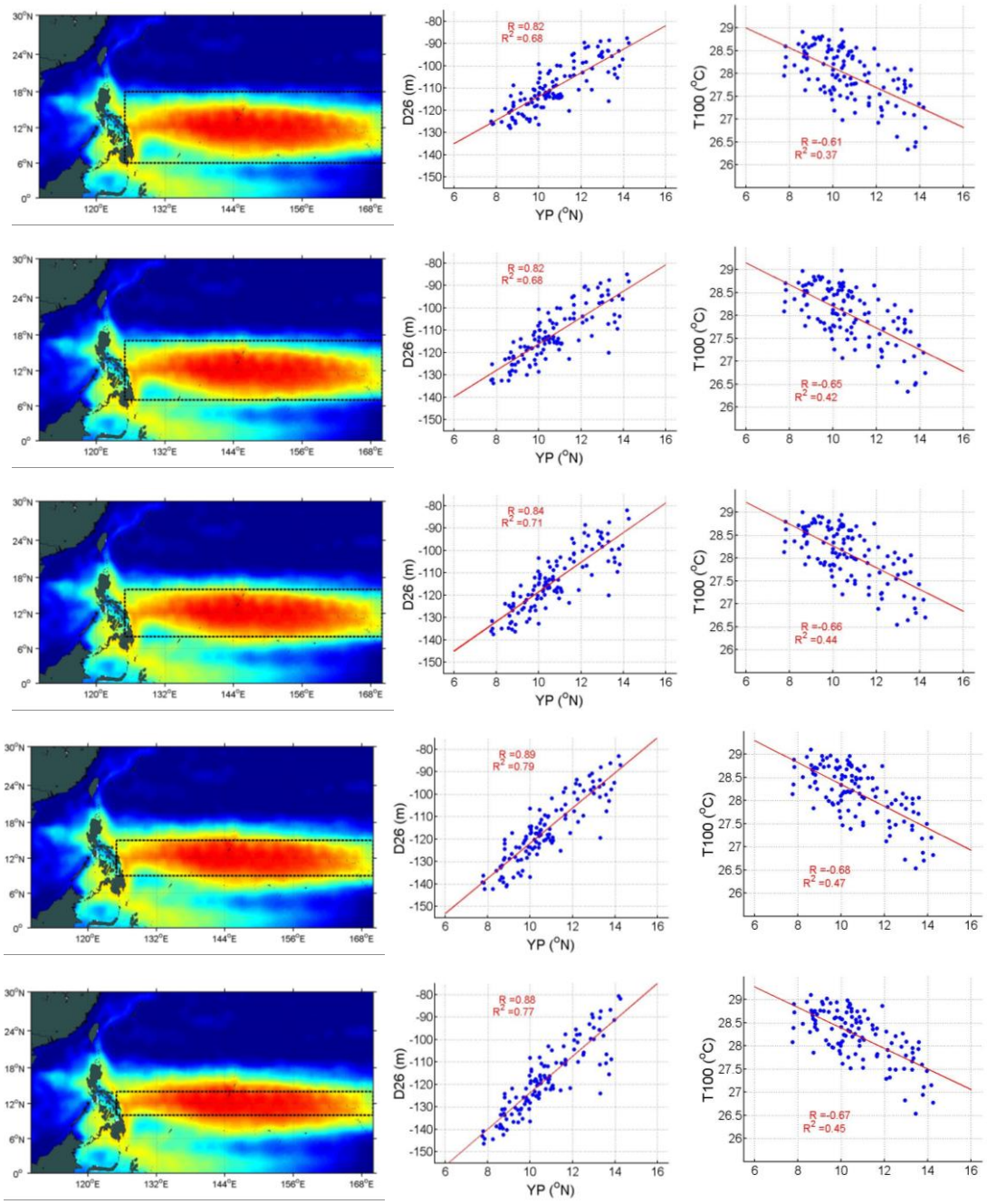

Figure 68. (a) Meridional Plot of D26 averaged along the 124-145°E region acquired using ARGO Float data from 2003 to 2012. Boxed highlighting NEC Bifurcation window (10-15°N)